Fall 12-18-2014

Incorporation of Charge Transfer into Classical Molecular Dynamics Force Fields with Applications in Physical Chemistry.

Marielle Soniat
University of New Orleans, mesoniat@uno.edu

Incorporation of Charge Transfer into Classical Molecular Dynamics Force Fields with Applications in Physical Chemistry.

A Dissertation

Submitted to the Graduate Faculty of the
University of New Orleans
in partial fulfillment of the
requirments for the degree of

Doctor of Philosophy
in
Chemistry

by

Marielle Soniat

B.S. Mississippi State University, 2007

December, 2014

Acknowledgements

First, I must thank my advisor, Dr. Steven W. Rick. He has been encouraging throughout my research and has allowed me to explore whatever interests I develop.

My committee members Dr. Lawrence R. Pratt, Dr. Christopher M. Summa, and Dr. Dhruva K. Chakravorty have also provided me with valuable assistance and advice.

My group members, most especially Dr. Alexis J. Lee and Dr. Sreeja Parameswaran, have been helpful in technical questions and helping me remember that there's a light at the end of the dissertation tunnel.

My colleagues in the wider science community, too numerous to name here, have challenged me to look further into my research, sparked ideas for new projects, and furthered my understanding of science outside my research area.

My family has supported this endeavor, since long before starting at UNO. My friends have kept me sane and not too antisocial.

Lastly, the Board of Regents and the LA-SiGMA program have provided financial support.

Table of Contents

List of Figures

List of Tables

Abstract

The presence of charge transfer (CT) interactions is clear in a variety of systems. In CT, some electron density is shifted from one molecule to another (non-bonded) molecule. The importance of this CT interaction is unclear. Previous attempts to look at the consequences of CT required the use of ab initio molecular dynamics (AIMD), a computationally intensive method. Herein, a method for including CT in force field (FF) simulations is described. It is efficient, produces charges in agreement with AIMD, and prevents long-ranged CT.

This CT MD method has been applied to monatomic ions in water. When solvated, ions do not have an integer charge. Anions give up some electron density to their ligands, and cations receive some electron density from their ligands. In bulk, the first solvation shell does not compensate for all CT, i.e. the charge is not smeared out over the first solvation shell. Rather, some charge is also found in the second solvation shell and further into the bulk. The charge of the first solvation shell depends on the balance between ion-water and water-water CT. When an interface is present, the charge outside of the second solvation shell will reside at the interface. This occurs even when the ion is over 15 Å away from the surface. The effect of long-ranged CT is mediated by changes in the hydrogen bonding patterns in water induced by the ions (not direct CT from the ions to distant waters).

The model has also been applied to water's "self-ions" hydronium and hydroxide. Trajectories from the multi-state empirical valence bond model (MS-EVB3) are analyzed. The differences between monatomic and molecular ions are explored. The direction of CT and the effect of hydrogen bonding with the ion are considered.

The damping of CT as ligands are added is discussed and a method to improve the MD model, in order to account for damping, is proposed.

Keywords: charge transfer, quantum mechanics, molecular dynamics, water, liquid-vapor interface, ion, zinc, hydronium, hydroxide,

Chapter 1

Introduction

1.1 What is CT?

Electron delocalization is a common phenomenon in quantum mechanics. Charge transfer (CT) occurs when electrons become delocalized over non-bonded pairs. There is an energy contribution E_{CT} equal to the stabilization of the cluster due to CT or electron delocalization.[1] In ion-water dimers, quantum mechanical (QM) charge partitioning schemes assign a non-integer charge to the ion and assign a net charge to the water molecule.[2] QM calculations show the occurrence of CT even in the electronic ground state and separate from basis set superposition error (BSSE).[3, 4, 5]

CT is related to polarizability. Polarizability is the "redistribution of electron density of a molecule in the presence of an electric field."[3] The electric field may be due to other molecules in a system. The change in electron distribution lowers the overall energy of the system, giving rise to a "polarization energy." The polarization of a molecule depends on the arrangement of all other molecules in the system. As such, it is a non-additive, many-body term, as opposed to a pairwise additive term. Polarizability is usually defined as the intra-molecular rearrangement of electron density, whereas CT refers to the inter-molecular rearrangement of electron density.[3] The distinction between the two is somewhat arbitrary. For instance, for large molecules, polarizability may be defined as rearrangement within a fragment of the molecule and CT as rearrangement between frag-

ments. (These terms then depend on the definition of the fragments.)[6] Both polarization and CT tend to stabilize a system.[7]

CT is often explained and modeled in terms of an interplay between ionization energy of the donor and electron affinity of the acceptor. The overlap integral between the orbitals exchanging charge is also relevant.[8]

1.2 Evidence for CT

1.2.1 Quantum Mechanics Calculations

Electronic structure calculations have shown CT in ion-water systems,[9, 10, 11, 12, 13, 14] hydrogen bonded systems,[5, 15] solid salts,[16] proteins in water,[7, 17] ions in biological ion channels,[18, 19, 20] and ionic liquids.[21]

Thompson and Hynes [15] and van der Vaart and Merz [5] review the controversy over whether hydrogen bonds (HB's) are purely electrostatic or involve CT. CT has been shown to be a typical feature of hydrogen bonds,[22] with 0.005 to 0.050 *e* transferred.[23] In natural energy decomposition (NEDA, part of natural bond order (NBO) analysis), this corresponds to 3-30 kcal/mol.[5, 24] The energy due to this local covalency explains the trends in total binding energy for different types of HB's.[23] Galvez, Gomez, and Pacios [25] show that electrostatic effects dominate HB's at $R \geq R_{eq} + 1$Å. At shorter distances, polarization and CT dominate the interaction.[25]

Thompson and Hynes [15] look at CT in HB complexes in light of the Mulliken view of proton transfer. In this view, there is strong coupling between the X-H·Y and $A^- \cdot HY^+$ states, and transfer of the proton and electron of hydrogen are concerted, not sequential. This picture implicitly involves transfer of electron density from the lone pair of Y to the anti-bonding orbital of X-H. Such a picture is shown explicitly in an NBO analysis in which the occupancy of a halide lone pair decreases as the X-H anti-bonding orbital occupancy increases. In HB, this resonance decreases the X-H bond strength and lowers its stretch frequency. The non-linear relationship between X-H stretch frequency

and binding energy/enthalpy can be captured with a single valence state (no CT), but the frequency shifts are too small. They predict that CT should show an isotope effect in the classical vibrational turning points, since X-D has a different stretch frequency than X-H.[15]

Dal Peraro et al. looked at the charge of ions in water using AIMD.[26] They find that anions' orbitals are spread out and overlap with their first solvation shell (1ss), resulting in a loss of ≈25% of electron density. In contrast, the cations' volumes are overlapped by orbitals of waters in the 1ss, and they lose ≈12% of their charge. Additionally, CT between water and the ionic termini of a zwitterionic diglycine (GG) molecule is much greater than CT due to HB's between water and the peptide backbone.

Marenich et al. [27] show that the magnitude of CT between molecules is equal to or greater than the change in atomic partial charges upon polarization for ions and neutral molecules.

CT energy has been included in a variety of energy decomposition (ED) methods.[3] Because there are no quantum operators for the energy components (only the total energy), ambiguity exists in how to divide up the energy contributions. Thus, what exactly CT energy refers to and how much energy per electron transferred vary between the methods. As an example, in water dimers, E_{CT} is only 20% of the total interaction energy in the Morokuma scheme and perturbation-based analyses but the dominant term (up to 60%) in natural energy decomposition analysis (NEDA, part of the natural bond order (NBO) analysis) and semiempirical divide and conquer decomposition (SDCD).[5, 15] The magnitude of CT energy varies with the system type, and it can be less than, greater than, or equal to the polarization energy.[3]

Morokuma [28] includes a CT term in his energy decomposition scheme. CT is defined as the movement of electrons from occupied orbitals of one molecule to the unoccupied orbitals of another molecule. E_{CT} is defined as the difference in interaction energy

between a complex in which electrons are allowed to delocalize and a complex in which this is prohibited.[28]

In Intermolecular Perturbation Theory (IMPT) [29] defines induction energy as a "term involving one-electron excitations ... from on of the occupied orbitals to a virtual orbital *on the same molecule*." When molecules are close together, the induction in modified by the CT term. In this case, the excitation is from the occupied orbital of one molecule to the virtual orbitals of the other molecule. The functional form of $E_{CT} = -Be^{r-\rho(\Omega)}$ where B is a parameter, r is the distance, and $\rho(\Omega)$ is an orientational term.[29] Since the amount of CT is also exponentially dependent on distance, the relation between energy and amount of CT should be linear. In Stone's scheme the proportionality is approximately 42 kcal/mol per electron transferred.

Most other energy partitioning schemes [3, 30, 31, 32] are based on one of the above concepts. Debate rages over which ED method is best.[3] Most have some drawbacks, typically related to the handling of basis sets or their convergence. Many of the methods can only use single-determinant (Hartree-Fock) wavefunctions and so neglect correlation.[1, 3, 5, 29]

1.2.2 Experiment

Few experiments give direct access to atomic partial charge or charge transfer values.[33] Bader's atoms in molecules (AIM) method can be applied to experimental electron density from X-ray crystallography.[34] X-ray absorption spectroscopy (XAS) and photoelectron spectroscopy (PES) probe mixing between the ligand electrons and metal orbitals (i.e. covalency or CT).[35] CT was shown to alter the spectrum of Mg^{2+} in water, compared to Ca^{2+}.[36]

The difference in dipole moment of a dimer versus the geometric sum of the dipoles of the isolated monomers could, in theory, be used to estimate CT if the change in

dipole of the monomers in the complex can be accounted for; however, this is usually not possible.[33]

A method exists to estimate CT from nuclear quadrupole coupling constants (aka hyperfine structure).[33] In molecular beam (MB) scattering experiments, the quantum integral cross section Q is measured as a function of beam velocity v.[8] The pattern of $\Delta Q(v)$ due to "glory" quantum interference depends on the depth and location of the potential energy minimum. The average cross section $\bar{Q}(v)$ is related to the strength of the long-ranged interaction. The information obtained from MB experiments is similar to that of nuclear quadrupole coupling. The MB experiments are combined with high-level *ab initio* calculations of electron density distribution. The CD method considers the difference between the charge distribution in a dimer versus the monomers. Systems that have been studied with this method are mainly water or ammonia bound to noble gases or diatomic gases; such systems were chosen because electrostatic effects are minimal, allowing for more clear analysis of CT. Because van der Waals (vdW) terms are similar in these systems, deviation from vdW plus induction is attributed to CT. For example, an improved Lennard-Jones (ILJ) [37] model fits the Ne-water interaction well but fails for the Xe-water interaction for which the potential energy minimum is lower than predicted by ILJ.[8]

A model for E_{CT} is proposed in Ref. [8] in which $E_{CT} = (B/I)e^{-A\sqrt{I}}$ where I is the ionization potential of the electron donor, and A and B are parameters. The estimated energy stabilization due to CT is ≈58 kcal/mol per electron transferred.[8] Such a large energy contribution reproduces the interaction potentials of water with noble gases and molecular hydrogen calculated from experiment [38, 39, 40, 41] though slightly larger than from SAPT(DFT) (version CT-SM09).[8, 42] This energy contribution is larger than the Coulombic energy expected for point charges of the same magnitude separated by the same distance. The stabilization is instead due to the decrease in kinetic energy of the

electrons when they delocalize over the larger system, in the same manner as seen in covalent bonds.[8]

Using the CD method, Pirani et al. find CT from ammonia and water to the hydrogen molecule of 0.0024 and 0.0029 e, respectively.[41] These values are of the same order of magnitude as AIM values.

Vibrational spectra can be interpreted in terms of CT.[15, 43, 44, 45] In vibrational spectroscopy, hydrogen bonding in a complex of the form X-H·Y results in lengthening (weakening) of the X-H bond, which in turn results in a red-shift in the X-H vibrational frequency (compared to the monomer).[22] Typically, this is interpreted as due to CT from Y to X. The electron density is transferred into the X-H σ^* anti-bonding orbital. There are also rare cases of blue-shifted HB's. In these cases, electron density is shifted to a distant part of the HB donor, resulting in a shortening of the X-H bond.[22]

Thompson and Hynes show that without including CT in a model of vibrational frequencies, the frequency shift upon hydrogen bonding is too small.[15] Robertson et al.[43] show that CT is the source of differences in the spectra of $NO^-{\cdot}H_2O$ and $O_2^-{\cdot}H_2O$. They estimate that at least half of the red-shift in $O_2^-{\cdot}H_2O$ is due to CT.[43] The lack of CT explains the weakness of the red-shift in $NO_3^-{\cdot}6H_2O$ complexes.[44]

Infrared (IR) intensities reflect the electronic structure.[46] Because CT alters the dipoles in a system, it is expected to alter IR intensities.[47] The correlation between atomic charge and IR intensity is expected to be high when contributions from charge flux and dipole flux to the dipole moment derivatives are small.[46] Calculations using the QTAIM/CCFDF framework show that those fluxes are large contributors to the IR intensity and so the correlation between IR intensity and QTAIM charges is low.[46]

In Raman spectra, the red shift in X-H stretch frequency due to CT is also observed. However, the Raman intensity is dependent on polarizability of halide solutes, not CT.[48] CT from halides to water does alter the H-O-H bend angle of water and causes an increase in Raman intensity for the water bending mode.[45] Further studies of halides in

water show that the preresonance Raman cross section of water is increased by CT from halides.[49]

1.3 Why is CT important?

Though the amount of electron density shifted between the pairs is generally small ($< 0.1e$), CT has been posed as a possible explanation for: specific ion effects,[50] ion channel selectivity,[18] the electrostatic potential of biomolecules,[6] and electrophoretic mobility of hydrophobic particles in water,[51, 52] among others.

The study of CT in large systems has been limited by the high computational cost of ab initio molecular dynamics (AIMD).[9, 26, 53, 54] Recently, classical point-charge models which include CT have been developed for molecular mechanics (MM) calculations.[2, 55] These models describe properties of water and ions that are in agreement with experiment and *ab initio* methods. In particular, the charge of waters and ions in bulk and the charge of the solvation shells around ions are the same as in AIMD.[2, 26] Additionally, the use of potential functions allows for easy separation of the energy contributions of CT and its effect on the Coulombic energy.

The importance of CT in a particular system is often quantified by comparing the CT energy and the polarization energy. Generally, chemical intuition can give a reasonable impression of how polarizable a system is. By comparing the CT energy, we can find out if CT is more or less important than polarization. For example, benzene is polarizable. In complex with cations, the CT energy is much less than the polarization energy. However, in complex with transition metal ions, the CT energy is greater.[3] In another example, the water-zinc CT energy is significant when few waters are present but decreases, relative to the polarization energy, as more waters are added.[3]

1.3.1 Previous Studies of CT

Some studies are bringing to light the consequences of CT. Most of the following studies are quantum mechanics studies, which prohibit large system size or long simulation times. Speed is gained by using semi-empirical methods but can also result in loss of accuracy. In depth discussion of the advantages and disadvantages of the various methods are carried out elsewhere [56] and are beyond the scope of this discussion. Nevertheless, whatever the quantitative accuracy, the qualitative results from different methods are expected to be important.

Mo and Gao [57] use BLW-ED to show that E_{CT} is linearly correlated with q_{CT} in Lewis acid-base complexes with 234 kcal/mol per electron transferred. Electron density is transferred from the base to the acid. Polarization and CT make approximately equal contributions to the induced dipoles. Thus, experiments on nuclear hyperfine structure overestimate CT, due to their neglect of polarization.[57]

In a later study, Mo and Gao [58] find -0.022e and +0.025e transferred from acetate and methylammonium ions to water, respectively. From this, they claim that polarization is the main many-body effect for acetate and methylammonium ions. The polarization of the waters by the ion is the main contributor. This contrasts with larger amounts of CT found by van der Vaart and Merz [5] for the same ions. They find -0.0475e and +0.0511e from acetate and methylammonium ions to water, respectively, at the MP2/aug-cc-pVTZ level with the same charge partitioning method.

In studies of proteins in water, Nadig et al.[59] find 2e are transferred from CspA protein to its hydration shell. For dimers of amino acid mimics and water (including acetate and methylammonium ions), the CT energy is double that of the polarization energy.[59] Polarization and CT are more significant for charged residues of CspA than for neutral residues.[7] Polarization is more important for the protein and affects the neutral residues more than CT. However, CT has more effect on the water surrounding CspA than polarization.[7]

Komeiji et al.[60] find CT from the neural ubiquitin protein to water. They show that this CT increases the protein's dipole moment. Additionally, CT between the solvent and protein stabilizes the protein.[60] Anisimov, Bugaenko, and Cavasotto,[61] while discussing the drawbacks of semi-empirical methods, support the qualitative conclusions of Komeiji et al. They especially emphasize the role CT plays in reducing the Coulombic attraction in salt bridges and the ability of neutral amino acids to become charged.[61]

Anisimov and Bliznyuk [6] find large CT from the GroEL-GroES chaperonin tetramer to water. They also consider the charge distribution of individual amino acids. The neutral amino acids have an average charge of zero, since they are equally likely to accept or donate charge (over all the various orientations within the tetramer). In contrast, the charged amino acids have a non-integer average charge. The cationic Arg and Lys have charges around +0.91e, and the anionic Asp and Glu have charges around -0.84e.[6]

Church et al.[62] find that polarization and CT are equally important to electrostatics in the interaction of Cl^- with neutral amino acids in the ClC transport protein binding site. Without polarization and CT, those interactions would be repulsive. Only for Cl^- interactions with cationic amino acids was electrostatics the dominant force. Cl^- loses about 25% of its charge from lone pair orbitals to X-H anti-bonding orbitals.[62]

In a *de novo* designed di-zinc metalloprotein (DFsc), CT is shown to be essential for the asymmetric coordination of the zinc ions.[63]

CT in concentrated NaCl solution was studied by Sellner, Valiev, and Kathmann.[53] They find that ion charges are not equal to $\pm 1e$, nor are they equal and opposite. The chloride charge varies with NaCl concentration, and the water molecules become negatively charged overall. Most of the negative charge is concentrated in the ions' first solvation shells. The sodium charge is less sensitive to concentration or its local solvation structure.[53]

Most recently, Yao, Kanai, and Berkowitz [64] used our model to study the diffusion of ions in water. They find that diffusion in the CT model agrees with ab initio molecular

dynamics (AIMD). The CT model allows the water dynamics to depend on ion type, whereas this behavior is not captured in fixed-charge or polarizable FF. In AIMD, anions increase the diffusivity of water, and cations decrease it. A net negative charge within the water decreases the hydrogen bond strength/lifetime, whereas the opposite is true for a net positive charge.[64]

1.4 Previous Methods for CT Force Fields

When developing potential models for molecular simulations, assigning a neutral charge to a molecule, or assigning an integer charge to an ion is a choice, made for convenience or based on intuition. It is more physically realistic to assign charges based on the electron density, resulting in molecular or ionic charges which depend upon their environment. The local rearrangement of charge affects both short- and long-ranged interactions. Such rearrangements may be within a molecule (polarization) or between molecules (charge transfer).

The inclusion of multi-body effects in molecular dynamics (MD) force fields is usually accomplished by adding polarizability.[65, 66] A multitude of dipole-polarizable force fields have been developed both for neutral molecules and ions.[67, 68, 69, 70, 71, 72] Some potentials also include polarizable quadrupoles.[73, 74] However, CT raises the question: Are we even getting the monopoles correct?

A few models have been developed which include charge transfer effects, often by including a charge transfer contribution to the energy but not actually changing the particles' charges.[73, 75, 76, 77, 78, 79] Charge-transfer models are largely derived from *ab initio* calculations. They have been primarily applied to dimers and small clusters but are fairly complex.[15, 73, 76, 80, 81] In a simpler technique used for ionic liquids, charge transfer has been added by assigning non-integer, but geometry independent, charges to the ions.[82] Such a method also can account for effective (average) polarization.[83]

Some methods include CT by getting atomic charges from QM calculations during the simulation. In the Adaptive Polarized Protein-Specific Charge (APPC) method,[63] the dynamics are paused every so often, and the charges are reset based on their QM values for that conformation. This allowed use of the standard Amber FF without refitting of parameters.[63] In the X-pol method,[84] the system is split into fragments, and QM charges are calculated for each fragment at each time step. Inter-fragment electrostatics are handled in a manner similar to QM/MM. However, this does not allow charge to move between fragments.

The Sum of Interacting Fragment *Ab Initio* (SIBFA) FF [85] produces CT energies which are in good agreement with *ab initio* values. The energy is influenced by the ionization potential of the electron donor and the electron affinity and "self-potential" of the electron acceptor. Each of these values are modified by the local electrostatic environment.

Reactive force fields may account for CT effects. As a reaction occurs, the partial charges of the reactants changes. This behavior is captured in the Variable Charge Central Force (VCCF) model [86] and the ReaxFF method.[87] Multi-State Empirical Valence Bond (MS-EVB) models [88] implicitly include CT due to the superposition of states.

1.4.1 Our Model

A new method for treating charge transfer has been developed recently for liquid water [55] and ions in water.[2] The Discrete Charge Transfer (DCT) method transfers a fixed amount of charge from one particle to another, if the two particles are within a prescribed distance. Though CT is most accurately modeled as an exponential, a switching function is used so that the amount of charge transferred goes smoothly to zero, thereby preventing long-ranged CT. The DCT model avoids the problems which have plagued other attempts at creating charge-transfer models,[81, 89, 90, 91] such as systems becoming conductive, and charge transfer at large distances and in the wrong direction. The DCT model is also an efficient method to treat charge transfer when simulating large systems.

Bibliography

[1] A. J. Misquitta, J. Chem. Theor. Comput. **9**, 5313 (2013).

[2] M. Soniat and S. W. Rick, J. Chem. Phys. **137**, 044511 (2012).

[3] G. A. Cisneros, M. Karttunen, P. Ren, and C. Sagui, Chem. Rev. **114**, 779 (2014).

[4] Y. Mo, J. Gao, and S. D. Peyerimhoff, J. Chem. Phys. **112**, 5530 (2000).

[5] A. van der Vaart and K. M. Merz, Jr., J. Chem. Phys. **116**, 7380 (2002).

[6] V. M. Anisimov and A. A. Bliznyuk, J. Phys. Chem. B **116**, 6261 (2012).

[7] A. van der Vaart and K. M. Merz, Jr., J. Am. Chem. Soc. **121**, 9182 (1999).

[8] D. Cappelletti, E. Ronca, L. Belpassi, F. Tarantelli, and F. Pirani, Acc. Chem. Res. **45**, 1571 (2012).

[9] S. Varma and S. B. Rempe, Biophys. J. **99**, 3394 (2010).

[10] Z. Zhao, D. M. Rogers, and T. L. Beck, J. Chem. Phys. **132**, 014502 (2010).

[11] A. C. Olleta, H. M. Lee, and K. S. Kim, J. Chem. Phys. **126**, 144311 (2007).

[12] D. Majundar, J. Kim, and K. S. Kim, J. Chem. Phys. **112**, 101 (2000).

[13] S. S. M. C. Godinho, P. Cabral do Couto, and B. J. Costa Cabral, Chem. Phys. Lett. **399**, 200 (2004).

[14] M. Tanaka and M. Aida, J. Solution Chem. **33**, 887 (2004).

[15] W. H. Thompson and J. T. Hynes, J. Am. Chem. Soc. **122**, 6278 (2000).

[16] A. Trzesowska and R. Kruszynski, J. Mol. Struct. (Theochem) **714**, 175 (2005).

[17] I. S. Ufimtsev, N. Luehr, and T. J. Martinez, J. Phys. Chem. Lett. **2**, 1789 (2011).

[18] D. Bucher et al., Biophys. Chem. **124**, 292 (2006).

[19] P. Huetz, C. Boiteux, M. Compoint, C. Ramseyer, and C. Girardet, J. Chem. Phys. **124**, 044703 (2006).

[20] S. Kraszewski, C. Boiteux, C. Ramseyer, and C. Girardet, Phys. Chem. Chem. Phys. **11**, 8606 (2009).

[21] J. Schmidt et al., J. Phys. Chem. B **114**, 6150 (2010).

[22] J. Muñoz, X. Fradera, M. Orozco, and F. J. Luque, Rev. Mod. Quantum Chem. , 1615 (2002).

[23] A. M. Pendas, M. A. Blanco, and E. Francisco, J. Chem. Phys. **125**, 184112 (2006).

[24] A. E. Reed, L. A. Curtiss, and F. Weinhold, Chem. Rev. **88**, 899 (1988).

[25] O. Gálvez, P. C. Gómez, and L. F. Pacios, J. Chem. Phys. **115**, 11166 (2001).

[26] M. Dal Peraro, S. Raugei, P. Carloni, and M. L. Klein, ChemPhysChem **6**, 1715 (2005).

[27] A. V. Marenich, R. M. Olson, A. C. Chamberlin, C. J. Cramer, and D. G. Truhlar, J. Chem. Theor. Comput. **3**, 2055 (2007).

[28] K. Morokuma, Acc. Chem. Res. **10**, 294 (1977).

[29] A. J. Stone, Chem. Phys. Lett. **211**, 101 (1993).

[30] R. Z. Khaliullin, A. T. Bell, and M. Head-Gordon, J. Chem. Phys. **128**, 184112 (2008).

[31] W. J. Stevens and W. H. Fink, Chem. Phys. Lett. **139**, 15 (1987).

[32] E. D. Glendening, J. Phys. Chem. A **109**, 11936 (2005).

[33] B. Szefczyk, W. A. Sokalski, and J. Leszczynski, J. Chem. Phys. **117**, 6952 (2002).

[34] E. D. Stevens, M. K. Dowd, G. P. Johnson, and A. D. French, Carbohydrate Res. **345**, 1469 (2010), Special Issue: Selected Papers from the 15th European Carbohydrate Symposium, Vienna 2009.

[35] R. H. Holm, P. Kennepohl, and E. I. Solomon, Chem. Rev. **96**, 2239 (1996).

[36] C. D. Cappa, J. D. Smith, B. M. Messer, R. C. Cohen, and R. J. Saykally, J. Phys. Chem. B **110**, 5301 (2006).

[37] F. Pirani et al., Phys. Chem. Chem. Phys. **10**, 5489 (2008).

[38] L. F. Roncaratti, L. Belpassi, D. Cappelletti, F. Pirani, and F. Tarantelli, J. Phys. Chem. A **113**, 15223 (2009), PMID: 19705824.

[39] L. Belpassi, F. Tarantelli, F. Pirani, P. Candori, and D. Cappelletti, Phys. Chem. Chem. Phys. **11**, 9970 (2009).

[40] L. Belpassi et al., J. Am. Chem. Soc. **132**, 13046 (2010).

[41] F. Pirani, D. Cappelletti, L. Belpassi, and F. Tarantelli, J. Phys. Chem. A **117**, 12601 (2013).

[42] A. J. Stone and A. J. Misquitta, Chem. Phys. Lett. **473**, 201 (2009).

[43] W. H. Robertson, M. A. Johnson, E. M. Myshakin, and K. D. Jordon, J. Phys. Chem. A **106**, 10010 (2002).

[44] S. G. Ramesh, S. Re, and J. T. Hynes, J. Phys. Chem. A **112**, 3391 (2008).

[45] K. Xiong and S. A. Asher, J. Phys. Chem. A **115**, 9345 (2011).

[46] A. F. Silva, W. E. Richter, H. G. C. Meneses, S. H. D. M. Faria, and R. E. Bruns, J. Phys. Chem. A **116**, 8238 (2012).

[47] H. Torii, J. Chem. Theor. Comput. **10**, 1219 (2014).

[48] D.-Y. Wu et al., J. Phys. Chem. A **112**, 1313 (2008).

[49] M. Ahmed, A. K. Singh, J. A. Mondal, and S. K. Sarkar, J. Phys. Chem. B **117**, 9728 (2013).

[50] P. Lo Nostro and B. W. Ninham, Chem. Rev. **112**, 2286 (2012).

[51] R. Vácha et al., J. Am. Chem. Soc. **133**, 10204 (2011).

[52] R. Vácha et al., J. Phys. Chem. Lett. **3**, 107 (2012).

[53] B. Sellner, M. Valiev, and S. M. Kathmann, J. Phys. Chem. B **117**, 10869 (2013).

[54] Q. Wan, L. Spanu, G. A. Galli, and F. Gygi, J. Chem. Theor. Comput. (2013).

[55] A. J. Lee and S. W. Rick, J. Chem. Phys. **134**, 184507 (2011).

[56] C. J. Cramer, *Essentials of Computational Chemistry: Theories and Models*, John Wiley Sons, Inc., West Sussex, England, 2nd edition, 2004.

[57] Y. Mo and J. Gao, J. Phys. Chem. A **105**, 6530 (2001).

[58] Y. Mo and J. Gao, J. Phys. Chem. B **110**, 2976 (2006).

[59] G. Nadig, L. C. Van Zant, S. L. Dixon, and K. M. Merz, Jr, J. Am. Chem. Soc. **120**, 5593 (1998).

[60] Y. Komeiji, T. Ishida, D. G. Fedorov, and K. Kitaura, J. Comput. Chem. **28**, 1750 (2007).

[61] V. M. Anisimov, V. L. Bugaenko, and C. N. Cavasotto, ChemPhysChem **10**, 3194 (2009).

[62] J. Church, S. Pezeshki, C. Davis, and H. Lin, J. Phys. Chem. B **117**, 16029 (2013).

[63] Y. L. Li, Y. Mei, D. W. Zhang, D. Q. Xie, and J. Z. H. Zhang, J. Phys. Chem. B **115**, 10154 (2011).

[64] Y. Yao, Y. Kanai, and M. L. Berkowitz, J. Phys. Chem. Lett. **5**, 2711 (2014).

[65] S. W. Rick and S. J. Stuart, in *Reviews in Computational Chemistry*, edited by K. B. Lipkowitz and D. B. Boyd, pages 89–146, Wiley, New York, 2002.

[66] P. Cieplak, F. Y. Dupradeau, Y. Duan, and J. Wang, J. Phys.: Condens. Matter **21**, 333102 (2009).

[67] L. X. Dang and T. Chang, J. Chem. Phys. **106**, 8149 (1997).

[68] D. E. Smith and L. X. Dang, J. Chem. Phys. **100**, 3757 (1994).

[69] S. J. Stuart and B. J. Berne, J. Phys. Chem. **100**, 11934 (1996).

[70] A. Grossfield, P. Ren, and J. W. Ponder, J. Am. Chem. Soc. **125**, 15671 (2003).

[71] D. Jiao, C. King, A. Grossfield, T. A. Darden, and P. Ren, J. Phys. Chem. B **110**, 1855 (2006).

[72] H. Yu et al., J. Chem. Theor. Comput. **6**, 774 (2010).

[73] C. Millot et al., J. Phys. Chem. A **102**, 754 (1998).

[74] A. Holt, J. Boström, G. Karlström, and R. Lindh, J. Comput. Chem. **31**, 1583 (2010).

[75] K. Honda, J. Chem. Phys. **117**, 3558 (2002).

[76] J. Piquemal, J. Chevreau, and N. Gresh, J. Chem. Theor. Comput. **3**, 824 (2007).

[77] R. Kumar, F. F. Wang, G. R. Jenness, and K. D. Jordan, J. Chem. Phys. **132**, 014309 (2010).

[78] C. Clavaguéra-Sarrio et al., J. Phys. Chem. B **107**, 3051 (2003).

[79] D. Hagberg, G. Karlström, B. O. Roos, and L. Gagliardi, J. Am. Chem. Soc. **127**, 14250 (2005).

[80] R. Chelli, V. Schettino, and P. Procacci, J. Chem. Phys. **122**, 234107 (2005).

[81] R. Chelli, M. Pagliai, P. Procacci, G. Cardini, and V. Schettino, J. Chem. Phys. **122**, 074504 (2005).

[82] T. G. A. Youngs and C. Hardacre, ChemPhysChem **9**, 1548 (2008).

[83] I. Leontyev and A. Stuchebrukhov, Phys. Chem. Chem. Phys. **13**, 2613 (2011).

[84] W. Xie, M. Orozco, D. G. Truhlar, and J. Gao, J. Chem. Theor. Comput. **5**, 459 (2009).

[85] N. Gresh, G. A. Cisneros, T. A. Darden, and J.-P. Piquemal, J. Chem. Theor. Comput. **3**, 1960 (2007).

[86] C. W. David, J. Chem. Phys. **104**, 7255 (1996).

[87] A. C. T. van Duin, S. Dasgupta, F. Lorant, and W. A. Goddard, J. Phys. Chem. A **105**, 9396 (2001).

[88] Y. Wu, H. Chen, F. Wang, F. Paesani, and G. A. Voth, J. Phys. Chem. B **112**, 467 (2007).

[89] S. W. Rick, S. J. Stuart, and B. J. Berne, J. Chem. Phys. **101**, 6141 (1994).

[90] S. M. Valone and S. R. Atlas, J. Chem. Phys. **120**, 7264 (2004).

[91] J. Chen and T. J. Martínez, Chem. Phys. Lett. **438**, 315 (2007).

Chapter 2

Quantum Chemical Characterization of Charge Transfer

Charge transfer was recognized as a contributor to molecular binding as early as the 1930's by Mulliken.[1] However, his scheme to calculate partial charges of atoms in molecules (and thus the amount of CT) suffers from severe deficiencies.[2] Subsequently, a variety of methods have been proposed for calculating partial atomic charges, each with its own advantages and drawbacks.

We choose to use Bader's Quantum Theory of Atoms in Molecules (QTAIM or AIM).[3] In AIM, originally developed for X-ray crystallography studies, the electron density is measured directly. In the absence of an X-ray structure, the electron density can be calculated with quantum mechanics. With a reasonable definition of atomic volumes, the electron density within a region can be summed and assigned to an atom.[2] For more details, see Section 2.1 below.

This chapter deals with some practical considerations of CT calculations, in order to establish "best practices" for them.

2.1 Quantum Theory of Atoms in Molecules

In quantum mechanics, a fundamental principle is that everything about a system is know if its wavefunction Ψ is known. In chemistry, we often wish to break the total

system into smaller pieces, such as molecules or atoms. If there is such a breakdown, the wavefunction itself must predict a unique partition and fully describe each subsystem.[3]

With the proper choice of boundary surfaces between subsystems, the total system can be partitioned in a physically reasonable manner.[3] While the wavefunction is not an observable, it's square, the electron density $\rho = \Psi^2$ is. The topology of ρ can be used to define the subsystems, without resorting to orbitals (another non-observable) or extra assumptions. The boundaries of each atom are the "zero-flux surface" surrounding its nucleus. Mathematically, this boundary surface is

$$\{ \vec{r} \mid \nabla\rho \cdot \vec{n} = 0 \} . \tag{2.1}$$

This is the set of all points $\vec{r}$ for which the gradient of the electron density $\nabla\rho$ dotted with the unit vector normal to the surface $\vec{n}$ is zero. This occurs when there is a minimum in the electron density, between two (or more) nuclei. Such a surface defines the volume Ω_k for each nucleus.[2]

The charge q_k within each volume is found by subtracting the sum of the electron density within the volume from the nuclear charge Z_k. Mathematically,

$$q_k = Z_k - \int_{\Omega_k} \rho(\vec{r}) d\vec{r} . \tag{2.2}$$

Practically, this means that the charge of a molecule q_m is the sum of the charges of all its constituent atoms,

$$q_m = \sum_{k}^{M} q_k . \tag{2.3}$$

CT is then the difference between the molecular charge from AIM and the molecular formal charge,

$$q_{CT} = \mid q_{\text{formal}} - q_m \mid . \tag{2.4}$$

2.1.1 Comparison to Other Charge Partitioning Methods

Table 2.1: NaCl CT using different charge partitioning methods with STO's.

Method	q_{ct} (e)
AIM	0.033
MDC-m	0.006
MDC-d	0.074
MDC-q	0.010
Mulliken	0.046
Hirshfeld	0.158
Voroni	0.090

In Table 2.1, different charge partitioning are compared. These CT amounts are for NaCl optimized with M06-2X/ATZP in ADF. Note that ADF uses Slater-type orbitals (STO's).

In Table 2.2, the charge partitioning methods are compared with GTO's. The values are for NaCl at the HF/aug-cc-pvTZ level.

In a study of ionic liquids, Bader charges are 15% larger than ChelpG charges.[4] Szefczyk, Sokalski, and Leszczynski [5] compare partial charges from AIM, ChelpG, and NPA to experimental estimates from nuclear quadrupole coupling. For Lewis acid-base adducts, they find that ChelpG has the lowest percent error (around 15%). AIM has around 50% error (both with cc-pVQZ). However, Zhao, Rogers, and Beck [6] find that ChelpG gives unreasonably large amounts of CT in anion-water clusters. Adding a point dipole to the chloride anion brings the ChelpG calculation closer to the AIM values. Because ChelpG is an ESP-based method, charges for buried atoms, such as the ion in the center of cluster, are not very reliable.[2]

2.2 Dependence on Basis Set

Stone[7] warns against confusing CT with basis set superposition error (BSSE). The use of small basis sets is expected to result in artificially large CT. However, with an infinite basis set, BSSE approaches zero, whereas CT approaches a (non-zero) constant.[8]

Table 2.2: NaCl CT using different charge partitioning methods with GTO's.

Method	q_{ct} (e)
AIM	0.082
MK	0.1497
MK +D	0.1498
MK +AD	0.0944
MK +D + AD	0.0944
ChelpG	0.1591
ChelpG + D	0.1498
ChelpG + AD	0.117
ChelpG + D + AD	0.117

Table 2.3: CT of NaCl convergence with STO basis sets.

basis	distance Å	q_{ct} e
SZ	2.206	0.135
TZP	2.358	0.110
TZ2P	2.358	0.101
ATZP	2.359	0.105
ATZ2P	2.359	0.105
QZ4P	2.359	0.099
ET-QZ3P	2.358	0.104

With STO's, the amount of CT converges at the TZP level when evaluated with M06-2X.

Figure 2.1 compares several different families of GTO's. All the CT values are for NaCl at a distance of 2.93Å at the HF level in NWChem. Pople's 6-31G basis set family includes: 6-31+G*, 6-311++G(2d,2p), 6-31G(3df,3pd), and 6-311++G(3df,3pd). The "+" adds diffuse functions; The asterisk or "(a,b)" are for extra "zeta" basis sets, where a is for heavy atoms, and b is for hydrogens.

The Dunning basis set family includes: cc-pVDZ, cc-pVTZ, cc-pVQZ, cc-pV5Z, cc-pCVDZ, cc-pCVTZ, cc-pCVQZ, cc-pCV5Z, aug-cc-pVDZ, aug-cc-pVTZ, aug-cc-pVQZ, aug-cc-pCVDZ, aug-cc-pCVTZ, and aug-cc-pCVQZ. The "V" is for extra zeta's on the valence electrons only; The "CV" has extra zeta's on the core and valence electrons; "aug" adds diffuse functions.

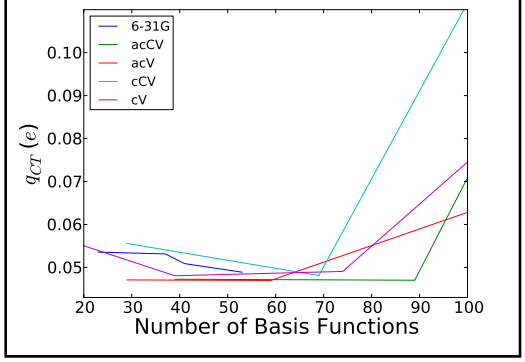

Figure 2.1: CT of NaCl convergence with GTO basis sets.

The amounts of CT are fairly consistent in the range of 50-70 basis functions. The single-zeta basis sets often show more CT than double- and triple-zeta basis sets. The aug-cc-pvDZ and aug-cc-pvTZ sets, which have 29 and 59 basis functions, respectively, are well-converged. A problem arises when more than 70 basis functions are present; in this case, larger amounts of CT are seen again. However, these results are less trustworthy than those with fewer basis functions because the sum of the total electron density is greater than the total number of electrons should be.

Note that the STO's converge well, and summing over their total electron density does not result in extra electrons. Indeed, the STO'S are expected to be more consistent

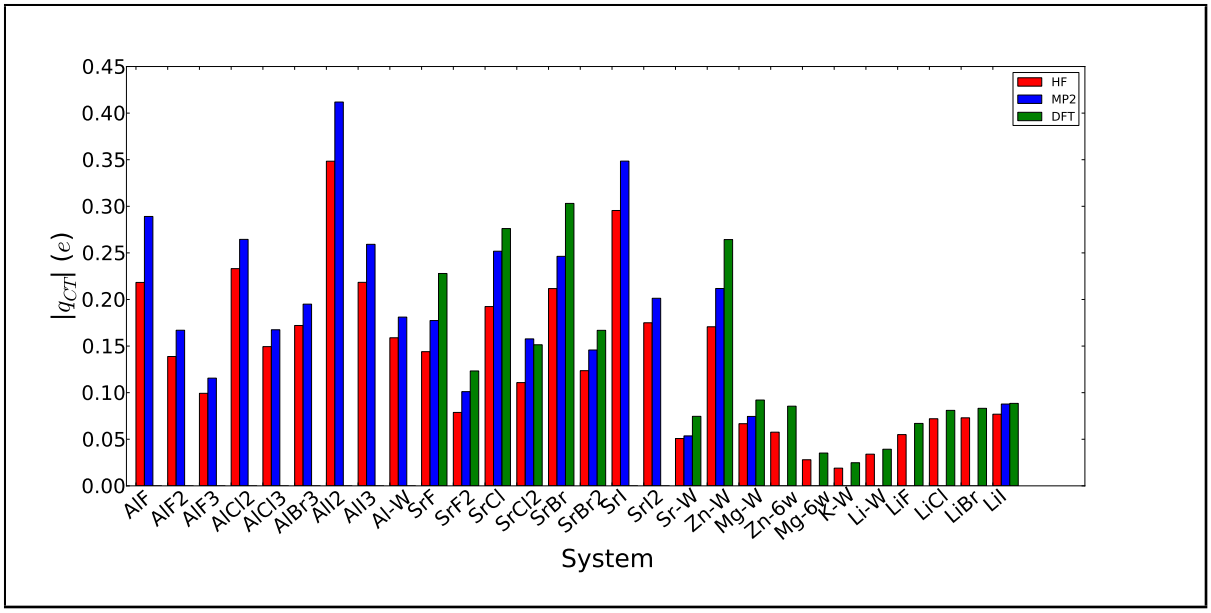

Figure 2.2: Comparison of CT with HF, MP2, and DFT.

in their CT predictions due to their more realistic decay in orbital probability far from the nucleus and better description of the electron density peak near the nucleus. However, efficient implementation of STO's is only available in a single software package to date.[9]

2.3 Dependence on Level of Theory

Table 2.4: CT of NaCl with different density functionals.

DF	distance Å	q_{ct} e
KMLYP	2.342	0.100
M06	2.374	0.103
M06-2X	2.359	0.105
M06-HF	2.376	0.107
TPSSH	2.377	0.114
PBE0	2.367	0.116
CAM-B3LYP	2.363	0.117
B3LYP	2.375	0.123
X3LYP	2.373	0.126
BLYP	2.391	0.142
B3LYP-GD3BJ	2.390	0.148

In Table 2.4, CT from various density functionals is arranged in order from least to most CT. All calculations are done with the ATZP STO in ADF. There is a 0.05e spread in the amounts of CT. No pattern emerges with respect to the "level" of DFT, e.g. GGA vs. hybrid GGA vs. meta-GGA.

As shown in Figure 2.2, CT typically increases in the order of HF $<$ MP2 $<$ DFT. This

is consistent with the known under-polarization of HF, due to lack of electron correlation, and the known over-polarization of DFT, due to self-interaction error.[2] CT from MP2 is 20 ± 8% greater than from HF; CT from DFT is 35 ± 16% greater than from HF. Because MP2 calculations are more computationally expensive, it is important to be able to estimate these values from lower levels of theory. Studies which have compared partial charges from CCSD, CCSD(T), and MP2 generally find no difference between the methods.[10, 11] Similarly, quantum mechanical calculation of polarizability is shown to be most accurate at the MP2/aug-cc-pVTZ level, with no further gain in accuracy when using CCSD.[11]

PBE0 is used for all systems involving Al^{3+} and Sr^{2+}. TPSS is used for all Zn^{2+} and Mg^{2+} systems. M06-2X is used for the remaining systems. The smallest difference between HF and DFT is found with the M06-2X functional; however, it is not clear if this difference is due to the functional or the use of STO basis sets. This is consistent with Table 2.4, in which the M06 family is shown to have lower amounts of CT than other functionals.

2.4 Other Methodological Considerations

The amount of CT depends exponentially on distance, which is depicted in Figure 2.3. This trend is seen for both ion-ion and ion-water pairs. In many cases, the decay is very slow, and so charge is transferred even when the monomers are 5 or more Å away. However, CT at this distance is not relevant to condensed phases. So, in the MD model, CT is cut off at shorter distances than this.

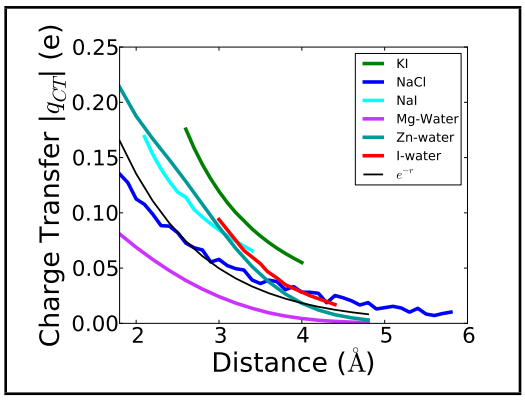

Figure 2.3: CT has an exponential decay with increasing distance.

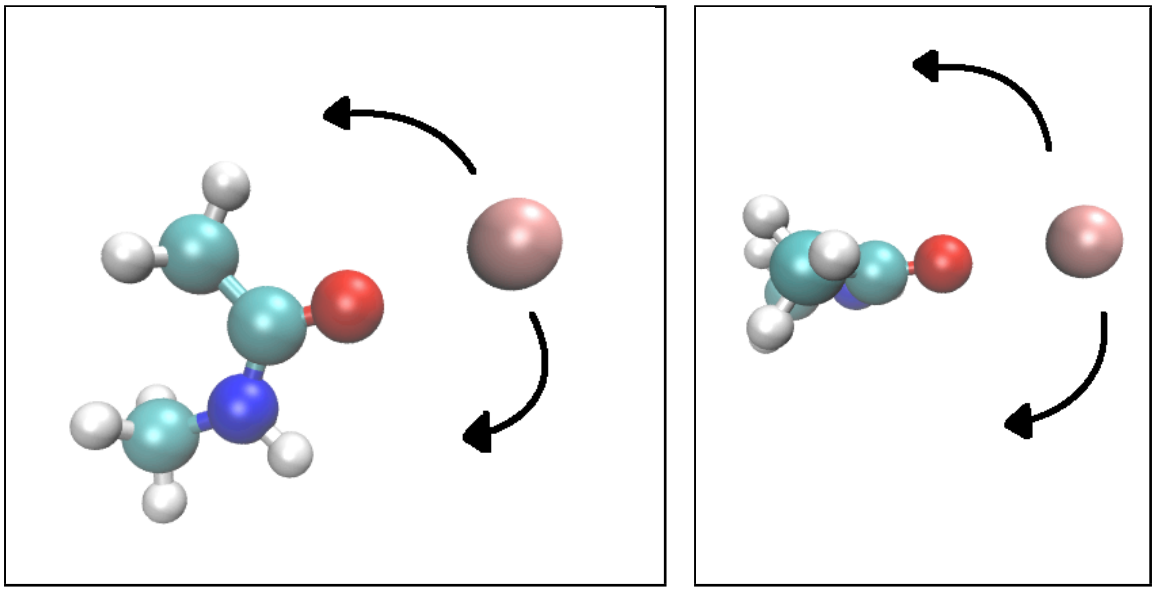

(a) (b)

Figure 2.4: Ion-NMA structures. (a) shows in-plane displacement of the ion. (b) shows out-of-plane displacement of the ion.

In interactions between molecules, the angle can affect the interaction in addition to the distance. How much does the angle affect CT? To determine this, we used a cation coordinated to N-methylacetamide (NMA). Figure 2.4 shows the in- and out-of-plane displacements of the ion. Only the angle varies; the distance is kept constant.

Figure 2.5 compares the CT between sodium and NMA for different distances and angles. The angle is from the carbonyl carbon to the carbonyl oxygen to the ion. The charge of sodium is almost the same despite variation in the angles from -180° to +180°. In contrast, the charge varies greatly with small changes in distance from the carbonyl oxygen to the ion. CT does reach a maximum when the ion is coordinated in the region of the oxygen lone pairs. However, this difference is still minor

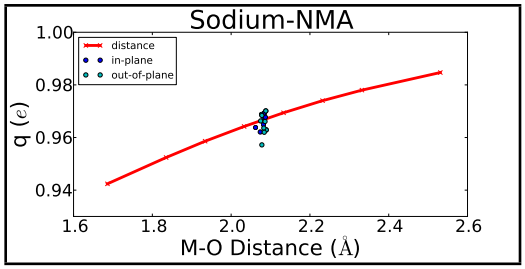

Figure 2.5: CT depends strongly on distance but not on angle.

compared to the distance dependence. Thus, a model that depends only on distances and neglects angles is reasonable from this data.

2.5 CT Data

The following tables show the amounts of CT at the clusters' minimum-energy geometry. Additional CT data can be found in Appendix A.

2.5.1 Monovalent Cations

Table 2.5: Distances in MX alkali-halide dimers in Å.

	F	Cl	Br	I	OH2
Li	1.558	2.020	2.175	2.410	1.815
Na	1.920	2.35	2.506	2.740	2.17
K	2.186	2.71	2.850	3.100	2.67
Rb	2.379	2.886	3.057	3.373	2.840
Cs	2.434	3.009	3.194	3.563	2.953

Table 2.6: Amounts of CT MX alkali-halide dimers in e.

	F	Cl	Br	I	OH2
Li	0.055	0.072	0.073	0.079	0.034
Na	0.057	0.082	0.091	0.100	0.028
K	0.072	0.104	0.130	0.109	0.021
Rb	0.049	0.070	0.081	0.163	0.009
Cs	0.048	0.066	0.074	0.108	0.011

The methods for each cluster are in Table B.1. Additionally, all references relevant to the methods can be found in Appendix B. The alkali-halide dimer distances are listed in Table 2.5, and CT is listed in Table 2.6.

For most of the alkali-halide dimers, q_{CT} increases going down the halide series. This trend is broken with K^+, for which CT from Br^- is maximum and CT from I^- then decreases. Going down the alkali metal ion group, CT increases to K^+, where it reaches a maximum, then decreases further down the group. The exception to this is with the RbI dimer, in which CT from I^- is greater to Rb^+ than to K^+. The CT from water decreases going down the alkali metal ion group, with a minimum for Rb^+.

2.5.2 Divalent Cations

Single counter-ion.

Table 2.7: Distances in $[MX]^+$ alkaline earth-halide dimers in Å.

	F	Cl	Br	I	OH2
Be	1.3260	1.7260	1.8706	2.0712	1.4912
Mg	1.7265	2.1243	2.2727	2.4670	1.9329
Ca	1.8647	2.3128	2.4666	2.6857	2.2200
Sr	1.9920	2.4633	2.6135	2.8997	2.3917
Ba	2.1007	2.5907	2.7508	3.0372	2.5829

Table 2.8: Amounts of CT in $[MX]^+$ alkaline earth-halide dimers in *e*.

	F	Cl	Br	I	OH2
Be	0.1347	0.1936	0.2238	0.2819	0.0957
Mg	0.1090	0.1981	0.2430	0.3187	0.0745
Ca	0.1681	0.2171	0.2367	0.2878	0.0710
Sr	0.1774	0.2518	0.2463	0.3485	0.0536
Ba	0.2962	0.1370	0.3992	0.3287	0.0851

The methods for each cluster with alkaline earth metals are in Table B.2. The distances for alkaline earth-halide dimers are listed in Table 2.7, and CT is listed in Table 2.8.

Again, the amounts of CT tend to increase as one moves down the halide group. However, CT in $[SrCl]^+$ is greater than in $[SrBr]^+$. Additionally, CT is at a minimum for $[BaCl]^+$ in the barium series. Moving down the alkaline earth metal ion group, CT trends are inconsistent for the different halide series. For F^-, CT has a minimum with Mg^{2+}. For Cl^-, CT increases moving down the group, but drops off steeply with Ba^{2+}. CT from Br^- increases down the series except when paired with Ca^{2+}. CT from I^- also increases going down the series, except when paired with Mg^{2+}.

Two counter-ions, i.e. a neutral system.

Table 2.9: Distances in MX_2 alkaline earth-halide trimers in Å.

	F	Cl	Br	I
Be	1.3910	1.8040	1.9550	2.1630
Mg	1.7695	2.1865	2.3354	2.5435
Ca	2.0175	2.4619	2.6125	2.8333
Sr	2.1556	2.6227	2.7762	3.0380
Ba	2.2842	2.7801	2.9375	3.2110

In order to study a neutral system, the divalent cation is paired with two halide anions, placed symmetrically on either side of the cation. The distances for alkaline earth-halide trimers are listed in Table 2.9, and CT is listed in Table 2.10.

Table 2.10: Amounts of CT in MX_2 alkaline earth-halide trimers in *e*.

	F	Cl	Br	I
Be	0.0940	0.1215	0.1313	0.1479
Mg	0.0782	0.1174	0.1328	0.1583
Ca	0.0934	0.1252	0.1374	0.1661
Sr	0.1011	0.1577	0.1458	0.2013
Ba	0.1583	0.0827	0.1473	0.2097

Comparing Table 2.10 and Table 2.8, it is clear that CT per halide ligand is reduced when two halides are present. The trends moving down the halide group are maintained here. CT increases as the halide gets larger, with the exceptions mentioned above continued here for $SrCl_2$, $SrBr_2$, and $BaCl_2$. As for the halides, F^- has the same trend as before, with a minimum in CT for Mg^{2+}. CT from Cl^- does not have a consistent trend. It decreases moving from Be^{2+} to Mg^{2+}, then increases from Mg^{2+} to Ca^{2+} to Sr^{2+}, then decreases drastically from Sr^{2+} to Ba^{2+}. CT from Br^- and I^- increase monotonically moving down the alkaline earth series.

Zinc

Table 2.11 and 2.12 show distances and CT, respectively, for zinc-halide clusters.

Table 2.11: Distances in Zn-X zinc-halide clusters in Å.

n_X	F	Cl	Br	I
1	1.7049	2.068	2.1796	2.3897
2	1.7223	2.111	2.2145	2.4328

Calculations with Cl^- are done in ADF. The optimizations are performed with M06-2X. For one Cl^-, the QZ4P basis set is used; because of computational limita-

tions, the smaller ATZP basis is used for two Cl^-. The CT amounts are from HF-level calculations. Other calculations are done in Gaussian09. The optimizations are done with PBE0, and the CT amounts are from HF. The AIM calculations are done with AIMAll. Zn and I use the ECP's MDF10 and MWB46, respectively, and aug-cc-pvTZ is used for F and Br.

Table 2.12: Amounts of CT in Zn-X zinc-halide clusters in *e*.

n_X	F	Cl	Br	I
1	0.2921	0.519	0.6739	0.9556
2	0.2070	0.327	0.3957	0.5429

CT increases as the halides become larger. Note the large amount of CT for $[ZnI]^+$: the iodide becomes nearly neutral and reduces the zinc charge by half. Such strong CT is reduced when another iodide is added, but charges on iodide ions are half of what is expected based on the ion's formal charge.

2.5.3 Trivalent Cations

Table 2.13: Distances in Al-X aluminum-halide clusters in Å.

n_X	F	Cl	Br	I	OH2
1	1.5813	1.9919	2.1499	2.3561	1.7372
2	1.5955	2.0032	2.1533	2.3628	
3	1.6376	2.0756	2.2354	2.4600	

The trivalent cation Al is also investigated. All clusters are optimized with PBE0 in Gaussian09. The CT amounts are from MP2 calculations, analyzed with AIMAll. The basis sets are: aug-cc-pvTZ for F, Cl, Br, and O; the ECP MWB46 for I; and cc-pvTZ for Al and H.

Table 2.14: Amounts of CT in Al-X aluminum-halide clusters in *e*.

n_X	F	Cl	Br	I	OH2
1	0.2891	0.5848	0.7420	1.0434	0.1811
2	0.1670	0.2645	0.3148	0.4119	
3	0.1156	0.1675	0.1950	0.2592	

Table 2.13 and 2.14 show distances and CT, respectively, for zinc-halide clusters. Again, CT increases moving down the halide series. Furthermore, the amount of CT per halide ligand decreases as more halides are added.

2.5.4 Halide Anions

Dimers are optimized with the M06-2X density functional. The STO basis set is QZ4P, and CT amounts are calculated at the Hartree-Fock level of theory with the Amsterdam Density Functional (ADF) software. [12, 13, 14, 15, 16, 17] For comparison, the optimization is repeated with M06-2X with GTO's. The AIM calculations are based on MP2 single-point energies. The basis sets are: aug-cc-pvDZ for O, F, Cl, and Br; cc-pvDZ for H; and ECP MWB46 for I. The ion-hydrogen distances are larger for the GTO basis sets.

CT follows basically the same pattern for STO's and GTO's, where F^- transfers the most charge, and Cl^-, Br^-, and I^- have nearly the same amount of CT in the ion-water dimers. Iodide is usually expected to have the maximum amount of CT due to its small electron affinity but the ion-water distance is also larger for this ion.[18] The energy of the CT state is lower for fluoride due to its higher homolytic bond dissociation energy (the determinant of relative acidity). [18]

The same basis sets and MP2 are used in the calculations with 6 waters. The clusters are optimized with PBE0. Ion-hydrogen distances increase in the clusters, with a standard deviation of 0.2 Å. Interestingly, the trend for CT reverses in the 6-water clusters, with I^- transferring the most charge per water molecule. This may be due to a smaller difference between r_{i-H} in the dimer and the cluster with I^-. These results contradict those of Ramesh, Re, and Hynes,[19] who find that F^- has the greatest amount of CT in the 6-water clusters. Note that the experimental change in O-H stretch frequency decreases down the halide series.

Table 2.15: Halide-Water CT.

	1 water STO			1 water GTO			6 waters GTO	
Ion	$r_{i-\mathrm{H}}$ Å	$r_{i-\mathrm{O}}$ Å	q_{CT} e	$r_{i-\mathrm{H}}$ Å	$r_{i-\mathrm{O}}$ Å	q_{CT} e	$< r_{i-\mathrm{H}} >$ Å	q_{CT} e
F	1.313	2.398	0.076	1.325	2.408	0.108	1.810	0.023
Cl	2.157	3.114	0.051	2.165	3.118	0.065	2.419	0.031
Br	2.394	3.323	0.048	2.416	3.324	0.061	2.621	0.032
I	2.714	3.583	0.047	2.792	3.601	0.070	2.961	0.037

Bibliography

[1] R. S. Mulliken, J. Chem. Phys. **7**, 20 (1939).

[2] C. J. Cramer, *Essentials of Computational Chemistry: Theories and Models*, John Wiley Sons, Inc., West Sussex, England, 2nd edition, 2004.

[3] R. F. W. Bader, Acc. Chem. Res. **18**, 9 (1985).

[4] J. Schmidt et al., J. Phys. Chem. B **114**, 6150 (2010).

[5] B. Szefczyk, W. A. Sokalski, and J. Leszczynski, J. Chem. Phys. **117**, 6952 (2002).

[6] Z. Zhao, D. M. Rogers, and T. L. Beck, J. Chem. Phys. **132**, 014502 (2010).

[7] A. J. Stone, *The Theory of Intermolecular Forces*, Oxford Univerity Press, USA, 1997.

[8] G. A. Cisneros, M. Karttunen, P. Ren, and C. Sagui, Chem. Rev. **114**, 779 (2014).

[9] *ADF2013*, SCM, Theoretical Chemsitry, Vrije Universiteit, Amsterdam, The Netherlands, 2013.

[10] A. C. Olleta, H. M. Lee, and K. S. Kim, J. Chem. Phys. **126**, 144311 (2007).

[11] A. L. Hickey and C. N. Rowley, J. Phys. Chem. A **118**, 3678 (2014).

[12] Y. Zhao and D. G. Truhlar, Theor. Chem. Acct. **120**, 215 (2008).

[13] F. te Velde et al., J. Comput. Chem. **22**, 931 (2001).

[14] C. Fonseca Guerra, J. G. Snijders, F. te Velde, and E. J. Baerends, Theor. Chem. Acct. **99**, 391 (1998).

[15] E. van Lenthe and E. J. Baerends, J. Comput. Chem. **24**, 1142 (2003).

[16] J. I. Rodriguez et al., Chem. Phys. Lett. **472**, 149 (2009).

[17] J. I. Rodríguez, J. Comput. Chem. **34**, 681 (2013).

[18] W. H. Thompson and J. T. Hynes, J. Am. Chem. Soc. **122**, 6278 (2000).

[19] S. G. Ramesh, S. Re, and J. T. Hynes, J. Phys. Chem. A **112**, 3391 (2008).

Chapter 3

The Model

3.1 The Potential

The model for ions described here expands on the basic model of ions, which includes only charge, dispersion, and repulsion interaction. Multi-body effects are incorporated via polarizability and charge transfer for both ions and water. Polarizability for the ions is treated using the Drude oscillator model.[1, 2] The total energy for the system is described by equation 3.2, below, which includes a Lennard-Jones (LJ) potential for dispersion and repulsion energies, the Coulombic energy between charge sites, the charge transfer (CT) energy, and the polarization energy,

$$U_{total} = U_{LJ} + U_{Coulomb} + U_{CT} + U_{self,Drude} + U_{self,FQ} \tag{3.1}$$

$$\begin{aligned} &= \sum_{i=1}^{N+M-1} \sum_{j<i} \left(4\epsilon \left[\left(\frac{\sigma}{r_{i\gamma j\delta}} \right)^{12} - \left(\frac{\sigma}{r_{i\gamma j\delta}} \right)^{6} \right] + \sum_{\alpha\beta} \frac{q_{i\alpha} q_{j\beta}}{r_{i\alpha j\beta}} S_{ij}(r_{i\alpha j\beta}) \right) \\ &+ \sum_{i=1}^{N+M-1} \sum_{j<i} \left(-\mu_{ij}^{CT} |q_{ij}^{CT}| + \frac{1}{2} \eta_{ij}^{CT} (q_{ij}^{CT})^2 \right) \\ &+ \sum_{m=1}^{M} \frac{1}{2} k_D x_{mD}^2 + \sum_{l=1}^{N} \left(\sum_{\alpha} \tilde{\chi}_{\alpha}^{0} q_{l\alpha} + \frac{1}{2} \sum_{\alpha} \sum_{\beta} q_{l\alpha} q_{l\beta} J_{\alpha\beta}(r_{l\alpha l\beta}) - E_l^{gp} \right), \end{aligned} \tag{3.2}$$

where N is the total number of water molecules, and M is the number of ions. The indices i and j denote separate particles, either ions or water. The indices γ and δ denote the LJ interaction sites, which are located at ion centers and on the oxygen atom of the water molecules. The indices α and β denote charge sites, either atom sites on water, ion centers, or Drude charge sites. In the Drude model, both the monopole and dipole intermolecular interactions are handled in the normal Coulomb summation. Sums over m are over ions only, and sums over l are over waters only. Distances between charge sites are given by $r_{i\alpha j\beta}$.

The electrostatic interactions are damped using the function S_{ij}, which acts only at short range and does not disturb the long-range interactions. We use the full gas-phase polarizability for all ions with Thole-type damping, suggested by the work of Masia, Probst, and Rey.[3, 4] The damping is applied to all electrostatic interactions of ions (mono- and dipole) via equation 3.3,

$$S_{ij} = 1 - \left(1 + \frac{r_{ij}}{2a_{ij}}\right) e^{-r_{ij}/a_{ij}}, \tag{3.3}$$

where a_{ij} is a user-defined constant, which controls the strength of damping. As in previous work, [5, 6] we set $S_{ij} = 1$ for water-water interactions. Previous work using the TIP4P-FQ model with a Drude model for chloride also damped all electrostatic interactions. We find, like Stuart and Berne, that using an unscreened Coulombic interaction between the ions and water leads to poor prediction of many properties, including the water structure around the ion.[1]

In the charge transfer part of the equation for the total energy (Equation 3.2, above), the negative of the Mulliken electronegativity, μ_{ij}^{CT}, represents the tendency of an atom to attract electrons in intermolecular CT. The hardness, η_{ij}^{CT}, represents the atoms' resistance to losing electrons in intermolecular CT.[5] The charge-transfer energy, which contains these two parameters, partially compensates for the loss of electrostatic energy upon charge transfer. The amount of charge transferred, q_{CT}, which depends on the pair type

and the distance, is given by the switching function,

$$q_{CT} = \begin{cases} Q_{ij}^{CT} & \text{if } r_{ij} < R_1^{CT}, \\ \frac{1}{2}Q_{ij}^{CT}[1 + \cos(\pi \frac{r_{ij} - R_1^{CT}}{R_2^{CT} - R_1^{CT}})] & \text{if } R_1^{CT} \leq r_{ij} \leq R_2^{CT}, \\ 0 & \text{if } r_{ij} > R_2^{CT}, \end{cases} \tag{3.4}$$

where Q_{ij}^{CT} is the maximum amount of CT for each pair and depends on the pair type. The distances R_1^{CT} and R_2^{CT} define where the switching function starts and ends, respectively, for each pair type. In our potential, CT is treated in a purely distance-dependent fashion. Charges of solvated ions are not required to be integers and water molecules can become charged, either through charge transfer with ions or other water molecules.[6] Assigning a maximum amount of charge transfer, Q^{CT}, prevents q_{CT} from becoming extremely large at short distances. The combination of R_1, R_2, and Q_{CT} are chosen so that $q_{CT}^{MD} = q_{CT}^{QM}$ at the equilibrium separation of the dimers. As the distance increases, the switching function ensures a smooth approach to zero and prevents long-range CT. It also prevents the CT model from becoming conductive. The switching function is the same as that used for TIP4P-FQ+DCT and was chosen to be consistent with that model.

In the Drude model, the dipole-dipole and dipole-charge interactions are handled in the Coulomb sums. The Drude model has an additional energy contribution based on the polarizability of the ion, denoted at $U_{self,Drude}$ in Equation 1, above. The displacement of the Drude oscillator from equilibrium is x_{mD}. The Drude spring constant k_D was set to 1000 kcal/mol/Å^2, and the Drude charge q_D is determined by the equation

$$q_D = -\sqrt{ak_D}, \tag{3.5}$$

where a is the polarizability. This is the same method used by Yu *et al.*[2] Drude oscillators avoid the instabilities in point-inducible dipoles, and long-range effects are easily incorporated into Ewald sums.

The remaining terms are related to the polarizability of the water, which is handled by the fluctuating charge (FQ) method.[5, 6] The parameters χ_a^0 and $J_{a\beta}$ correspond to μ_{ij}^{CT} and η_{ij}^{CT}, respectively, but here refer to intramolecular charge transfer. The intramolecular charge interactions are described by the Coulomb overlap integral

$$J_{a\beta}(r_{la l\beta}) = \int dr_{la} dr_{l\beta} |\phi_{n_a}(r_{la})|^2 \frac{1}{|r_{la} - r_{l\beta} - r|} |\phi_{n_\beta}(r_{l\beta})|^2 \tag{3.6}$$

of Slater functions

$$\phi_a(r) = A_{n_a} r^{n_a - 1} e^{-\zeta_a r}, \tag{3.7}$$

where A_{n_a} is a normalization constant, n_a is the principal quantum number of charge site a, and ζ_a is considered an adjustable parameter.

The last line of Equation 2 (part of $U_{self,FQ}$) constrains the total charge of the system to remain constant. The term λ_l is an undetermined multiplier for the charge constraint, and Q_t^l is the total charge on a water molecule, as determined by the total amount of charge transfer to and from the ions and other water molecules.

3.2 Parameterization

The adjustable parameters in this model are:

i. LJ parameters for each ion (well-depth, ϵ, and LJ equilibrium distance, σ),

ii. CT energy parameters between each pair (chemical potential, μ^{CT}, and hardness, η^{CT}),

iii. CT cut-off distances for each pair(R_1^{CT} and R_2^{CT}),

iv. amount of charge transfer for each pair (Q_{CT}),

v. Drude charge for each ion (q_D), and

vi. the damping constant for pairs (a_{ij}).

Each ion has a single Drude charge parameter and a single set of Lennard-Jones parameters. The Lennard-Jones interactions between unlike atoms use parameters from the Lorentz-Berthelot combining rules. Charge is transferred from the ion center, so the Drude charge is not affected by CT. The charge transfer parameter, Q_{CT}, and the cut-off parameters are chosen to best fit the switching function to our electronic structure calculations.

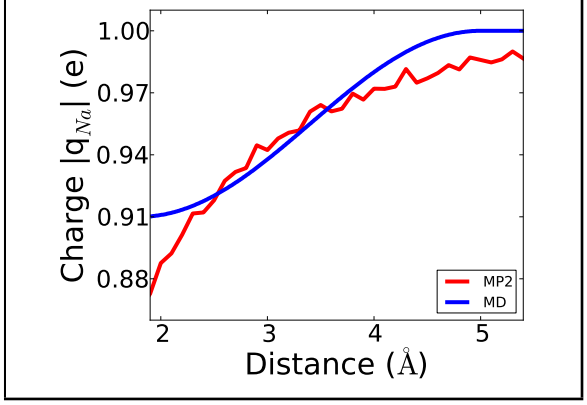

Figure 3.1: Comparison of the Ion Charge from the QM Calculations to the MD Switching Function. The curves pictured are for NaCl; the other dimers are qualitatively similar. The red diamonds show the absolute value of QTAIM ion charges, which were calculated at intervals of 0.1Å. The blue line represents absolute values of charges of the ions from our switching function.

For ion-water interactions, the damping constant, a_{ij}, is chosen as the minimum amount needed to prevent over-polarization. The remaining parameters (ϵ, σ, μ^{CT}, η^{CT}) are adjusted to fit the dimer and aqueous properties. The parameters used in the simulations are listed in Tables 3.1 and 3.2.

Ion-water parameters are fit with respect to:

i. dimer energy minimum,

ii. distance at the energy minimum of dimer,

iii. amount of charge transfer at the dimer minimum,

iv. location of the first maximum and first minimum of the radial distribution function, and

v. the average dipole in the liquid phase (for chloride).

The height of $g(r)$ at the maximum and minimum and single-ion hydration free energies were also considered in order to differentiate between parameter sets that had very similar aqueous structure otherwise.

Once parameters were established for the ion-water interactions, additional parameters for the ion-ion interactions were determined using only the properties of the ion dimers. For ion-ion interactions, the damping constant, a_{ij}, is chosen so that the dipole moment of the ion pair is in agreement with experiment.

3.2.1 Automated Parameter Optimization

The parameterization of a model with so many parameters is complex. It is possible to automate the search of parameter space for the optimal parameter set. For this, we use the downhill simplex optimization method (SOP) of Nelder and Mead.[7][8] (Note that this method is totally unrelated to the simplex method of linear programming.) The advantage of SOP is that it does not use derivatives and so is faster than many other optimization methods.

A simplex is a geometrical object which has $N + 1$ vertices in N-dimensional space. Here, N is the number of parameters which need to be optimized. We take $N + 1$ initial guesses at the N parameters; we use each of these guesses in the calculation of dimer and aqueous properties. We have target properties for the dimer from *ab initio* calculations and experiment. We define a difference function, m,

$$m = \sum_i w_i^2 (p_{\mathrm{calc},i} - p_{\mathrm{target},i})^2 \ , \tag{3.8}$$

where w is the weight for each property p_i.

We then attempt to minimized the difference function, which occurs when the calculated and target properties are the same. Basically, the vertices except the one with the largest difference define a polygon. A vector is calculated from the vertex with the largest merit to the center of the polygon. In a "conservation" step, the vector is doubled

Table 3.1: Lennard-Jones and Drude Parameters. The Lennard-Jones well-depth, ϵ, and distance, σ, for interactions of ions with water are listed. The Drude charge and polarizabilities of ions are shown. Also included are the Lennard-Jones parameters for the TIP4P-FQ+DCT water model.[6] LJ parameters for ion-ion interactions are determined by Lorentz-Berthelot rules.

	ϵ	σ	q_D	a
	kcal/mol	Å	e	Å^3
Na^+	0.0407	2.320	-0.687597	0.157
K^+	0.0497	3.030	-1.580968	0.830
Cl^-	0.1490	3.720	-4.062989	5.482
I^-	0.1854	4.695	-5.562578	10.275
H_2O	0.2633	3.171		

so that the new vertex is a reflection of the largest-difference vertex. There could also be an "expansion" step, in which the vector is tripled, or a "contraction" step in which the vector is halved. The new vertex is used to calculate dimer and aqueous properties. Then the steps are repeated until the difference function converges to a minimum.[9]

While SOP is an elegant solution for quick optimization, it is in essence a trial and error method. Especially when exploring a rough merit function surface, there is no guarantee that the absolute minimum will be found. Indeed, the merit function surface is extremely rough; changes in the fifth decimal place of parameters can result in changes in merit in the first decimal place. However, SOP remains a useful method to find good regions of parameter space quickly, and the merit function helps to quantify small differences in aqueous properties.

3.3 Currently Available Parameter Sets

Tables 3.1 and 3.2 show the parameters for all members in our CT model to date.

3.3.1 Quantum Calculations and Dimer Properties

The equilibrium dimer distance and charge transfer at equilibrium are shown in Table 3.3, where these values are compared to experiment and to other *ab initio* calcula-

Table 3.2: Charge Transfer Parameters. The maximum amount of CT, the CT cut-offs, and the energy parameters are listed for each pair. The damping for each pair is also shown.

Pair	Q_{CT} e	r_{CT1} Å	r_{CT2} Å	μ_{CT} kcal/mol/e	η_{CT} kcal/mol/e^2	a Å
Na^+ - H_2O	0.033	1.7	3.3	275.33	1602.6	0.10
K^+ - H_2O	0.024	2.0	3.7	304.57	6306.7	0.10
Cl^- - H_2O	0.057	1.9	3.1	95.51	995.8	0.60
I^- - H_2O	0.075	2.0	3.6	26.80	-896.2	0.66
NaCl	0.090	1.8	5.0	535.35	232.4	1.175
KCl	0.085	2.0	5.5	468.63	663.9	1.164

tions. The binding energies and distance at equilibrium agree with experiment, though MP2 results in distances slightly longer than those from experiment. Figure 3.2 compares QM calculations to our CT (MD) model (Equation 3.4). From the QM calculations, the amount of charge transferred is found to be distance-dependent, as shown in Figure 3.2. This compares well with previous studies.[10, 11]

The NaCl dimer has a dipole moment equal to 9.0 Debye,[12] and the dimer bond distance is 2.36 Å.[13] Assigning the ions charge of plus or minus one would give the pair a dipole moment equal to 11.3 Debye. Our model transfers 0.083 e of charge from Cl^- to Na^+, which reduces the dipole moment to 10.4 Debye. Choosing a_{ij} equal to 1.175 Å gives induced dipoles of 1.42 Debye for Cl^- and 0.04 Debye for Na^+, reducing the total dipole to 9.0 Debye. A similar effect is found for KCl, where the charge transfer and polarizability both reduce the dipole of the pair.

Trimers

Figure 3.3.1 shows the direction of CT between water, anions, and cations. Charge is transferred from an anion to water or a cation. A cation will accept charge from a water, and the hydrogen bond acceptor donates electron density to the hydrogen bond donor.

Table 3.4 shows the charge of an ion and two waters arranged as in Figure 3.3.1. The water that is further from the cation, and only hydrogen bonded to the first water, has

Table 3.3: Dimer Properties. The results of the present MD model are compared with quantum mechanical calculations. Experimental results for E_{min} and r_{min} are given in the second row in the middle columns. Note that Q^{CT} in Table 3.2 is greater than q^{CT} here because the equilibrium distances are within the range of the switching function in Equation 3.4 (*i.e.* $r_{eq} > R_{CT1}$).

Pair		E_{min} kcal/mol	r_{min} Å	q_{CT} e	Reference
Na^+ - H_2O	MD	-23.72	2.25	0.024	
	QM		2.17	0.028	
	Exp.	-24.0	2.26		[14]
K^+ - H_2O	MD	-17.82	2.60	0.024	
	QM		2.67	0.021	
	Exp.	-17.9	2.60		[14]
Cl^- - H_2O	MD	-20.30	2.95	0.056	
	QM		3.08	0.069	
	QM	-13.6	3.09		[15]
I^- - H_2O	MD	-13.52	3.40	0.061	
	QM		3.583	0.047	
	QM	-10.5			[16]
NaCl	MD	-128.98	2.37	0.083	
	QM		2.35	0.082	
	QM	-131.9	2.36		[17]
KCl	MD	-117.39	2.70	0.083	
	QM		2.71	0.104	
	QM	-115.8	2.67		[17]

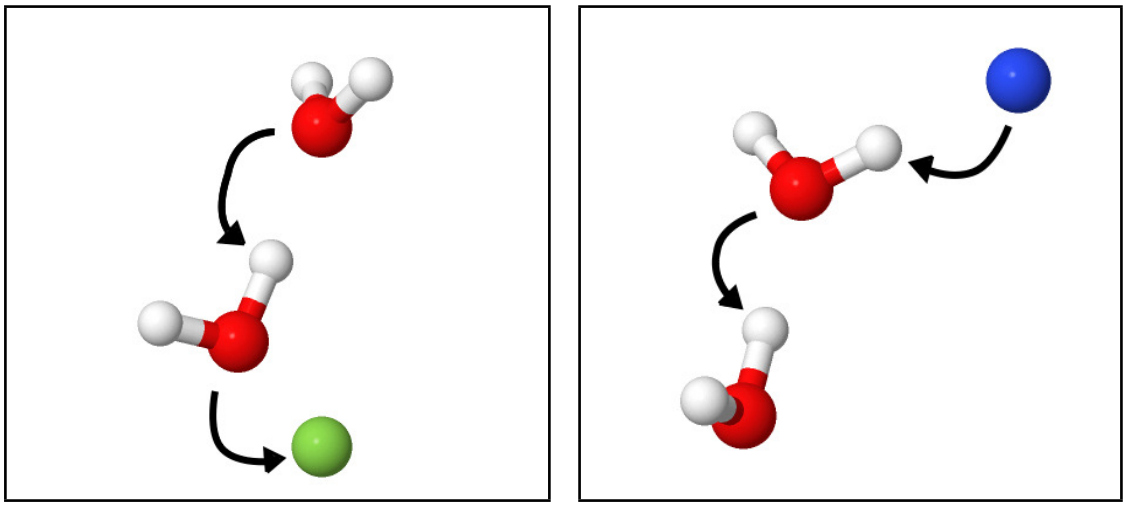

(a) (b)

Figure 3.2: Direction of Charge Transfer. a) The cation receives charge from the first shell water, which in turn receives charge from the second shell water. b) The anion transfers charge to the first shell water, which donates charge to the second shell water.

Table 3.4: Trimers of Ions with Two Waters. The charges of ions and waters in ion-water-water trimers, arranged as depicted in Figure 3.3.1, are listed. Units are in *e*.

Charge of:	Ion	Closest Water	Second Water
Na^+	+0.9717	+0.0001	+0.0276
K^+	+0.9881	-0.0081	+0.0201
Cl^-	-0.9451	-0.0344	-0.0205

the same charge that would be expected if only the waters were present. This indicates that the ion does not affect CT between water molecules that it is not directly coordinated to.

3.3.2 Equilibrium Aqueous Structure

The structural properties of charge transfer ions in water are listed in Table 3.5 and are illustrated in Figure 3.3.2. The cations are parameterized to have radial distribution functions (RDF) consistent with Tongraar, Liedl, and Rode.[18] The current best theoretical estimates for coordination numbers of alkali metals are from Varma and Rempe.[19] The

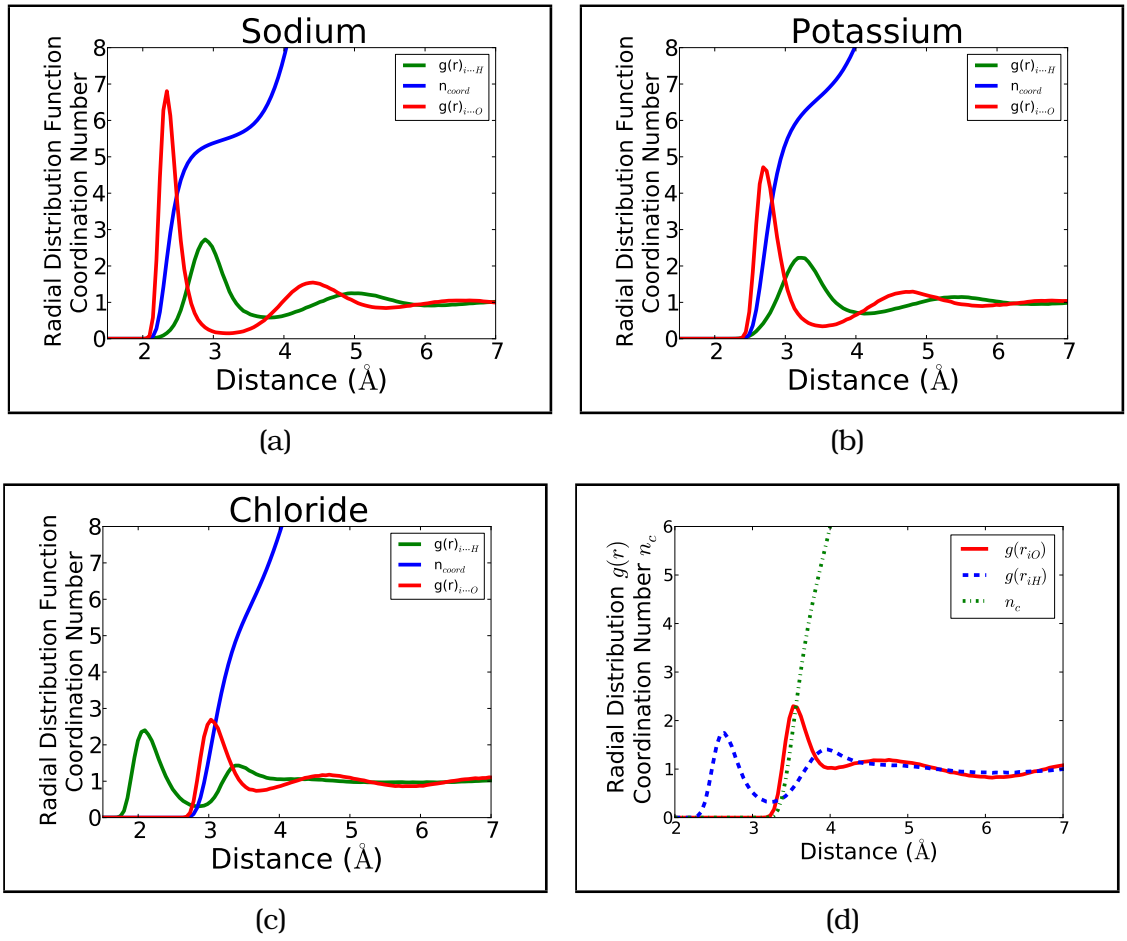

Figure 3.3: Radial Distribution Functions.

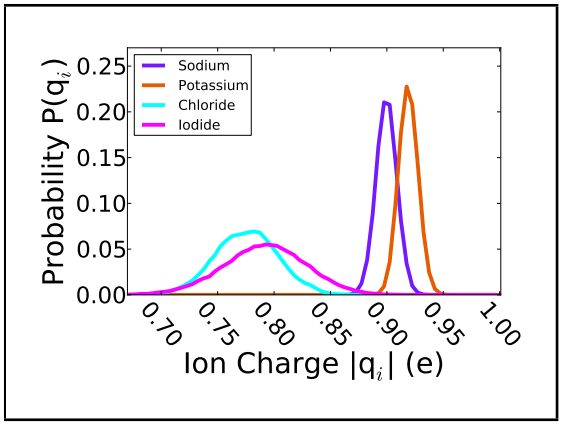

Figure 3.4: Ionic Charge Distributions.

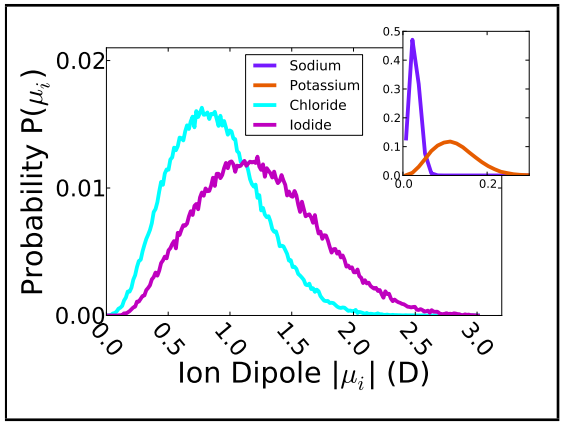

Figure 3.5: Ionic Dipole Distributions.

alkali metals, Na^+ and K^+, are strongly coordinated by four water molecules. As the atomic number increases, loosely coordinated waters are added– one for Na^+ and two for K^+. Thus the total hydration numbers are 5 for Na^+ and 6 for K^+.[19] Our coordination number is determined by integration of the ion-water oxygen radial distribution function to the first minimum. Compared to Varma and Rempe, our coordination number of 5.5 for Na^+ is acceptable, but our coordination number of 6.7 for K^+ is high. Our results are also similar to the results for the polarizable Drude model of Yu *et al.*,[2] but the coordination number for K^+ is smaller than the QM/MM results of Tongraar, Liedl, and Rode.[18] The chloride ion is parameterized to have a coordination number near 6, as is indicated experimentally.[20] Our result of 6.4 is higher than that of Zhao, Rogers, and Beck, who report an average coordination number of 5.9 for chloride, using the polarizable AMOEBA model.[21]

The charge distributions of the ions from our MD simulations are shown in Figure 3.4. Our charge distributions are supported by electronic structure calculations of ions with their first solvation shell. Zhao, Rogers, and Beck find that chloride transfers 0.03-0.05 electrons to each water in its solvation shell, resulting in a total charge of about −0.8 e for chloride.[21] Using Car-Parrinello MD, dal Peraro *el al.* find that Cl^- transfers 0.26 e to water, making the chloride charge −0.74 e.[22] Our average chloride charge is

−0.775 e. Varma and Rempe find a charge near 0.9 e for both sodium and potassium, when coordinated to six waters.[23] Our average values of 0.900 and 0.919 e (for Na^+ and K^+, respectively) are close to their values, as well as those of dal Peraro *et al.* (0.88 e for Na^+ and 0.87 e for K^+). The cations show a sharp peak in their probability distributions. The broader peak in the chloride charge distribution is due to greater CT and thereby greater sensitivity to fluctuations as compared to the cations. The distribution of the ion dipoles is shown in Figure 3.5. The dipole moments of waters around the ions are also reduced comported to bulk waters' dipoles, consistent with *ab initio* MD of the chloride ion.[21, 24]

The average ionic dipole of the iodide model is the same as that calculated by *ab initio* methods.[24, 25] Because a charge transfer (CT) model is used, the iodide charge varies, due to solvent fluctuations around the ion. The waters around the ion also have different charges from what is found in bulk. The average charge and dipole of a water in the first solvation shell are listed in Table 3.5. An attempt to create an iodide model with reduced polarizability (50% of the gas-phase polarizability based on Ref. [26]) was unsuccessful. The reduced polarizability model could not produce a dipole and a RDF consistent with AIMD simultaneously.

Table 3.5: Equilibrium Properties of Single Ions in Water. The radial distribution function is described by r_{max}, g_{max}, r_{min}, and g_{min}. The average coordination number is n_{coord}. The average charge and dipole of the ion are $< q_{ion} >$ and $< \mu_{ion} >$, respectively. The average charge and dipole of the waters of the first solvation shell are also listed as $< q_{shell} >$ and $< \mu_{shell} >$, respectively.

Ion	r_{max} Å	g_{max}	r_{min} Å	g_{min}	n_{coord}	$< q_{ion} >$ e	$< \mu_{ion} >$ D	$< q_{shell} >$ e	$< \mu_{shell} >$ D	Ref.
Na^+	2.34	6.81	3.23	0.15	5.5	0.900	0.028	-0.009	2.57	
	2.33	5.5	3.0	0.5	5.6					[18]
	2.38	7.42	3.24	0.20	5.6	1		0		[2]
K^+	2.68	4.71	3.52	0.34	6.7	0.919	0.122	-0.010	2.51	
	2.81	3.4	3.7	0.6	8.3					[18]
	2.74	4.80	3.56	0.45	6.9	1		0		[2]
Cl^-	3.03	2.69	3.72	0.74	6.4	-0.775	0.888	-0.019	2.54	
	3.2	3.1	4.0	0.9	5.9	-0.8	0.6		2.5	[21]
	3.16	3.15	3.78	0.72	6.5	-1		0		[2]
I^-	3.52	2.30	4.07	1.02	6.5	-0.792	1.23	-0.022	2.47	
	3.58	2.55	4.20	0.72	6.0		1.3			[25]

Bibliography

[1] S. J. Stuart and B. J. Berne, J. Phys. Chem. **100**, 11934 (1996).

[2] H. Yu et al., J. Chem. Theor. Comput. **6**, 774 (2010).

[3] M. Masia, M. Probst, and R. Rey, Chem. Phys. Lett. **420**, 267 (2006).

[4] M. Masia, M. Probst, and R. Rey, J. Chem. Phys. **123**, 164505 (2005).

[5] S. W. Rick, S. J. Stuart, and B. J. Berne, J. Chem. Phys. **101**, 6141 (1994).

[6] A. J. Lee and S. W. Rick, J. Chem. Phys. **134**, 184507 (2011).

[7] J. A. Nelder and R. Mead, Comput. J. **7**, 308 (1965).

[8] J. A. Nelder and R. Mead, Comput. J. **8**, 27 (1965).

[9] W. H. Press, B. P. Flannery, S. A. Teukolsky, and W. T. Vetterling, *Numerical Recipes: The Art of Scientific Computing*, Cambridge Univeristy Press, 1986.

[10] O. Gálvez, P. C. Gómez, and L. F. Pacios, J. Chem. Phys. **115**, 11166 (2001).

[11] L. Belpassi et al., J. Am. Chem. Soc. **132**, 13046 (2010).

[12] P. Vimalchand, M. D. Donohue, and I. Celmins, ACS Syposium Series **300**, 297 (1986).

[13] A. A. Radzig and B. M. Smirnov, *Reference Data on Atoms, Molecules, and Ions*, Springer, Berlin, 1985.

[14] I. Dzidic and P. Kebarle, J. Phys. Chem. **74**, 1466 (1970).

[15] J. Kim, H. M. Lee, S. B. Suh, D. Majumdar, and K. S. Kim, J. Chem. Phys. **113**, 5259 (2000).

[16] A. Tongraar, S. Hannongbua, and B. M. Rode, J. Phys. Chem. A **114**, 4334 (2010).

[17] Y. Wang, P. Nordlander, and N. H. Tolk, J. Chem. Phys. **89**, 4163 (1988).

[18] A. Tongraar, K. R. Liedl, and B. M. Rode, J. Phys. Chem. A **102**, 10340 (1998).

[19] S. Varma and S. B. Rempe, Biophys. Chem. **124**, 192 (2006).

[20] S. Cummings et al., Nature **287**, 714 (1980).

[21] Z. Zhao, D. M. Rogers, and T. L. Beck, J. Chem. Phys. **132**, 014502 (2010).

[22] M. Dal Peraro, S. Raugei, P. Carloni, and M. L. Klein, ChemPhysChem **6**, 1715 (2005).

[23] S. Varma and S. B. Rempe, Biophys. J. **99**, 3394 (2010).

[24] E. Guàrdia, I. Skarmoutsos, and M. Masia, J. Chem. Theor. Comput. **5**, 1449 (2009).

[25] J. L. Fulton et al., J. Phys. Chem. B **114**, 12926 (2010).

[26] B. A. Bauer, T. R. Lucas, A. Krishtal, C. Van Alsenoy, and S. Patel, J. Phys. Chem. A **114**, 8984 (2010).

Chapter 4

Single Ions in Bulk Water

4.1 Introduction

A common method to validate ion models is to test their aqueous single-ion properties. This allows us to confirm that each ion model is working properly before combining the ion model with other solutes. Though experiment can only access aqueous properties of whole salts, much work has gone into separating out the effects of individual constituents of the salts.[1] For instance, the hydration free energies and diffusion constants of single ions are currently agreed upon. These values are calculated for the ion models listed in Chapter 3. Additionally, the differences between CT and non-CT models for ions are explored.

4.2 Methods

Calculations of thermodynamic properties were done using a system of a single ion with 256 water molecules in the TPN ensemble with periodic boundary conditions, using our own code. All simulations used the TIP4P-FQ+DCT water model.[2] This model is polarizable using the fluctuating charge scheme, as discussed in the original work by Rick, Stuart, and Berne.[3] The temperature is kept at 298 K using a Nosé-Hoover thermostat, and the pressure is kept at 1 atm using an Anderson barostat.[4] The charge equilibration for the fluctuating charges is handled via an extended Lagrangian approach

[3] using charge normal modes.[2, 5] The Drude variables are given a mass equal to 0.4 amu, which is subtracted from the mass of the ion center. The positions of the ion are propagated as described by Lamoureux and Roux.[6] The simulations use a 1 fs time step and Ewald summation for the long-range electrostatics.[4] The bonds were constrained using the SHAKE algorithm.[4] The charge degrees of freedom (Drude and charges on atom sites of water) were kept at 1 K. The diffusion constants were determined using the Stokes-Einstein equation. Diffusion simulations of single ions were performed in the EVN ensemble using systems of 256, 512, and 1024 waters, to check for system-size dependence.

Free energies are calculated relative to the hydration free energy values calculated by Warren and Patel for a non-polarizable ion in TIP4P-FQ.[7] (We used Set A of their ion parameter sets.) Warren and Patel applied several corrections to their absolute hydration free energies which allowed for calculation of real hydration free energies.[7] Therefore, our results are also real hydration free energies. Free energy perturbation theory is performed in which the ions from Warren and Patel are morphed into our ions, and the water is morphed from TIP4P-FQ [3] to TIP4P-FQ+DCT. The transition is done in twenty steps, with 50 ps of simulation time for each step. Double-wide sampling is used. Free energy calculations for neutral ion pairs are also performed, using thermodynamic integration in 16 steps, with 500 ps of simulation time for each. Both the single-ion and ion-pair simulations include 512 water molecules.

4.3 Results

4.3.1 Charge of Solvating Water Molecules

Water in the first solvation shell has a partial negative charge for both cations and anions (see Table 3.5 and Figure 4.3.1). This result is explained by the arrangement of waters in the second solvation shell (Figure 3.3.1). A first solvation shell water donates negative charge to the cation, which would give it a partial positive charge in a gas-

phase dimer. In aqueous phase, the waters of the first solvation shell also accept charge from waters in the second solvation shell. Because the first shell water can donate two hydrogen bonds but accept only one hydrogen bond while bound to the cation, the charge accepted from the second shell is greater than the charge donated, resulting in an overall negative partial charge. The negative charge of the first solvation shell is compensated by a slight positive charge spread over the second solvation shell, indicating that members of the second shell must accept slightly more hydrogen bonds than they donate. (The charge transfer between water molecules is solely determined from the hydrogen bond arrangement.)

In the case of chloride, the anion is donating charge to the waters in the first solvation shell, and the waters in the first solvation shell are donating charge to waters in the second solvation shell. The amount of charge transfer between the waters is not sufficient to compensate for the charge transferred from the ion, so the first solvation shell retains a negative charge. Dal Peraro *et al.* find that waters in the first solvation shell around Cl^- or K^+ have a negative charge of a magnitude close to our results and that the second solvation shell of K^+ has a small positive charge.[8]

The picture of the charge distribution among water, described above, is supported by quantum calculations on trimers (Table 3.4 and Figure 3.3.1). In the QTAIM calculations on geometry optimized trimers the water closest to the ion has a charge close to zero or negative in all cases. So, the first solvation shell water has a charge imbalance similar to that predicted by the MD CT model. The amount of charge transferred between the water molecules is 0.02 e for potassium and chloride. The value 0.02 e is consistent with QM calculations on water dimers at the same distance.[9] For sodium, the distance between the waters is smaller in the optimized structure, and so the charge transfer is greater.

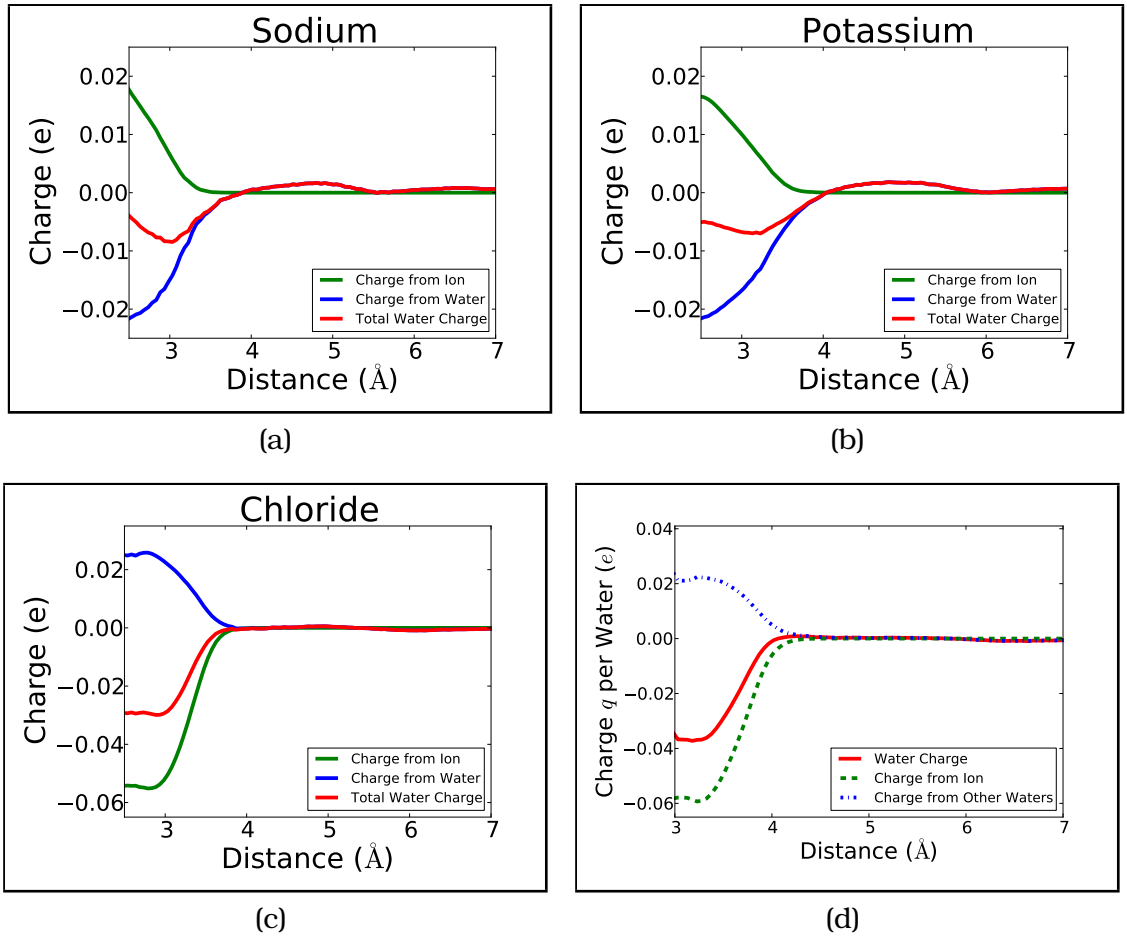

Figure 4.1: The Charge of Water Near the Ion. The distribution of charge in the solvation shells near each ion are shown. The charge gained from the ion is shown in green. The charge gained from other waters is shown in blue. The red line shows the total charge of the water molecules, based on their distance from the ion. The distances less than those at the onset of the ion-oxygen RDF are not shown.

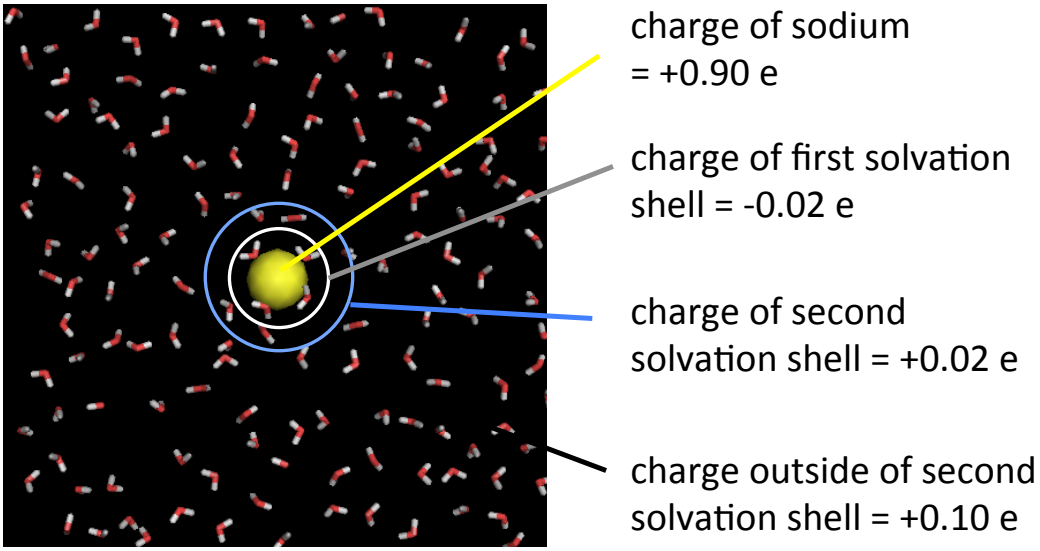

Figure 4.2: Some charge from the ion resides in the bulk water.

Single Ions Alter Water Charges in Bulk.

As shown in Figure 4.3.1, the waters of the first solvation shell have a negative charge, as was seen for both cations and anions in previous work.[8, 10, 11] Anions donate charge to their first solvation shell, making it negative. Those waters then donate charge to waters of the second shell, reducing the magnitude of their charge of the first shell from what is seen in small gas-phase anion-water clusters.[10] Cations receive charge from their first shell waters. However, second solvation shell waters donate more charge to the first shell than what is lost. And so the first shell of cations is also negative. Table 4.1 shows the total charge of the first and second solvation shells for Na^+, K^+, Cl^-, and I^- in bulk water.

Even out to the second solvation shell, the total charge ($\pm 1e$) has not been recovered, leaving $< q_{\text{left-over}} > \approx \pm 0.1e$ in the bulk water. Because the charge of water is based on its hydrogen bonding pattern, charged bulk water indicates that ions' effect on

Table 4.1: Charges of the ion ($< q_{\text{ion}} >$), its first solvation shell ($< q_{\text{1ss}} >$), its second solvation shell ($< q_{\text{2ss}} >$), and the remaining charge in bulk water ($< q_{\text{left-over}} >$). Charges are in units of e.

Ion	$< q_{\text{ion}} >$	$< q_{\text{1ss}} >$	$< q_{\text{2ss}} >$	$< q_{\text{left-over}} >$
Na^+	+0.900	-0.017	+0.017	+0.100
K^+	+0.919	-0.040	+0.022	+0.098
Cl^-	-0.775	-0.124	+0.001	-0.102
I^-	-0.791	-0.108	-0.031	-0.070

water structure is long-ranged in nature. Such long-ranged behavior is consistent with the results of Irudayam and Henchman.[12] Because (negative) charge is transferred from the hydrogen bond acceptor to the hydrogen bond donor, the $-0.1e$ of left-over charge in the anion simulations indicates an excess of hydrogen bond acceptors over donors. For cations, $+0.1e$ is left, and so there are excess hydrogen bond donors.

4.3.2 Asymmetry in the Solvation Shell of Anions

The solvation shell can be defined as all atoms that are within the first minimum of the ion-oxygen pair correlation function. For ions such as sodium, all oxygens in the first solvation shell are about the same distance from the ion. In contrast, several groups have reported that the first solvation shell around the chloride ion is asymmetric, both in clusters and in bulk solution.[13, 14, 15, 16] Asymmetry has been proposed to be a driving force for attraction of anions to the liquid-vapor interface.[15] Since non-polarizable models do not reflect experimental concentrations of anions at the liquid-vapor interface [17] and asymmetry decreases when polarizability decreases,[13] asymmetry has been attributed to the polarizability. The average of the positions of the oxygen atoms in the first solvation shell can be used to define the center of the first solvation shell. The difference between the average of the oxygens' positions and the position of the ion can be used to determine the degree of anisotropy of the first solvation shell.

We find a slight anisotropy in the chloride solvation, whereas the cations have more symmetric hydration shells (Figure 4.3.2). We find that charge transfer has a small effect on the asymmetry. Simulations of our chloride ion without charge transfer result in a more asymmetric solvation shell than when charge transfer is included. For chloride without charge transfer, the polarizability is reduced to 4.92 Å^3, so that the chloride ion dipole has the same average as the CT model. (The Drude charge was reduced to -3.850 e.) The slight negative charge in the solvation shell of the charge-transfer ion repels the negative Drude charge, thereby reducing the dipole moment of the ion. Thus, CT provides an additional damping force on the anion dipole, which results in more isotropic solvation. Furthermore, the negative charge transferred to the waters causes the first solvation shell molecules to repel each other and solvate the ion more symmetrically. As expected from its greater polarizability and less favorable hydration, iodide has a more asymmetric solvation shell than chloride.

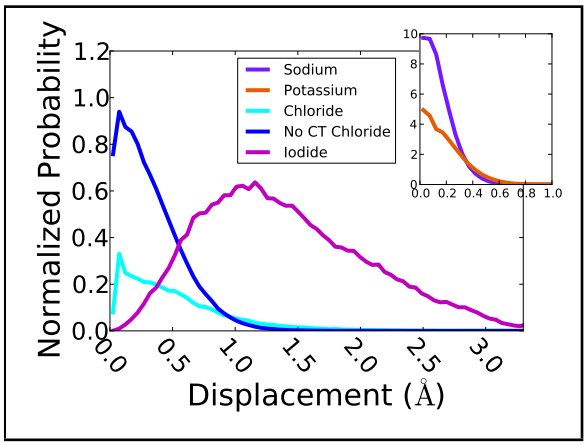

Figure 4.3: Asymmetry in the First Solvation Shell. Displacement refers to the distance between the center of mass of the first solvation shell and the ion's center. The inset shows sodium and potassium, which are much more symmetric than chloride. The larger plot show chloride with charge transfer and without charge transfer.

4.3.3 Free Energies

Direct comparison of solvation free energies determined by experiment and MD simulations remains ambiguous, due to the extra-thermodynamic assumptions necessary to set experimental single-ion free energies.[7] Our hydration free energies for single ions and ion pairs compare well with those of Tissandier *et al.* [18] (see Table 4.2). Because our

ion hydration free energies are relative to those of Warren and Patel,[7] our free energies are also real hydration free energies.

Table 4.2: Hydration Free Energy (ΔG_{hydr}). The single-ion hydration free energies and the ion-pair hydration free energies are compared to experimental values are from Tissandier *et al.*[18] Units are kcal/mol.

	Calculated	Experimental
Single Ions		
Na^+	-100.8 ± 0.6	-101 ± 2
K^+	-84.6 ± 0.7	-84 ± 2
Cl^-	-73.1 ± 0.3	-73 ± 2
I^-	-58.0 ± 0.2	-57 ± 2
Ion Pairs		
NaCl	-175.2 ± 0.4	-174 ± 4
KCl	-158.6 ± 0.4	-157 ± 4

Our model correctly predicts the hydration free energy difference between K^+ and Na^+ as −17.2 kcal/mol.[18] The calculations for the ion pairs are slightly more negative than the sum of the single-ion values, perhaps because the simulations are not at the infinite dilution limit and ion-ion interactions contribute. The ion pair energy, found from the difference of the potential energy of ionic solution and the pure liquid, is −181 ± 6 kcal/mol for NaCl and −164 ± 7 kcal/mol for KCl. These values compare well to the experimental values: −187 ± 2 kcal/mol for NaCl and −167 ± 2kcal/mol for KCl.[18]

4.3.4 Diffusion Constants

Table 4.3: Diffusion Constants. The diffusion constants of single ions in 512 waters are compared to experimental values from the *Handbook of Chemistry and Physics*.[19] Units are 10^{-5} cm^2/s.

	Calculated	Experimental
Na^+	1.0 ± 0.2	1.33
K^+	1.5 ± 0.1	1.98
Cl^-	1.9 ± 0.1	2.03
I^-	1.33 ± 0.1	2.05

Our calculated diffusion constants are compared to experimental values in Table 4.3. The diffusion constants are in good agreement with experiment and show the correct trend among the ions ($Cl^- > K^+ > Na^+$) but are all lower than the experimental values. The water model used for these studies also has a diffusion constant less than experiment (1.9 rather than 2.3 x10^{-5} cm^2/s),[2], which may influence

the results for the ion diffusion constants. The diffusion constant does not change if charge transfer is turned off and the polarizability reduced to give the same dipole, as described in Section 4.3.2 (*i.e.* $Q^{CT} = 0$ and $q_d = -3.850$). For transport properties in response to an electric field or a charge gradient, charge transfer may have a larger effect. Some researchers have found a system-size dependence in the calculation of diffusion constants.[20] However, we do not find any difference between the simulations at different system sizes. Yu *et al.* do not observe system-size dependence of diffusion constants either.[21]

4.4 Conclusions

Herein, we describe a method for including charge transfer for polarizable ions in MD simulations and developed parameters for the chloride, potassium, and sodium ions. The amount of charge transfer is parameterized to be consistent with the result of electronic structure calculation for ion-water and ion-ion pairs. In the liquid, CT to the first solvation shell results in charges for the ions that average to be about 0.9 *e* for the cations and $-0.77e$ for Cl^-, in agreement with *ab initio* results for solvated ions.[8, 13, 22] The charges of the ions show a distribution of values (Figure 3.4), representing the degree of fluctuations of the first solvation shell. Ion-ion parameters for the Lennard-Jones and charge transfer energies are chosen to reproduce the energy and structure of the dimer pairs. The resulting models properly reproduce the hydration free energies and enthalpies. Therefore, they accurately describe the interaction energies for both the dimers and in the aqueous phase (see Tables 3.3 and 4.2). The aqueous structures are consistent with previous MD simulations[21] and give coordination numbers consistent with experiment (Table 3.5). The ions also show accurate transport properties, as evidenced by the diffusion constants (Table 4.3). The chloride ion is parameterized to reproduce the distribution of its dipole moment in the liquid. Its value of 0.7 Debye compares well with quantum calculations of aqueous Cl^- that find the dipole moment is less than 1 Debye.[13, 23]

Charge transfer also affects the asymmetry of ion solvation. Comparing Cl^- simulations with and without CT, shows that charge transfer slightly reduces the anisotropy of the first solvation shell (Figure 4.3.2). Both the reduced dipole moment of the ion and the negative charge on the solvating waters make the solvation shell more symmetric.

For all three ions, the charge of water molecules in the first solvation shell is negative (Figure 4.3.1), despite the fact that charge transfer to the cations makes the water positive in a cation-water dimer. The geometry of the solvating waters is such that molecules next to K^+ or Na^+ donate more hydrogen bonds with other molecules than they accept. The arrangement of the water molecules results in a transfer of negative charge to the first solvation shell, outweighing the amount of charge transferred to the ion. The first solvation shell water molecules next to Cl^- acquire positive charge since they accept more hydrogen bonds with other waters than they donate, but this positive charge is not large enough to outweigh the negative charge from the chloride ion and so the first solvation shell waters are negative. The second solvation shell has a compensating positive charge. Our models predict that the solvating waters are negative and the charge of water molecules near the ions is not zero.

Bibliography

[1] P. Hunenberger, M. M. Reif, and J. Hirst, *Single-Ion Solvation Single Ion Solvation: Experimental and Theoretical Approaches to Elusive Thermodynamic Quantities*, RSC Theoretical and Computational Chemistry Series, 2011.

[2] A. J. Lee and S. W. Rick, J. Chem. Phys. **134**, 184507 (2011).

[3] S. W. Rick, S. J. Stuart, and B. J. Berne, J. Chem. Phys. **101**, 6141 (1994).

[4] M. P. Allen and D. J. Tildesley, *Computer Simulation of Liquids*, Oxford Univerity, 1987.

[5] L. R. Olano and S. W. Rick, J. Comput. Chem. **26**, 699 (2005).

[6] G. Lamoureux and B. Roux, J. Chem. Phys. **119**, 3025 (2003).

[7] G. L. Warren and S. Patel, J. Chem. Phys. **127**, 064509 (2007).

[8] M. Dal Peraro, S. Raugei, P. Carloni, and M. L. Klein, ChemPhysChem **6**, 1715 (2005).

[9] J. Korchowiec and T. Uchimaru, J. Chem. Phys. **112**, 1623 (2000).

[10] M. Soniat and S. W. Rick, J. Chem. Phys. **137**, 044511 (2012).

[11] B. Sellner, M. Valiev, and S. M. Kathmann, J. Phys. Chem. B **117**, 10869 (2013).

[12] S. J. Irudayam and R. H. Henchman, J. Chem. Phys. **137**, 034508 (2012).

[13] Z. Zhao, D. M. Rogers, and T. L. Beck, J. Chem. Phys. **132**, 014502 (2010).

[14] S. J. Stuart and B. J. Berne, J. Phys. Chem. **100**, 11934 (1996).

[15] C. D. Wick, J. Chem. Phys. **131**, 084715 (2009).

[16] P. Jungwirth and D. J. Tobias, J. Phys. Chem. B **104**, 7702 (2000).

[17] P. Jungwirth and D. J. Tobias, Chem. Rev. **106**, 1259 (2006).

[18] M. D. Tissandier et al., J. Phys. Chem. A **102**, 7787 (1998).

[19] W. M. Haynes, editor, *CRC Handbook of Chemistry and Physics*, CRC Press, Internet Version, 92nd edition, 2012.

[20] I.-C. Yeh and G. Hummer, J. Phys. Chem. B **108**, 15873 (2004).

[21] H. Yu et al., J. Chem. Theor. Comput. **6**, 774 (2010).

[22] S. Varma and S. B. Rempe, Biophys. Chem. **124**, 192 (2006).

[23] M. Masia, J. Chem. Phys. **128**, 184107 (2008).

Chapter 5

Ions at the Liquid-Vapor Interface of Water

5.1 Introduction

Electron delocalization is a common phenomenon in quantum mechanics. Charge transfer (CT) occurs when electrons become delocalized over non-bonded pairs. In ion-water dimers, quantum mechanical (QM) charge partitioning schemes assign a non-integer charge to the ion and assign a net charge to the water molecule.[1] QM calculations show the occurrence of CT even in the electronic ground state and separate from basis set superposition error.[2, 3] Experiments such as Raman spectroscopy[4, 5] and X-ray absorption spectroscopy[6] also show evidence for CT. Though the amount of electron density shifted between the pairs is generally small ($< 0.1e$), CT has been posed as a possible explanation for: specific ion effects,[7] ion channel selectivity,[8] the electrostatic potential of biomolecules,[9] and electrophoretic mobility of hydrophobic particles in water.[10, 11]

The study of CT in large systems has been limited by the high computational cost of ab initio molecular dynamics (AIMD).[12, 13, 14, 15] Recently, classical point-charge models which include CT have been developed for molecular mechanics (MM) calculations.[1, 16] These models describe properties of water and ions that are in agreement with experiment and *ab intitio* methods. In particular, the charge of waters and ions in bulk and the charge of the solvation shells around ions are the same as in AIMD.[1, 12]

Additionally, the use of potential functions allows for easy separation of the energy contributions of CT and its effect on the Coulombic energy.

Charge transfer is expected to be important at interfaces because interfaces break the symmetry found in bulk liquid. Previous studies using CT models [10, 17, 18] or adding CT perturbatively [10, 11] have established that a hydrogen bond imbalance creates a charged layer at the interface. From the Gibbs dividing surface (GDS) to 5 Å into the liquid, there is a region of excess of hydrogen bond acceptors creating a negative charge at the water/vapor interface. Above (towards the vapor phase) and below (towards the center of the liquid) the negative layer are regions of excess hydrogen bond donors; therefore, these areas have a positive charge. The integrated surface charge reaches a minimum of -20 $\mu e/\text{Å}^2$ at 3 Å below the GDS.[11, 17] A negative charge of the same magnitude is found at the water-oil interface, in reasonable agreement with ζ-potential measurements.[10]

Studies of aqueous ions find significant CT between an ion and neighboring water molecules.[1, 12, 13, 14, 19] Additionally, ions can have long-range effects on the hydrogen bond structure of bulk water.[20, 21, 22] The effects of (i) a charged layer at the pure liquid/vapor interface, (ii) water molecules with charges from CT with ions, and (iii) long-ranged perturbation of hydrogen bond structure from ionic solutes suggest that CT can lead to some interesting effects for ions at interfaces.

Though traditionally viewed as being absent from water's surface, some evidence suggests that ions are in fact present at water-hydrophobe interfaces and water's liquid-vapor interface. [23, 24, 25, 26, 27] When present at the interface, ions have an integral role in atmospheric chemistry via on-water reactions,[28] the function of biological membranes and proteins,[29, 30] and solute partitioning between aqueous and organic/ionic liquid phases[31] to name a few. Consequently, extensive efforts have been made to understand which properties, including polarizability and size, might stabilize ions at the interface.[24, 26, 27, 32, 33, 34, 35, 36, 37] What role charge transfer has in ion adsorption is, as of yet, unexplored.

The aim of this study is to determine how CT affects ions at and near the water-vapor interface. Does reduction of the magnitude of ionic charge result in more adsorption to the interface? How does the charge layering of pure water affect ionic attraction or repulsion to the interface? How is the charge distribution at the interface affected by the presence of an ion? And visa versa, how is the charge distribution around the ion affected by the surface? This study is novel in that it considers a charge distribution consistent with QM but in a system size accessible only by MM. Additionally, this study examines the differences in free energy profile when using an instantaneous interface rather than an average surface.

5.2 Methods

5.2.1 The Charge Transfer Model

A force field has been developed which incorporates charge transfer (CT) into classical molecular mechanics simulations.[1, 16] In this CT force field, the total charge of the system is conserved, but the charge of each molecule and ion can change. The amounts of CT between different species are based on quantum mechanical atoms-in-molecules (AIM) calculations. The model calculates charges for each species at each time step, based on the local coordination structure. There is an energy contribution which is a function of the amount of charge transfer, and the Coulombic energy is calculated using the instantaneous charges. The model also includes polarizability with the fluctuating charge (FQ) method in the water model TIP4P-FQ+DCT and Drude polarizability for the monatomic ions. For a more complete description of the model, see References [1] and [16].

5.2.2 Simulation of the Liquid-Vapor Interface

The potential of mean force (PMF) for an ion as a function of position perpendicular to the liquid/vapor interface (the z-direction) was calculated using umbrella sampling and the weighted histogram analysis method (WHAM).[38] The ions investigated are polariz-

able, charge-transfer versions of Na^+, K^+, Cl^-,[1] and I^- in TIP4P-FQ+DCT water.[16] The Gibbs dividing surface (GDS) is found by fitting to an error function, and is defined as the point where the water density is half that of the bulk density.[39, 40] Due to the presence of capillary waves on the water surface, ion positions near the GDS may represent a range of distances from the vapor. If the ion is in the trough of a wave, it is right at the surface; whereas if the ion is beneath the peak of a wave, it may be relatively far from the surface, despite having the same position in z.

Another method to define the surface of water is to use an instantaneous surface (INS), which describes the microscopic structure of the interface. The INS is defined using the method of Willard and Chandler,[41] in which the oxygen positions are convoluted with a Gaussian to represent the local water density. Then, the density at each point in a 3D grid is calculated. The grid points at which the water density is half that of the bulk are used to define the surface. Using data from the same simulations and the weights from WHAM, the data are reweighted to construct a PMF relative to the INS. Similarly to WHAM, the unbiased probability, $< P(z) >$, can be calculated from the biased simulations by

$$< P(z) >= \sum_{k=1}^{N_{windows}} < P(z) e^{+\beta U_{bias,k}} > Z_{bias,k}, \tag{5.1}$$

where $U_{bias,k}$ is the biasing potential, and $Z_{bias,k}$ is the partition function (weight) for the biased potential, determined from WHAM. Here, the coordinate z is with respect to the INS though the umbrella potential is still centered with respect to the center of the slab.

A choice must be made about whether to include the ion in the surface definition, i.e. whether the ion contributes to the density used to determine the position of the interface. Stern *et al.*[37] show that location of the free energy minimum in the PMF with respect to the INS changes if contributions from the ion density are included in the INS definition. We find the same thing is true for both cations and anions, as seen in Figure 5.2.2. Excluding the ion from the interface definition artificially makes the ion

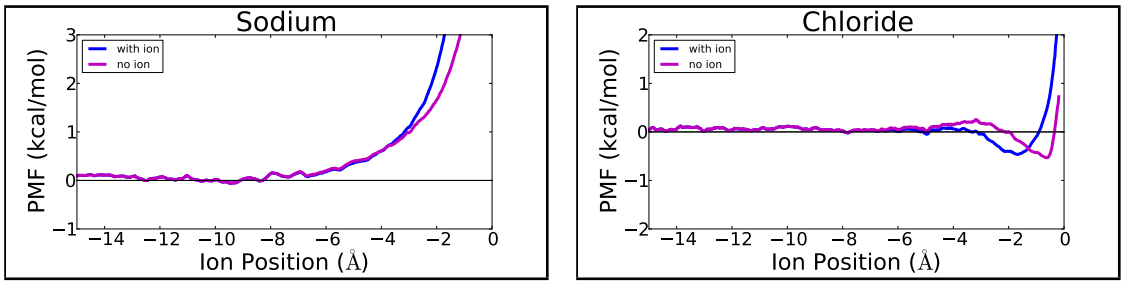

(a) (b)

Figure 5.1: Comparison of potentials of mean force (PMF) with respect to the instantaneous surface (INS) for different INS definitions. Excluding the ion from the interface definition causes the ion to approach closer to the surface.

"float" above the water. Therefore, we include the ion in the determination of the INS. For all PMF's, the relative free energy is set to zero at the center of the slab.

5.2.3 Simulation Details

There are 1024 TIP4P-FQ+DCT water molecules and a single ion in a simulation box of size 30 x 30 x 150 Å^3 (longer in z direction), resulting in a slab of liquid roughly 35 Å thick. The interface is along an xy plane, and in all figures, the interface (GDS or INS) is located at z = 0Å. The ion position is restrained at 1-Å intervals using a harmonic spring with a force constant of 4 kcal/mol/Å^2. A TVN ensemble is used with a Nose-Hoover thermostat to keep the temperature T = 298.2 K. Full Ewald summation with 3-dimensional periodic boundary conditions (3D PBC) are used. A surface correction from Ballenegger, Arnold, and Cerda (Eqn. 29 of Ref. [42]) is used for charged systems which include an interface. This correction reproduces a system with 2D periodicity when using 3D PBC. The effects of including this correction are small and do not qualitatively change the PMF results. A switching function was used[43] which continuously switches off the Lennard-Jones and real space Ewald interactions over a range from 12 to 12.5 Å. The coarse-graining length used for water and the ions for the INS calculation is 2.4 Å. The grid spacing between points is 1 Å. Production runs are at least 2 ns long, after 1 ps

equilibration time. The Verlet method with 1-fs timestep is used. Errors are determined by averaging over 500 ps blocks.

5.3 Results

5.3.1 Ionic Charges and Dipoles Change at the Interface

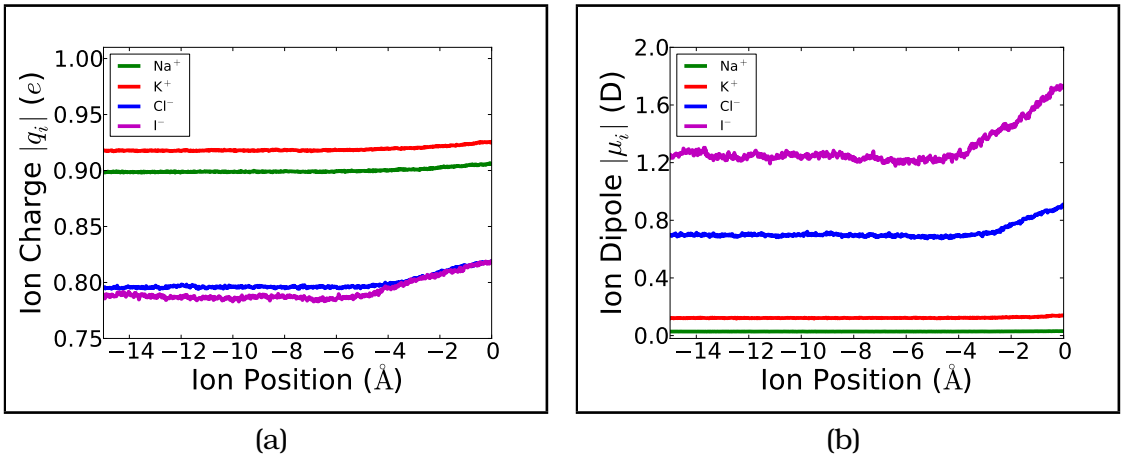

(a) (b)

Figure 5.2: Ionic charges and dipoles change near the interface. The interface is located at 0 Å, with more negative position closer to the center of the liquid phase. The dipole of the Cl^- model without CT is not significantly different from the model with CT in bulk nor at the interface (not shown).

The charge and dipole of each ion are plotted in Fig. 5.2. The cations' charges and dipoles are equal to their bulk values throughout the slab, with only a small increase in the charge at the interface. Because an ion's charge depends on its coordination number, constant charge indicates that the cations maintain their full coordination shell even at the interface. The nearly constant dipole of the cations indicates that the waters are arranged in the same way at the interface as in bulk.

In contrast, the anions' charges and dipoles depend on their distance from the interface. At the center of the slab, the anions' charges and dipoles are equal to their values in bulk. However, as the anions approach the interface, their charge approaches the formal charge of $-1e$. (Note that Fig. 5.2 plots the absolute value of the ion charge

$|q_i|$.) The increased magnitude of charge indicates that the anions have fewer neighbors to which charge is donated. The anions' dipoles also increase near the interface, indicating a more asymmetric solvation structure near the interface.

The dipoles of the waters around the ion also change as the ion approaches the surface. In bulk, dipoles for water in the first solvation shell are reduced, compared to the dipoles of bulk water.[1] At the surface, the dipoles of water molecules decrease in magnitude to 2.3 D from 2.6 D in bulk.[17] For waters bound to an ion, the dipoles decrease by $\approx$ 0.1 D at the surface. This results in dipoles which are larger for first-shell waters than for other surface waters, whereas the opposite is true in bulk water.

5.3.2 Free Energy Profiles for the Average Interface

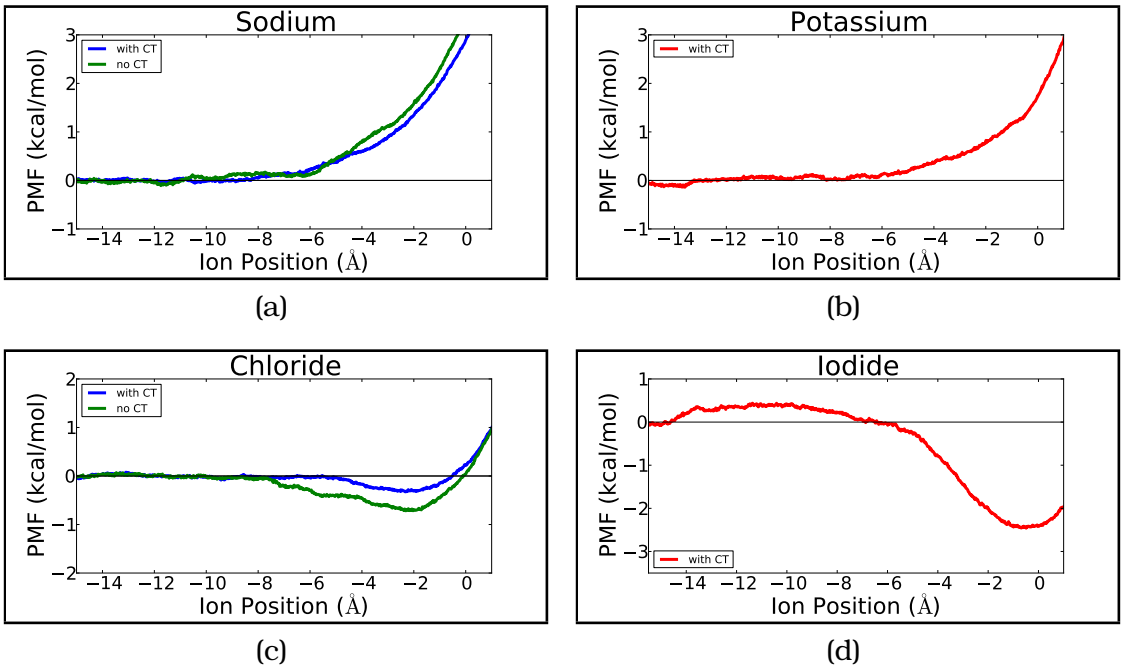

Figure 5.3: Potentials of mean force with respect to the Gibbs dividing surface. The interface is located at 0 Å, with more negative position closer to the center of the liquid phase. Cations are repelled from the interface, but anions are attracted to regions near the surface. PMF's are arbitrarily set to zero at the center of the slab for all species.

All the cations have similar potentials of mean force (PMF), shown in Figure 5.3. When cations are 6 Å below the Gibbs dividing surface (GDS), their free energy starts to

increase relative to bulk. So for cations, hydration in bulk is more favorable. The increase in free energy is less steep for potassium, as is expected because of its larger size and greater polarizability. For sodium, calculations are done with and without CT between the ion and water. The slight differences in steepness between sodium with and without CT are within error bars. There is a small difference in the bulk hydration free energy, $\Delta\Delta G_{hydr}$ = 2.7 ± 0.4 kcal/mol, between the two sodium models, with the CT model having less favorable hydration. The standard errors for the PMF's are listed in Table 5.1.

Table 5.1: Standard errors (N = number of blocks) in PMF's.

Ion		GDS kcal/mol	INS kcal/mol	N
Na^+		0.6	0.5	6
	no CT	0.6	0.5	5
K^+		0.2	0.2	4
Cl^-		0.7	0.6	7
	no CT	0.2	0.1	6
I^-		0.2	0.2	5

The anions have minima in free energy just below the GDS, indicating that they may be attached to the interface. The small minimum for Cl^- with CT near the GDS is not significantly different from zero. This is in agreement with previous studies which have found that Cl^- is neither enhanced at nor depleted from the interface.[44, 45] The minimum for the non-CT Cl^- model is significant. However, the difference between the two models cannot be ascribed solely to CT. The model without CT was designed with reduced polarizability in order maintain the same aqueous phase dipole without changing the Lennard-Jones parameters. Because of this, the non-CT Cl^- has a less favorable hydration free energy ($\Delta\Delta G_{hydr}$ = 4.3 ± 0.5 kcal/mol), which is also a driving force for surface adsorption.

Iodide shows strong surface adsorption, with free energy minimum of -2.7 kcal/mol, relative to bulk. Strong adsorption (-1.5 kcal/mol) is seen in some polarizable models,[46] while other polarizable models have less strong affinity for the surface (-0.8 kcal/mol).[47] Having too large a dipole in aqueous phase has been shown to cause too strong adsorption to the air-water interface.[48] Yet the model iodide's dipole at the surface (1.7 D) is the same as in AIMD simulations.[49] AIMD (using dispersion-corrected density functional theory) indicates an adsorption free energy of 0 to -1 kcal/mol.[49] Experiments also sug-

gest less strong adsorption of iodide at the surface than is predicted by most polarizable models.

5.3.3 Free Energy Profiles for the Instantaneous Interface

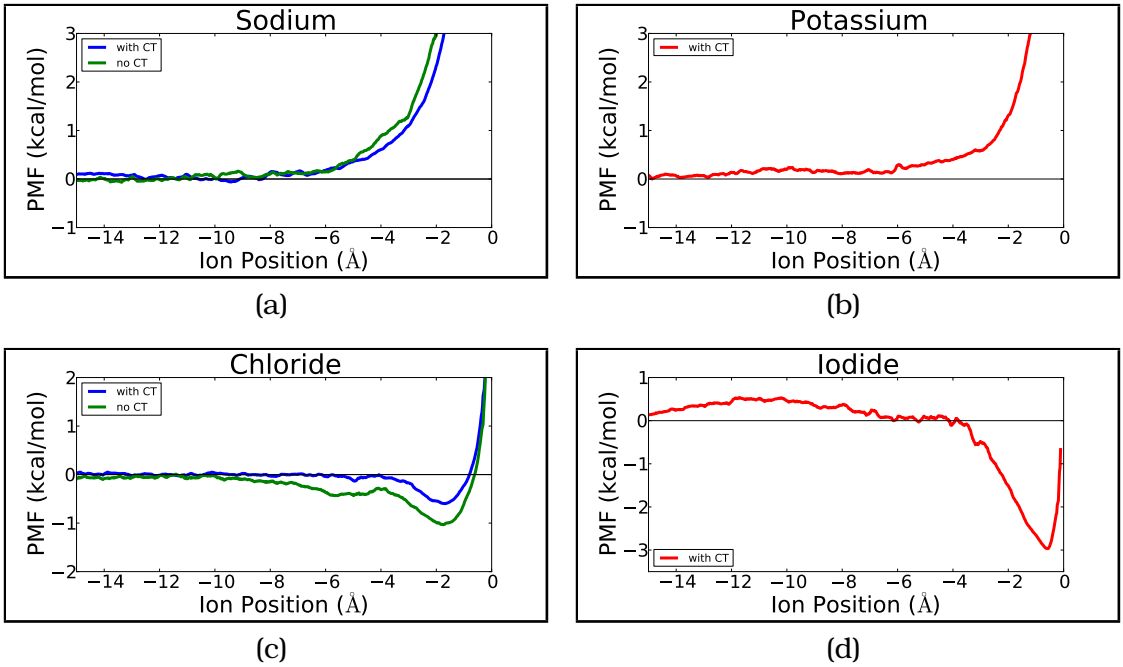

Figure 5.4: Potentials of mean force with respect to the instantaneous surface. The interface is located at 0 Å, with more negative position closer to the center of the liquid phase. The same trends are seen as in Figure 5.3 but with more sharply defined minima. PMF's are arbitrarily set to zero at the center of the slab for all species.

Qualitatively, the PMF's are similar for the instantaneous surface (INS) and the average surface (GDS), which can be seen in Figure 5.4. The cations are affected by the surface when they are 6 Å away. The non-CT Na^+ has slightly less affinity for the interface than CT Na^+, and K^+ is less strongly repelled than either sodium model. For the cations, the INS PMF is more steep near the interface, but there is still a longer ranged repulsion from the interface as well.

Use of the INS results in more localized free energy minima of the anions. I^- adsorbs most strongly and closest to the surface, and non-CT Cl^- adsorbs more strongly than CT Cl^-. The PMF's indicate that the anions are located in a narrow 2 Å-wide region,

rather than spread over a 5-6 Å range near the surface, as suggested by the conventional PMF. Also, the free energy minima decrease by 0.3 kcal/mol. Iodide adsorbs less than 1 Å from the INS. In a previous study of iodide at the instantaneous water liquid-vapor interface,[37] the adsorption is favorable by < 1 kcal/mol, around 1.8 Å below the INS. The enhanced free energy minimum and the shift of the minimum towards the INS are consistent with Stern *et al.* Similar effects are also seen in simulations with finite salt concentration.[50]

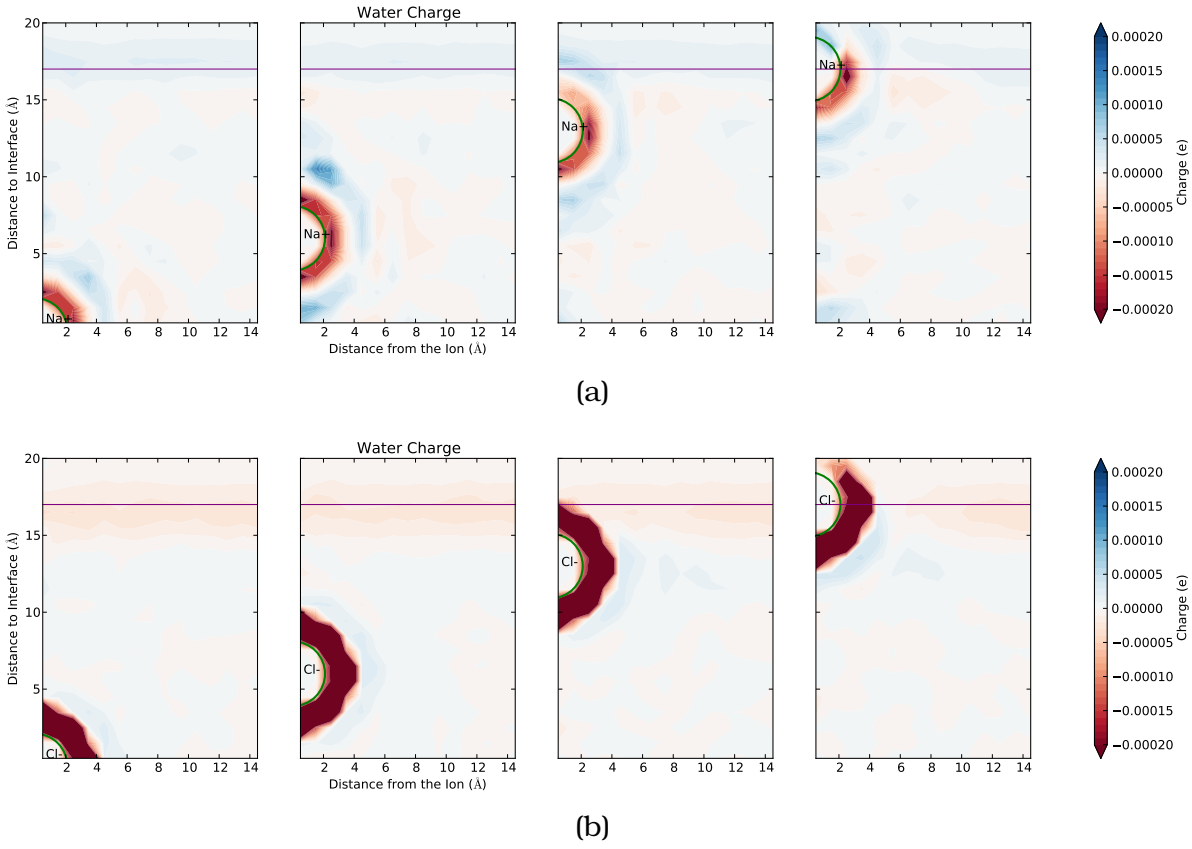

Figure 5.5: Two-dimensional distributions, showing the charge of water molecules based on their distance from the ion and from the surface for (a) sodium and (b) chloride ions. The purple line at 17 Å indicates the Gibbs dividing surface.

5.3.4 Surface Water Charge is Altered by Ions.

The presence of an interface can affect the charge distribution through charge transfer effects. In Figure 5.5, the water charge is plotted as a function of both its distance from the ion and from the interface. The negatively charged first solvation shell and positively charged second solvation shell for both anion and cation can be seen, as well as the charged surface layer. In the case of pure water, there is a negative layer centered 1.5 Å below the surface, shown in Figure 5.6(a).

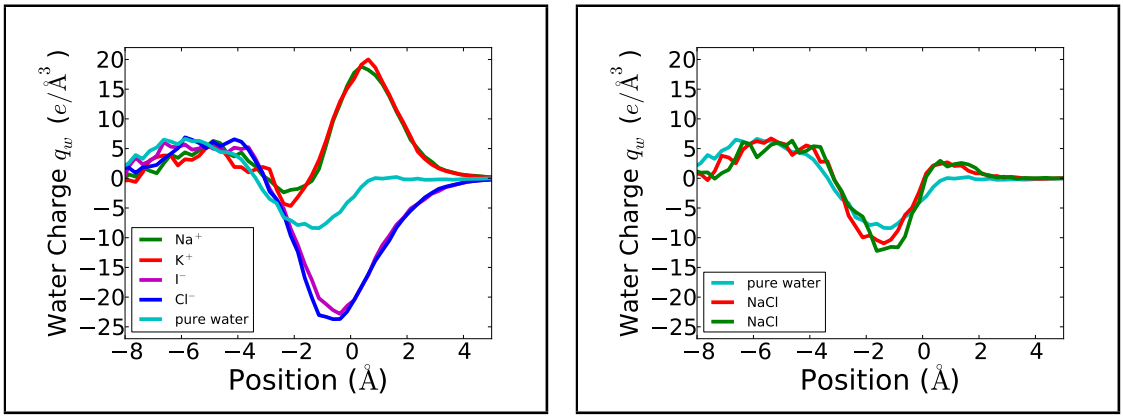

(a) (b)

Figure 5.6: Water charge density at the liquid-vapor interface. The y-axis is multiplied by 10^6. (a) The light blue line shows the charge of water molecules at the surface of neat water. With ions positioned at the center of the water slab, 17 Å away from the surface, the surface becomes more charged. Anions cause the surface to have more negative charge. Cations change the surface charge to positive. (b) With a neutral solution in which both ions have their full first and second solvation shell, the charge of waters at the surface is similar to that for pure water (blue line). The red line is for NaCl with Na^+ closer to the interface ($z(Na^+)$ = -7 Å, $z(Cl^-)$ = -17 Å). The green line is for the opposite configuration.

The negative layer is countered by a positive "sub-surface" layer, such that the slab is neutral 8 Å below the surface. The presence of an ion at the center of the slab alters the surface charge of the water. When a single anion is present, the negative charge at the surface is enhanced. In contrast, when a single cation is present, the surface charge

becomes positive, as seen in Figure 5.6(a). Integrating the charge to 3.5 Å below the GDS results in ±0.05e contributed to the surface layer from cat-/anions, shown in Figure 5.7.

Doubling that value to account for the two symmetric surfaces, the ±0.1e left-over from outside the ions' second solvation shell ($< q_{\text{left-over}} >$) is fully accounted for. Thus it appears that the excess charge outside the second solvation shell may become localized at the interface. Because the charge is based on water's hydrogen bonding patterns, the ion must be altering hydrogen bonding at the surface, even at long range.

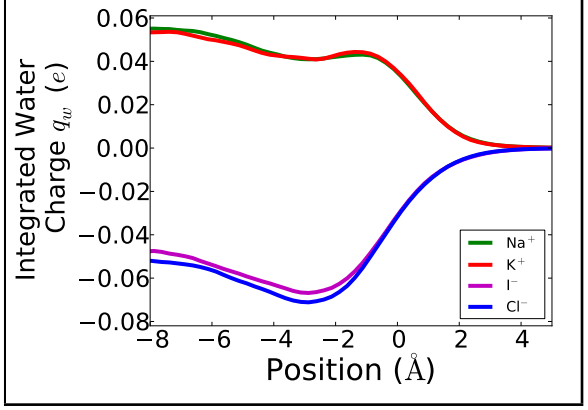

Figure 5.7: Integrated water charge (for a single surface) at the liquid-vapor interface shows that $< q_{\text{left-over}} >$ from Table 4.1 becomes localized at the interface. Single ions are located at z = -17 Å. The integrated water charge for neat water and for a neutral solution (i.e. NaCl) is zero.

When both Na^+ and Cl^- are present, excess charge from the cation and the anion largely cancel out, and the surface charge gets returns to a value close to that of the neat water case, as shown in Fig. 5.6(b). The results with both ions were generated with the two ions 10 Å from each other, with one ion at -17 Å and the other at -7 Å. The surface charge is not affected by which ion is closest to the surface. Though the ions' charges are not of equal magnitude, after charge transfer, the difference is largely compensated for in the first solvation shell such that they have equal and opposite $< q_{\text{left-over}} >$ which can delocalize to the interface. A contact-ion pair (CIP) is also tested, with the ions centered around the center of the slab. This configuration results in the same surface water charge results as the other simulations with Na^+ and Cl^-.

The charge of waters around the ion is only slightly affected by the surface. When the ion is at the surface (z_i = 0 Å), the ion disrupts the surface charge distribution up

to 8 Å away along the surface (see Fig. 5.5). This is consistent with the ion driving the orientation of waters in two solvation shells. The effects of chloride on water charge at the interface are smaller than those of sodium, consistent with Cl^- orienting its second solvation shell less strongly than Na^+.[51]

5.3.5 Charge Transfer Alters the Coulombic Interactions.

The charged surface alters the Coulombic interaction between the ion and the interface. The interactions that result from charge transfer can be quantified by U_δ, the Coulombic interaction of the ion with the net charge of a water molecule. Each water's charge, due to CT, is taken to be centered on the oxygen position. This energy as a function of ion position is shown in Figure 5.8 for sodium and chloride, where the energy at the center of the liquid phase ($z = -17$ Å) has been subtracted. The Coulombic energy for a point charge interacting with a charged surface is also plotted for comparison (also normalized to zero at the center). Note that only a single surface from the nearest image in included in these calculations, and so exact values are system-size dependent.

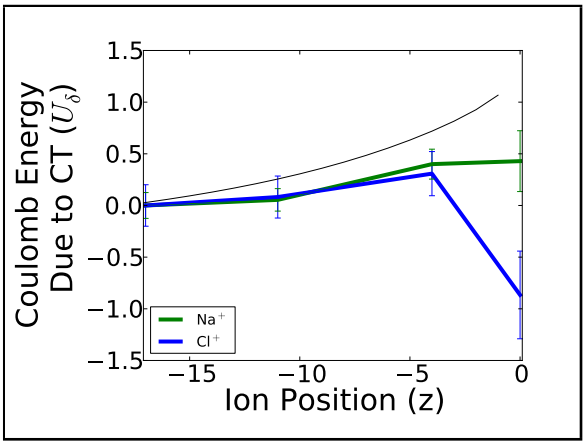

Figure 5.8: The Coulombic energy due to charge transfer, U_δ as a function of ion distance from the surface. The energy is normalized so that $U_\delta(z$ =-17 Å) = 0. The black line is the theoretical prediction for a point charge of $q = 0.85e$ being repelled from a charged surface of charge density $55.6\mu e/$ Å (the average of the charges for the two ions).

At the center of the slab, the energy U_δ is positive (unfavorable) for both ions, though there is no force from U_δ due to symmetry. For Na^+, positive U_δ at the center reflects the large amount of positive charge in $< q_{\text{left-over}} >$ compared to the smaller negative charge of the first solvation shell (see Tab. 4.1). But because the positive waters are

further away from the ion, the interactions nearly cancel, so that U_δ <1 kcal/mol. As Na^+ approaches the interface, U_δ increases, as is expected due to the like charges of the ion and the surface waters. For Cl^-, U_δ = 9.6 kcal/mol at the center. In this case, the unfavorable energy is due to repulsion between the anion and its negative first solvation shell. Again, U_δ increases as the ion gets closer to the interface. In bulk-like regions, solvation shell are symmetric, and so changes in U_δ are due to long-ranged interactions with the interface. Though U_δ is positive, it is compensated by the charge transfer energy, U_{CT}, for the nearest neighbor interactions. The CT energy compensates for the repulsive Coulombic interactions,[1] so that charge transfer is still energetically favorable.

At the interface, U_δ does not behave as expected for a point charge interacting with a charged surface. This deviation is due to the local effects of the solvation shells, which are not symmetric at the interface. As the sodium ion gets close to the surface, its second solvation shell is lost in the positive z direction. Without CT from the second to the first solvation shell, the first shell in the positive z direction becomes positively charged (see Fig. 5.5). The positively charged first shell waters on the vapor side increase the force pushing the cation into the bulk. For chloride, the loss of a negatively charged first shell water in the positive z direction results in U_δ being more favorable at the interface. Loss of that water also adds to the force pushing the ion towards the vapor.

5.4 Discussion

The role of charge transfer (CT) on the properties of ions near the liquid-vapor interface of water is examined. The potentials of mean force (PMF's) for Na^+, K^+, Cl^-, and I^- in TIP4P-FQ+DCT are calculated using a potential model which is both polarizable and has CT. We also study polarizable versions of Na^+ and Cl^-, which do not have CT, in order to better illuminate the role of CT. Our results address two questions: first, how charge is transferred among the particles of the system including its influence on interfacial

properties, and second, how charge transfer, among other interactions, influences the surface propensity of ions.

Charge transfer suggests a new mechanism for electrophoretic mobility. The present results show a new aspect of charge transfer at the interface. In bulk water, the charge transfer from the ion is spread out, and the full ion charge is not recovered even when the second solvation shell is included. Therefore, some excess charge ($\approx 0.1e$ of the same sign as the ion, see Table 4.1) resides in the third solvation shell or further away from the ion. In the presence of the liquid-vapor interface, the excess charge localizes at the interface, even when the ion is at the center of the slab (17 Å away). This enhances the charge at the surface, with a sign that matches the sign of the ion's charge. When a counter-ion is present, such that the solution is neutral overall, the excess charge at the interface largely cancels, and the charge at the interface returns to a value close to that of pure water.

The surface charge due to the ion may have relevance to electrophoretic mobility. It is known experimentally that the surface of the water/vapor or water/oil interface is negatively charged. Such hydrophobic bubbles move in response to an applied electric field.[52, 53, 54, 55, 56, 57] The charge that arises from CT at the neat water surface has been suggested a mechanism for this electrokinetic effect.[10, 11, 17] The CT model gives the correct sign of the surface charge but has a magnitude about a factor of ten too small to agree with the experimental ζ potential.[10, 11, 17] Other explanations for electrophoretic mobility include an excess of hydroxide ions at the surface[56, 57, 58] or surface active impurities.[59, 60] However, none of these hypotheses account for all the experimental data.[10, 11, 58, 61, 62, 63, 64, 65, 66, 67]

The long-ranged effects of ions on hydrogen bonding suggest a mechanism for surface charge in which ions are distant from the surface. The hydrogen bonding of the surface water molecules is changed by ions even when they are over 15 Å away. Long-ranged influences on hydrogen bonding of water molecules from the presence of ions has been seen in other simulations.[20] In our charge transfer model, the hydrogen

bond changes lead to surface charges that are 3 to 4 times larger than for pure water (Figure 5.6(a)), bringing the surface charge closer to the experimentally derived value, when a single ion is present. With this long-ranged mechanism, hydroxide ions or other impurities may lead to a more negative surface charge without being located near the surface.

Charge transfer does not affect ion surface propensity. Many properties have been investigated as the driving force for ion adsorption to the liquid-vapor surface. Among these are: ionic dipoles,[48] water dipoles,[68] ionic polarizability,[47, 49] water polarizability,[68] ion size,[33, 49, 69] asymmetry of the ionic hydration shell,[70] and overall hydration free energy (ΔG_{hyd}) of the ion.[33] Because charge transfer (CT) has some interesting effects on the charge of water molecules,[1, 17] it was suspected that CT may alter ion adsorption to the water liquid-vapor interface.

CT has been predicted to reduce ion repulsion from the interface due to a reduction in image charge repulsion.[71] Ions with CT have smaller charge magnitudes than ions in standard force fields, which retain their formal charge of ±1. Otten *et al.*[36] find that reducing the magnitude of ionic charge enhances minima in potential energy near the surface. However, they did not attempt to compute the change in free energy when changing the charge. Reducing ionic charge while keeping all other factors constant makes hydration less favorable, and therefore increases surface propensity.

The idea of greater adsorption for CT ions is contradicted by our data comparing ions with and without CT (Figures 5.3 and 5.4). The sodium models with and without CT have the very similar free energy of solvation, and so the differences between them should be due only to CT. However, the differences in their PMF's are insignificant. Additionally, potassium is able to approach closer to the interface than sodium, despite having a charge closer to $+1e$. For Cl^-, the model with $-1e$ charge has surface adsorption greater than the CT model. The greater adsorption of the non-CT Cl^- is ascribed to its less favorable

solvation free energy. Lastly, iodide has a much greater adsorption to the surface than chloride, despite having nearly the same charge.

An additional consideration with CT models is that the waters at the surface are also charged, with the same sign as the ion. The like charges increase the Coulombic repulsion between the ion and the surface. However, the charge at the surface is small, and so its effect is weak. At the surface, the forces are due to the charge and asymmetry of the ionic solvation shells. The Coulombic forces due to CT are small but act to reinforce the forces due to the water dipoles.

Furthermore, the PMF's for the polarizable, charge transfer models here are very similar to PMF's from other polarizable models. Experiment has shown a strong correlation between ion size and ionic solvation free energy in bulk to surface adsorption.[33] (The same experiment showed only a weak correlation between ionic polarizability and surface adsorption.) Indeed, it is the larger, less strongly hydrated (and more polarizable) ions which are less repelled from the interface. Moreover, the halide ions Cl^-, Br^-, and I^- transfer similar amounts of charge to water in the gas phase (see Tab. 2.15) and have similar aqueous phase coordination numbers. Figure 5.2(a) indicates that the halides have the similar charges in bulk and at the surface. That these ions have similar charges indicates that CT is not a source of the different adsorption behavior of these ions. Thus, the results indicate that CT of the ion has a minor role in overall free energy of surface adsorption. On the other hand, many studies point to the pivotal role of the water model in surface adsorption.[68, 72, 73] Only TIP4P-FQ+DCT is used in this study, and so charge transfer in the water model may still have an influence on ion absorption to the liquid/vapor interface.

5.5 Conclusions

Molecular dynamics simulations using a polarizable, charge-transfer (CT) force field are carried out to determine the role of CT on ion adsorption to the liquid-vapor interface

of water. Results show that the CT has little effect on the overall free energy of ion adsorption but has interesting implications for the surface charge of water. By comparing to ions without CT, it is seen that the reduced charge of the ions due to CT does not increase their surface propensity. Use of an instantaneous interface does not change the qualitative results from using an average interface. Nevertheless, the free energy minima for anions near the surface are more localized and within 2 Å of the instantaneous surface. The free energy profiles of cations are also affected, having a steeper increase closer to the instantaneous interface.

A fraction of the charge of the ion ends up on the bulk water molecules beyond the second solvation shell (Table 4.1) due to changes in the hydrogen bond structure of water induced by the ion. When an interface is present, this charge (negative for the anions and positive for cations) mostly resides on the interface (Figures 5.6 and 5.7). This surface charge repels the ion by a small amount. The surface charge is present even when the ion is far from the surface, showing that ions can have long-ranged effects on the structure of water. This surface charge due to the ion indicates a possible mechanism for the electrophoretic mobility of hydrophobic particles in water. It shows that the surface charge, and thus zeta potential, may be changed by hydroxide ions or other impurities without these species being located at the surface.

Bibliography

[1] M. Soniat and S. W. Rick, J. Chem. Phys. **137**, 044511 (2012).

[2] G. A. Cisneros, M. Karttunen, P. Ren, and C. Sagui, Chem. Rev. **114**, 779 (2014).

[3] Y. Mo, J. Gao, and S. D. Peyerimhoff, J. Chem. Phys. **112**, 5530 (2000).

[4] W. H. Thompson and J. T. Hynes, J. Am. Chem. Soc. **122**, 6278 (2000).

[5] S. G. Ramesh, S. Re, and J. T. Hynes, J. Phys. Chem. A **112**, 3391 (2008).

[6] C. D. Cappa, J. D. Smith, B. M. Messer, R. C. Cohen, and R. J. Saykally, J. Phys. Chem. B **110**, 5301 (2006).

[7] P. Lo Nostro and B. W. Ninham, Chem. Rev. **112**, 2286 (2012).

[8] D. Bucher et al., Biophys. Chem. **124**, 292 (2006).

[9] V. M. Anisimov and A. A. Bliznyuk, J. Phys. Chem. B **116**, 6261 (2012).

[10] R. Vácha et al., J. Am. Chem. Soc. **133**, 10204 (2011).

[11] R. Vácha et al., J. Phys. Chem. Lett. **3**, 107 (2012).

[12] M. Dal Peraro, S. Raugei, P. Carloni, and M. L. Klein, ChemPhysChem **6**, 1715 (2005).

[13] S. Varma and S. B. Rempe, Biophys. J. **99**, 3394 (2010).

[14] B. Sellner, M. Valiev, and S. M. Kathmann, J. Phys. Chem. B **117**, 10869 (2013).

[15] Q. Wan, L. Spanu, G. A. Galli, and F. Gygi, J. Chem. Theor. Comput. (2013).

[16] A. J. Lee and S. W. Rick, J. Chem. Phys. **134**, 184507 (2011).

[17] C. D. Wick, A. J. Lee, and S. W. Rick, J. Chem. Phys. **137**, 154701 (2012).

[18] A. J. Lee and S. W. Rick, J. Phys. Chem. Lett. **3**, 3199 (2012).

[19] Z. Zhao, D. M. Rogers, and T. L. Beck, J. Chem. Phys. **132**, 014502 (2010).

[20] S. J. Irudayam and R. H. Henchman, J. Chem. Phys. **137**, 034508 (2012).

[21] K. J. Tielrooij, N. Garcia-Araez, and H. J. Bakker, Science **328**, 1006 (2010).

[22] R. Mancinelli, A. Botti, F. Bruni, M. A. Ricci, and A. K. Soper, Phys. Chem. Chem. Phys. **9**, 2959 (2007).

[23] P. Jungwirth and D. J. Tobias, J. Phys. Chem. B **105**, 10468 (2001).

[24] P. Jungwirth and D. J. Tobias, Chem. Rev. **106**, 1259 (2006).

[25] P. B. Petersen and R. J. Saykally, Chem. Phys. Lett. **397**, 51 (2004).

[26] P. B. Petersen and R. J. Saykally, Ann. Rev. Phys. Chem. **57**, 333 (2006).

[27] C. D. Wick and O. T. Cummings, Chem. Phys. Lett. **513**, 161 (2011).

[28] E. M. Knipping et al., Science **288**, 301 (2000).

[29] P. Jungwirth and B. Winter, Ann. Rev. Phys. Chem. **59**, 343 (2008).

[30] W. Kunz, J. Henle, and B. Ninham, Curr. Opin. Colloid Int. Sci. **9**, 19 (2004).

[31] H. D. Willauer, J. G. Huddleston, and R. D. Rogers, Industrial Eng. Chem. Res. **41**, 1892 (2002).

[32] L. X. Dang, X. Sun, B. Ginovska-Pangovska, H. V. R. Annapureddy, and T. B. Truong, Faraday Discuss. **160**, 151 (2013).

[33] J. Cheng, C. D. Vecitis, M. R. Hoffmann, and A. J. Colussi, J. Phys. Chem. B **110**, 25598 (2006).

[34] K. D. Collins and M. W. Washabaugh, Q. Rev. Biophys. **18**, 323 (1985).

[35] Y. Levin, Phys. Rev. Lett. **102**, 147803 (2009).

[36] D. E. Otten, P. R. Shaffer, P. L. Geissler, and R. J. Saykally, Proc. Natl. Acad. Sci. **109**, 701 (2012).

[37] A. C. Stern, M. D. Baer, C. J. Mundy, and D. J. Tobias, J. Chem. Phys. **138**, 114709 (2013).

[38] S. Kumar, D. Bouzida, R. H. Swendsen, P. A. Kollman, and J. M. Rosenberg, J. Comput. Chem. **13**, 1011 (1992).

[39] A. E. Ismail, G. S. Grest, and M. J. Stevens, J. Chem. Phys. **125**, 014702 (2006).

[40] G. L. Warren and S. Patel, J. Phys. Chem. C **112**, 7455 (2008).

[41] A. P. Willard and D. Chandler, J. Phys. Chem. B **114**, 1954 (2010).

[42] V. Ballenegger, A. Arnold, and J. J. Cerda, J. Chem. Phys. **131**, 094107/1 (2009).

[43] H. W. Horn et al., J. Chem. Phys. **120**, 9665 (2004).

[44] M. D. Baer, I.-F. W. Kuo, H. Bluhm, and S. Ghosal, J. Phys. Chem. B **113**, 15843 (2009).

[45] M. Mucha et al., J. Phys. Chem. B **109**, 7617 (2005).

[46] L. X. Dang and T.-M. Chang, J. Phys. Chem. B **106**, 235 (2002).

[47] P. Jungwirth and D. J. Tobias, J. Phys. Chem. B **106**, 6361 (2002).

[48] C. D. Wick, J. Chem. Phys. **131**, 084715 (2009).

[49] M. D. Baer and C. J. Mundy, J. Phys. Chem. Lett. **2**, 1088 (2011).

[50] F. Bresme, E. Chacon, P. Tarazona, and A. Wynveen, J. Chem. Phys. **137**, 114706 (2012).

[51] S. Ou, Y. Hu, S. Patel, and H. Wan, J. Phys. Chem. B **117**, 11732 (2013).

[52] G. Quincke, Ann. Phys. Chem. **189**, 513 (1861).

[53] H. A. McTaggart, Philos. Mag. **27**, 297 (1914).

[54] J. C. Carruthers, Trans. Faraday Soc. **34**, 300 (1938).

[55] A. Graciaa, G. Morel, P. Saulner, J. Lachaise, and R. S. Schechter, J. Colloid Interface Sci. **172**, 131 (1995).

[56] K. G. Marinova et al., Langmiur **12**, 2045 (1996).

[57] J. K. Beattie and A. M. Djerdjev, Tran. Faraday Soc. **43**, 3568 (2004).

[58] P. Creux, J. Lachaise, A. Garciaa, J. K. Beattie, and A. M. Djerdjev, J. Phys. Chem. B **113**, 14146 (2009).

[59] R. Vácha, V. Buch, A. Milet, P. Devlin, and P. Jungwirth, Phys. Chem. Chem. Phys. **10**, 332 (2008).

[60] K. Roger and B. Cabane, Angew. Chem. Int. Ed. **51**, 5625 (2012).

[61] R. Vácha, V. Buch, A. Milet, P. Devlin, and P. Jungwirth, Phys. Chem. Chem. Phys. **9**, 4736 (2007).

[62] B. Winter, M. Faubel, R. Vácha, and P. Jungwirth, Chem. Phys. Lett. **474**, 241 (2009).

[63] J. K. Beattie, Chem. Phys. Lett. **481**, 17 (2009).

[64] A. Gray-Weale, Chem. Phys. Lett. **481**, 22 (2009).

[65] K. C. Jena, R. Scheu, and S. Roke, Angew. Chem. Int. Ed. **51**, 12938 (2012).

[66] J. K. Beattie and A. Gray-Weale, Angew. Chem. Int. Ed. **51**, 12941 (2011).

[67] K. Roger and B. Cabane, Angew. Chem. Int. Ed. **51**, 12943 (2012).

[68] S. J. Stuart and B. J. Berne, J. Phys. Chem. **100**, 11934 (1996).

[69] B. L. Eggimann and J. I. Siepmann, J. Phys. Chem. C **112**, 210 (2007).

[70] C. D. Wick and S. S. Xantheas, J. Phys. Chem. B **113**, 4141 (2009).

[71] O. T. Cummings and C. D. Wick, J. Chem. Phys. **139**, 064708 (2013).

[72] C. Krekeler and L. Delle Site, J. Phys.: Condens. Matter **19**, 192101 (2007).

[73] C. Caleman, J. S. Hub, P. J. van Maaren, and D. van der Spoel, Proc. Natl. Acad. Sci. **108**, 6838 (2011).

Chapter 6

Hydronium and Hydroxide at the Liquid-Vapor Interface of Water

6.1 Introduction

Understanding the chemistry of interfaces is vital for complex processes, such as heterogenous catalysis,[1] wetting behavior,[2] electrochemical processes,[3] and colloidal aggregation.[4] However, even seemingly simple interfaces, such as the liquid-vapor interface of water, are not fully characterized. Ion distribution[5] and the electrophoretic mobility of air bubbles[6] are two such unexplained phenomena which are dependent on the surface properties of water. Due to the difficulty of modeling hydronium and hydroxide, the aqueous and surface behavior of these species is even more mysterious.

The question of ion distribution with respect to the water-air interface was thought to be settled for many years. In the traditional view, based on the Debye-Hückel model, all ions are repelled from the interface. The increase in surface tension with the addition of salts, compared to pure water, was interpreted as supporting the Debye-Hückel viewpoint. However, simulations[7] and surface-sensitive experiments[8] showed that ions are able to reside at the air-water interface. This new evidence was synthesized with the surface tension data by showing that the region of enhanced ion concentration is counter-balanced by a region of ion depletion, i.e. the ion concentration changes non-monotonically.[9]

Large size, negative charge, and less favorable solvation free energy are the main drivers for expelling ions from the bulk. The Introduction of Ref. [5] provides an excellent review for monatomic ions and further references.

It is unclear whether the lessons learned from monatomic ions apply to hydronium and hydroxide. Acids, i.e. hydronium, decrease water's surface tension, indicating that hydronium should be present at the surface. The presence of bases, like that of salts, increases surface tension, indicating that hydroxide is excluded from the interface. Spectroscopic studies support this view.[6] However, air bubbles in water have the same electrophoretic mobility as negatively charged particles. Such negative surface charge indicates that hydroxide ions are present at the air-water interface, not hydronium.[6]

Charge transfer (CT) creates a negative charge at the air-water interface[10, 11] due to the hydrogen bond imbalance there. This negative layer is immobile because waters only have a net charge when located at the interface; their transition into bulk restores (on average) their hydrogen bond balance, and so they return to neutral. This negative charge was proposed as the source of air bubble electrophoretic mobility, [6] but the magnitude of the charge was too low. Recently, Soniat and Rick [12] showed that the negative charge at water's surface is enhanced by negative ions, even when the ions are distant from the interface. This novel result shows that ions can alter the surface of water even if they are excluded from the interface.

Polyatomic ions sometimes have unexpected solvation structures and can be amphiphilic in nature,[13] which is true of hydronium.[14] Hydronium and hydroxide are different from monatomic ions and from other polyatomic ions. From a quantum mechanical perspective, the excess or missing proton is equivalent to all other protons in the system. Typical non-reactive force fields in molecular mechanics must choose one of the oxygens and its nearby hydrogen(s) to be special and so cannot capture the diffuse nature of the charge excess/defect.[15] Multi-state empirical valence bond (MS-EVB) methods [16, 17, 18] allow bonds to break and form over the course of the simulation and describe

each time step as a linear combination of states. Thus, this method is closer to the true nature of aqueous systems of hydronium and hydroxide.

Herein, we explore how hydronium and hydroxide affect the liquid-vapor interface of water. How is CT different for molecular ions (compared to monatomic ions)? Is the surface charging different with H3O+/OH- than for monatomic ions? than for pure water? Additionally, we aim for a better understanding of the hydrogen bonding imbalance.

6.2 Methods

The trajectories from non-charge transfer simulations can be analyzed for their hydrogen bonding imbalance, which can in turn be used to predict molecular charges due to charge transfer (CT). Because the CT model is based on geometry, knowing the amounts of CT and the configuration is enough to predict the charges. This method has been applied previously to the water-oil interface.[6]

At an interface or in the solvation shell of an ion, there are an unequal number of hydrogen bond donors and acceptors, resulting in charged water molecules.

The hydrogen bond imbalance refers to the difference between the number of hydrogen bonds a water molecule accepts and the number of hydrogen bonds the same water donates. In bulk water, the number of hydrogen bonds accepted and donated is equal, on average. Thus, bulk water molecules are neutral. For each each extra hydrogen bond accepted, the water molecule gains $+0.02e$ of charge; conversely, for each extra hydrogen bond donated, the water molecule gains $-0.02e$.

Here, we analyze trajectories of hydronium and hydroxide generated with the multi-state empirical valence bond model. We compare how the liquid-vapor interface of water changes when the ion is at the interface (z_i = 15Å) to when the ion is away from the interface (z_i = 5Å).

6.2.1 The Multi-State Empirical Valence Bond Model

The multi-state empirical valence bond model (MS-EVB) describes the system as a linear combination of states.[16] This approach is necessary for describing the solvation of hydronium and hydroxide because the excess or missing proton is equivalent to all the hydrogens in a real system. Thus a typical non-reactive approach to molecular dynamics (MD) is inappropriate since one hydrogen must be distinguished from the others. Most notably, the non-reactive approach fails to capture the Grotthuss shuttling of protons and the mixing of Zundel and Eigen proton solvation states. In theory, all possible states would be needed to fully describe the system. However in practice, only the four (five) most frequently visited states account for $> 90\%$ of the hydronium (hydroxide) trajectory.

6.2.2 Determination of Amounts of Charge Transfer

Quantum calculations are performed on ion-water clusters using Gaussian software.[19] Clusters are optimized using the PBE0[20] functional with the aug-cc-pvTz on the oxygen and cc-pvTz on the hydrogen atoms. Charge transfer (CT) amounts are taken from Hartree-Fock (HF) single-point calculations on the optimized clusters. HF has been shown to give the most conservative estimates of CT (unpublished data).

While gas-phase structures of hydronium-water clusters are similar to their conformations in bulk,hydroxide-water clusters are distinct from their bulk counterparts.Additionally, previous CT calculations were done on ion-water dimers, which is ambiguous in this case due to the indistinguishability of the hydrogens of the ion versus the hydrogens of the water. Therefore, in addition to the optimized structures, CT is determined from snapshots from the trajectory. Using the snapshots, the hydroxide with its first solvation shell is isolated for a HF CT calculation. This is repeated for each of the five top-weighted states. Snapshots with the ion in both the bulk and at the surface are used to compare CT in the two environments. Snapshots from the hydronium trajectories are also analyzed to compare CT in the optimized clusters, at the surface and in the bulk.

All partial charges are assigned using the atoms in molecules (AIM) method[21] via the AIMAll (Version 14.06.21) software.[22]

For the MD simulations, the amount of CT and the distance cut-off for CT are tested to see how strongly these values affect the results. This two things affect mainly the first solvation shell and do not alter the results for the interface.

6.2.3 Simulation Details

Systems with 999 waters and 1 ion, either a proton or hydroxide, are simulated in a box of 31.07 x 31.07 x 100 Å. The thickness of the water slab is ≈31 Å, with z = 0Å as the center. The center of excess charge (CEC) is held at 1 Å intervals from z = 5 Å to 15 Å with a harmonic biasing potential of 5 kcal/mol. The CEC is defined as

$$\vec{r}_{\mathrm{CEC}} = \sum_i c_i^2 \vec{r}_{i,\mathrm{COC}} \tag{6.1}$$

where c_i^2 are the weights of each diabatic state i, and $\vec{r}_{i,\mathrm{COC}}$ is the center of charge (COC) coordinate for each state (typically the hydronium/hydroxide oxygen atom). A version of LAMPPS which is modified to handle the MS-EVB model is used to run the simulations.

For the excess proton, 9817 configurations are considered with the 4 top-weighted states each. These simulations are done in the NVT ensemble with T = 300 K. Particle-particle-particle mesh (PPPM) with 10^{-5} precision is used for long-ranged electrostatics. A 1.0 fs time step is used along with the Nosé-Hoover thermostat with a relaxation time of 0.05 ps.

For hydroxide, 6482 configurations are used with the top 5 states for each.

6.3 Results

6.3.1 Quantum Analysis of Gas-Phase Clusters

Hydronium

As stated previously, there is some ambiguity in declaring which hydrogen should be considered the excess proton. An isolated water molecule has hydrogens with partial charges of $+e$. An isolated H_3O^+ molecule (the Eigen state) has a total charge of $+1e$, with each hydrogen having the same partial charge ($+0.7824e$). Thus, the excess positive charge is distributed evenly over the identical hydrogens. In the $H_5O_2^+$ molecule (the Zundel state), the central hydrogen has a charge greater than the other hydrogens, indicating that it has the most proton-like character. Here we have a choice: to consider the Zundel state as a single molecule, in which case there is no CT, or to assign the proton to one water and consider CT from the Eigen state to the water. If we use the later method, there is $+0.0735e$ transferred from the cation to the water. cf [23].

As more waters are added, the Eigen state becomes more prevalent, and the additional waters have less Zundel-like properties. When three waters surround a central H_3O^+ (one water coordinated to each hydrogen), $+0.0377e$ are transferred to each water. This value is what is used in the trajectory analysis.

A rarely visited state in the aqueous simulation is one in which a fourth water is coordinated to the hydronium oxygen. However, as this state is important for the dynamics of proton shuttling,[] it cannot be ignored.

Hydroxide

In the isolated hydroxide, the partial charge on the hydrogen is reduced from the pure water case to $+0.4793e$. Again, when only one water is present, the hydrogen between the two oxygens cannot be definitively assigned to either oxygen.

As more waters are added, all waters are coordinated to the oxygen in the optimized structures, up to five waters. In the $OH^-(H_2O)_5$ structure, $-0.0363e$ are transferred to each water. A sixth water added to the hydrogen side optimizes to a structure with three waters coordinated to the hydroxide oxygen and the extra two waters in the ion's second solvation shell. Performing the CT analysis on the unoptimized structure, $-0.007e$ are transferred to the water coordinated to the hydroxide hydrogen.

However, structures with waters coordinated to the hydrogen are more common in the liquid. Therefore, snapshots from the trajectory are analyzed to better understand CT in more relevant structures.

6.3.2 Quantum Analysis of Snapshots

Hydronium

For a hydronium ion at z_i = 5Å and z_i = 15Å, i.e. in a bulk-like and a surface environment, eight configurations are selected. Each of the four top-weighted states are analyzed for their CT in relation to the number of hydronium oxygen and hydronium hydrogen partners.

The most common and the most highly weighted states are the same for the hydronium ion. That state has a water molecule coordinated to each hydronium hydrogen and no water on the hydronium oxygen. In the rare case of a water coordinated to the hydronium oxygen, the water transfers an average of 0.017 e to the ion when in bulk but only 0.007 e when at the surface. For waters coordinated to the hydrogens of hydronium, the same amount of CT occurs in bulk and at the surface. When there are two waters, 0.087 e are transferred to hydronium from each water; this value is reduced to 0.059 e when three waters are present. This is more CT than is seen in the gas-phase clusters with the same coordination state. This data indicates that the waters are closer to hydronium in aqueous solution than in the gas phase.

No matter its coordination state, hydronium maintains a charge around $+0.82e$ in these snapshots.

Hydroxide

For a hydroxide ion at z_i = 5Å and z_i = 15Å, i.e. in a bulk-like and a surface environment, ten configurations are selected. Each of the five top-weighted states are analyzed for their CT in relation to the number of hydroxide oxygen and hydroxide hydrogen partners.

In the bulk, the most common state has three waters next to the hydroxide oxygen. A water next to the hydroxide hydrogen as well occurs about two thirds of the time. However, the most highly weighted states tend to have four waters next to the hydroxide oxygen and a water next to the hydroxide hydrogen as well. The CT from hydroxide to the water next to its hydrogen is about $-0.025e$, which is what is used in the trajectory analysis. CT from the hydroxide to the waters next to its oxygen is still difficult to assign due to some damping of the CT per water as more waters are added. The amount of $-0.060e$ is used as a compromise between the amount of CT with three and four hydroxide oxygen neighbors. In the clusters and in the bulk, the amount of CT when four or five waters are coordinated to the oxygen is about the same. However, CT to three waters in the bulk is much greater than to three waters in the clusters. This may be due to the specific configurations, as the amount of CT is highly dependent on the distances between the ion and the water molecule.

At the surface, binding of waters to the hydroxide hydrogen is greatly reduced. The most common and the most highly weighted states still have three and four waters coordinated to the hydroxide oxygen, respectively. The CT per water is reduced when three waters coordinate the hydroxide oxygen at the surface, compared to the same configuration in bulk. This may indicate that $O_h \cdots H_w$ distances are increased at the surface. Other configurations have the same amounts of CT in the bulk and at the surface.

Oddly, the hydroxide charge is less negative (more CT overall) when fewer waters are present. When more waters are present, the hydroxide charge is closer to its formal charge of $-1e$. This may be due to steric hindrance between water molecules in the ion's first solvation shell. As more waters are added, they become crowded and so are further away from the ion. When only a few waters are present, the hydroxide can bind more strongly to each of them and thus transfer more charge overall. confirm that the gas-phase and aq.-phase distances are different.

For hydroxide, in addition to hydronium, the amount of CT is greater in the condensed phase than in the gas phase. This is in contrast to typical ions, where CT is damped in the condensed phase. The increase in CT may be due to a decrease in $O_h \cdots O_w$ distance for the ions in the aqueous phase compared to the gas phase. For hydronium, the average $O_h \cdots O_w$ distance in the liquid is 2.51 Å. The most common configuration has an optimized distance of 2.60 Å in the gas phase. For hydroxide, the average $O_h \cdots O_w$ distance in the liquid is 2.68 Å. This distance is the same as the as the most highly weighted configuration in its optimized structure. Interestingly, water-water oxygen-oxygen distances are also shorter in the liquid by 0.1 Å compared to gas phase.[24, 25]

6.3.3 Molecular Dynamics Simulation Results

Hydronium

The charge of the hydronium ion increases by 0.002 e as it approaches the interface, which is shown in Figure 6.1. Such a slight change in charge is consistent with the snapshots discussed in Section 6.3.2, in which the same coordination states are seen at the surface and in the bulk.

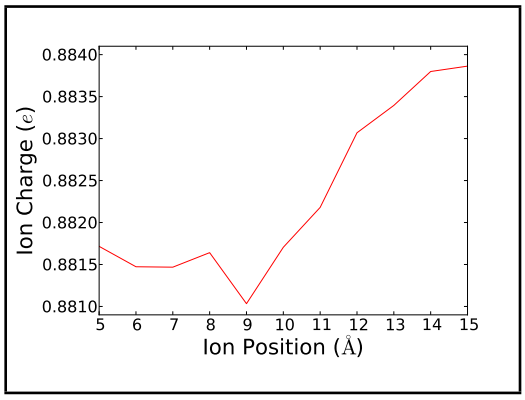

Figure 6.1: Hydronium Charge Based on Its Distance from the Interface.

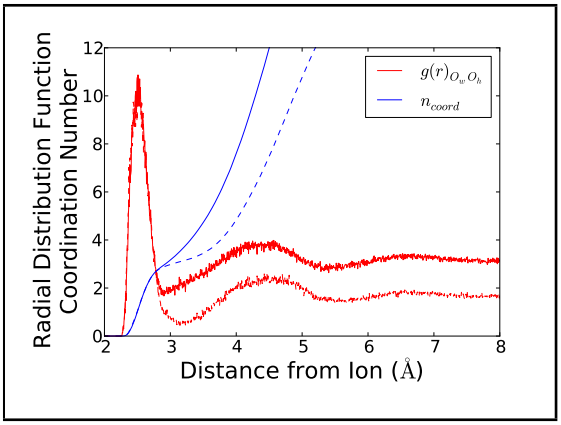

Figure 6.2: Radial Distribution Function of Hydronium. Dashed lines are for the ion at the surface, whereas solid lines are for the ion near the center of the slab.

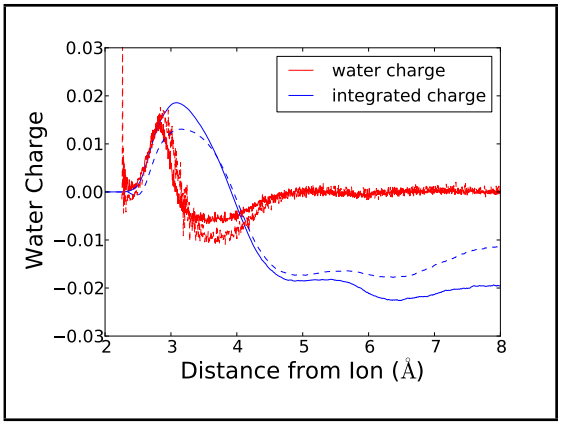

Figure 6.3: Charge of Waters in the First Solvation Shell of Hydronium. Dashed lines are for the ion at the surface, whereas solid lines are for the ion near the center of the slab.

The oxygen-oxygen radial distribution function (RDF) for hydronium to water is shown in Figure 6.2. Fig. 6.2 compares the solvation structure in a more bulk-like environment (≈ 10Å) from the surface to the hydronium solvation structure at the surface. The distance of waters in the first solvation shell is the same in bulk and at the surface. However, the coordination number for hydronium at the surface has a slight plateau due to the vacuum layer resulting in fewer waters in the second solvation shell. The charge of the waters based on their distance from the hydronium ion is shown in Figure 6.3. The first solvation shell is positive, integrating to a maximum of +0.0186*e* for the ion away from the surface. The second solvation shell is negative; integra-

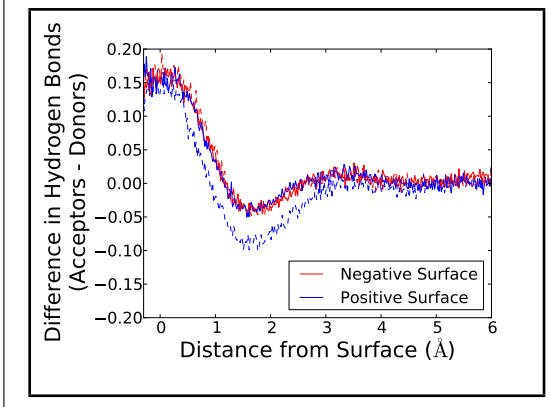

Figure 6.4: Hydrogen Bond Imbalance for Hydronium Based on Distance from the Instantaneous Interface. The negative interface is further away from the ion, and the positive interface is closer to the ion. Dashed lines are for the ion at the surface, whereas solid lines are for the ion near the center of the slab. The imbalance is reported as acceptors minus donors.

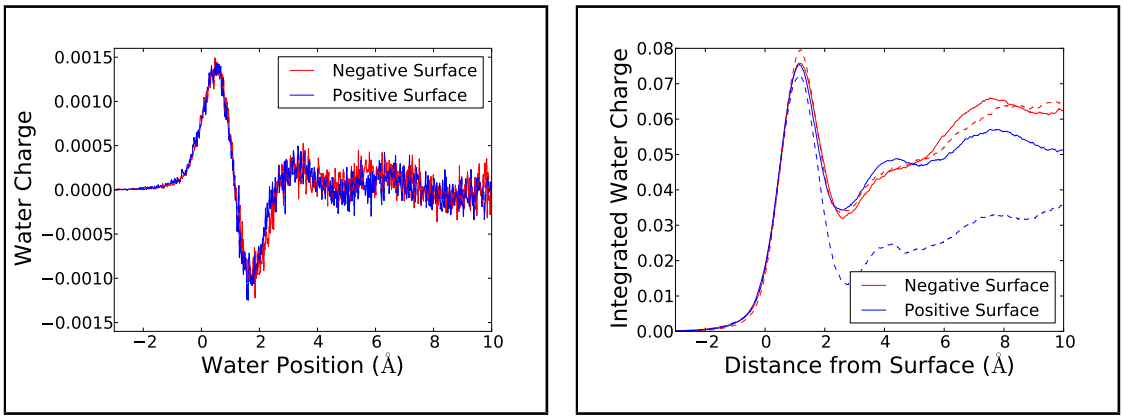

(a) (b)

Figure 6.5: Water Charge Based on Its Distance from the Instantaneous Interface When Hydronium is Present. Dashed lines are for the ion at the surface, whereas solid lines are for the ion near the center of the slab. (a) Water Charge with respect to the z-direction (e/Å) (b) Total Charge integrating from the vapor into the liquid phase (e)

tion shows that the second solvation shell contains $-0.0185e$. This leaves the charge missing from the hydronium ($+0.1183e$) outside of the second solvation shell.

Figure 6.4 shows the hydrogen bond imbalance for hydronium. When the ion is away from either surface, the hydrogen bond imbalance is the same, resulting in the same charge at each surface. The greater number of acceptors versus donors when the distance from the interface is < 1Å results in a positive charge on the waters in that region. When the ion is at the (positive) surface, the hydrogen bond imbalance is altered by the ion, whereas the distant surface is unaffected. In this case, the hydrogen bond imbalance is reduced. However, because the hydronium transfers positive charge to its first solvation shell, the surface charge is not as reduced as one would expect from the hydrogen bond imbalance.

The charge outside of the first and second solvation shells becomes localized at the interface. Figure 6.5 shows the water charge at the instantaneous surface. The "negative surface" refers to the surface further away from the ion; the "positive surface"

is closest to the ion. In Figure 6.5(a), the water charge per Angstrom is shown. A layer of positive charge nearest the vapor is followed by a negative layer just inside the liquid layer. Integration of the charge gives a clearer picture of the total amount of charge at the interface and is shown in Figure 6.5(b). When hydronium is near the center of the slab (solid lines), the charge is the same at both surfaces. Note that when the ion is far from the surface, the surface charge is solely due to hydrogen bonding imbalances in the water, i.e. there is no long-range charge transfer from the ion to the surface. When hydronium is at the surface, the positive charge of that surface decreases slightly, and the positive charge of the opposite surface increases to compensate. When at the surface, the ion is directly affecting the surface charge of water since the first solvation shell waters to which it transfers charge are also at the surface.

Hydroxide

The charge of the hydroxide decreases by $\approx 0.01e$ as it approaches the surface. The calculated charge approaching the formal charge of $-1e$ indicates a change in solvation structure, with fewer waters available to accept electron density from the ion. This is reflected in the snapshots by a decrease in states with

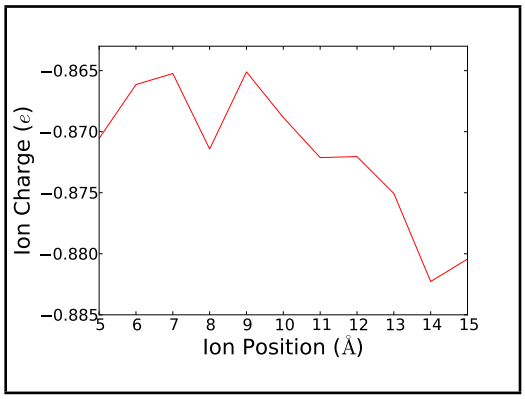

Figure 6.6: Hydroxide Charge Based on Its Distance from the Interface.

The radial distribution function (RDF) of OH^- (Fig. 6.7) shows little difference between the ion at the surface and the ion in a bulk-like environment.

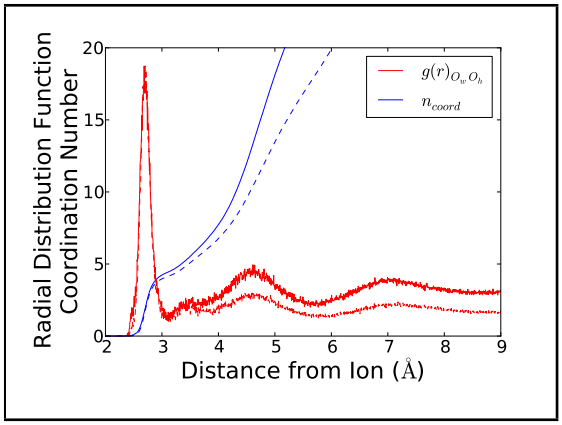

Figure 6.7: Radial Distribution Function of Hydroxide. Dashed lines are for the ion at the surface, whereas solid lines are for the ion near the center of the slab.

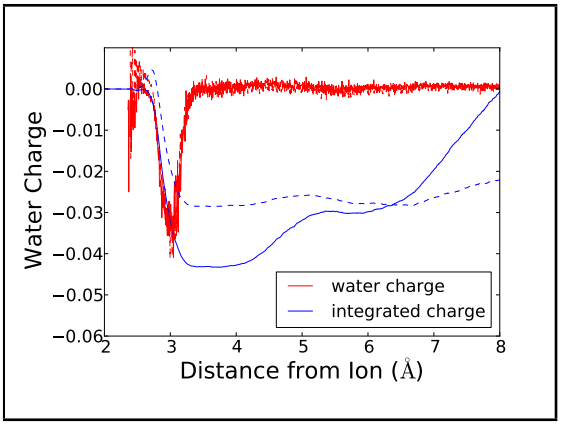

Figure 6.8: Charge of Waters in the First Solvation Shell of Hydroxide. Dashed lines are for the ion at the surface, whereas solid lines are for the ion near the center of the slab.

The hydrogen bond imbalance for hydroxide is shown in Figure 6.9. Both surfaces are the same when hydroxide is near the center. However, the hydroxide at the (positive) surface alters both the near and distant surfaces. The excess of hydrogen bond acceptors increases when hydroxide is at the surface, resulting in a less negative water charge at the surface, even though the ion's first solvation shell is negative.

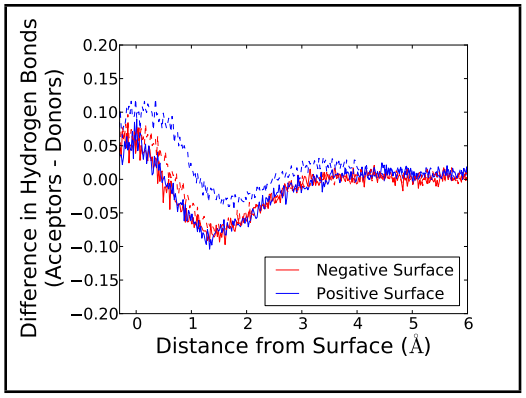

Figure 6.9: Hydrogen Bond Imbalance for Hydroxide Based on Distance from the Instantaneous Interface. The negative interface is further away from the ion, and the positive interface is closer to the ion. Dashed lines are for the ion at the surface, whereas solid lines are for the ion near the center of the slab. The imbalance is reported as acceptors minus donors.

For hydroxide, the positive water layer at the surface is reduced nearly to zero, and the negative charge dominates the surface. Oddly, the positive charge increases slightly when the anion is at the surface. This can be understood as having less negative charge in the water because the hydroxide charge is more negative when near the surface.

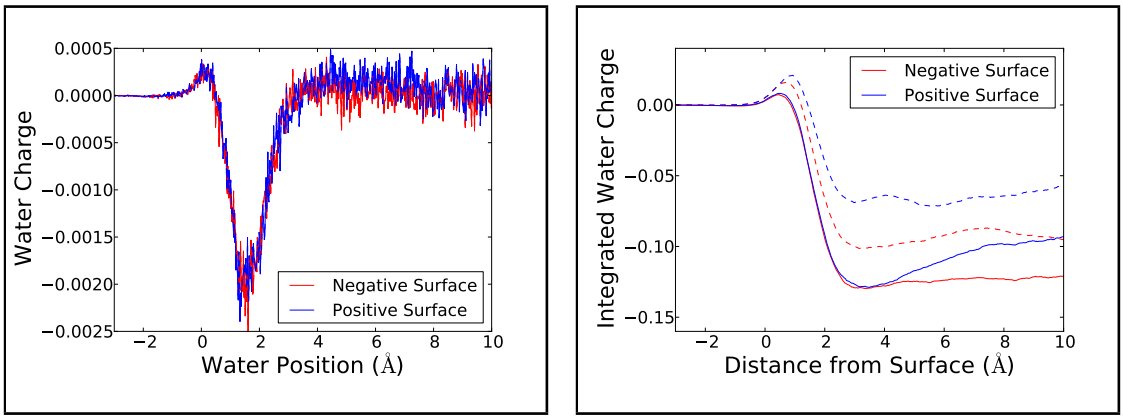

(a) (b)

Figure 6.10: Water Charge Based on Its Distance from the Instantaneous Interface When Hydroxide is Present. Dashed lines are for the ion at the surface, whereas solid lines are for the ion near the center of the slab. (a) Water Charge with respect to the z-direction (e/Å) (b) Total Charge integrating from the vapor into the liquid phase (e)

6.4 Discussion

Debate over the surface propensity of hydronium and hydroxide is on-going.[15, 18] For the purposes of the charge transfer (CT) analysis, we are not concerned with the energetics of a particular model, so long as the solvation structures are correct.

Hydronium and hydroxide are interesting polyatomic ions due to their hydrogen bonding ability. Hydrogen bonding places an additional constraint of the solvation of the ions, in addition to the packing constraint which dominates monatomic ion solvation. Waters may also be hydrogen bond acceptors or donors with respect to the ion, in contrast to monatomic ions in which all waters have similar orientations around the ion. The ability of first-shell waters to be donors or acceptors results in directionally-dependent CT.

The amounts of CT are different in the snapshots, compared to gas-phase and bulk. This difference due to the difference in O_h-H_h bond lengths. As the O_h-H_h bond is stretched, common in the aqueous phase, the hydrogen gains more proton character (for our purposes, a charge closer to $+1e$). When considering that hydrogen as part of an Eigen

state, it more charge is transferred from the hydronium to the waters. This is confirmed by quantum calculations. Work is underway to incorporated bond-length dependence of CT into the MD model. Such a bond-length dependent CT scheme may also show how CT is different at the surface, due to differing populations of Zundel and Eigen states at the surface compared to bulk.

The charge of the first solvation shell is different for hydronium than for the previous cases with cations. With Na^+ and K^+, the water-water CT from the second solvation shell (2ss) to the first solvation shell (1ss) overwhelms the CT from the 1ss to the ion, resulting in a negative 1ss. The positive charge in the 1ss of hydronium is due to the large amount of ion-water CT compared to the smaller amount of water-water CT. Hydroxide, on the other hand, is similar to Cl^- and I^- in that is has a negative 1ss and charge is transferred from the 1ss to the 2ss.

Similar to the monatomic ions, integration of the water charges from the ion center through the 2ss does not account for the total $\pm 1e$ charge of the system. Such delocalization of charge indicates that ions have long-ranged effects on water. Since there is no long-ranged CT (CT from the ion only affects waters in the 1ss), the charge outside the 2ss must be mediated by changes in hydrogen bonding patterns. Changes in hydrogen bonding patterns can be seen at the interface, when compared to pure water.[11] The charge at the surface, induced by the hydrogen bonding patterns, accounts for the charge outside the 2ss of hydronium or hydroxide when the ions are away from the interface. So, just as with monatomic ions, the charge missing from the first two solvation shells resides at the water surface, when a surface is present.

Do we need explicit CT in MS-EVB?

Bibliography

[1] W. A. Brown and D. A. King, J. Phys. Chem. B **104**, 2578 (2000).

[2] M. Järn, F. J. Brieler, M. Kuemmel, D. Grosso, and M. Lindén, Chem. Materials **20**, 1476 (2008).

[3] F. Bedioui, T. Nyokong, and J. H. Zagal, Internat. J. Electrochem. (2012).

[4] M. Y. Lin et al., Nature **339**, 360 (1989).

[5] A. C. Stern, M. D. Baer, C. J. Mundy, and D. J. Tobias, J. Chem. Phys. **138**, 114709 (2013).

[6] R. Vácha et al., J. Am. Chem. Soc. **133**, 10204 (2011).

[7] P. Jungwirth and D. J. Tobias, J. Phys. Chem. B **106**, 6361 (2002).

[8] S. Ghosal et al., Science **307**, 563 (2005).

[9] D. J. V. A. dos Santos, F. Müller-Plathe, and V. C. Weiss, J. Phys. Chem. C **112**, 19431 (2008).

[10] R. Vacha et al., J. Phys. Chem. B **114**, 9504 (2010).

[11] C. D. Wick, A. J. Lee, and S. W. Rick, J. Chem. Phys. **137**, 154701 (2012).

[12] M. Soniat and S. W. Rick, J. Chem. Phys. **140**, (2014).

[13] M. D. Baer et al., J. Phys. Chem. Lett. **2**, 2650 (2011).

[14] S. S. Iyengar, T. J. Day, and G. A. Voth, Internat. J. Mass Spec. **241**, 197 (2005), Special Issue in Honour of William L. Hase.

[15] R. Kumar, C. Knight, and G. A. Voth, Faraday Discuss. **167**, 263 (2013).

[16] Y. Wu, H. Chen, F. Wang, F. Paesani, and G. A. Voth, J. Phys. Chem. B **112**, 467 (2007).

[17] C. Knight, G. E. Lindberg, and G. A. Voth.

[18] C. D. Wick, J. Phys. Chem. C **116**, 4026 (2012).

[19] M. J. Frisch et al., Gaussian 09 Revision A.1, Gaussian Inc. Wallingford CT 2009.

[20] C. Adamo and V. Barone, J. Chem. Phys. **110**, 6158 (1999).

[21] R. F. W. Bader, *Atoms in Molecules- A Quantum Theory*, Oxford Univerity Press, Oxford, 1990.

[22] T. G. S. Todd A. Keith, Aimall (version 14.06.21), overland park ks, usa, (aim.tkgristmill.com), 2014.

[23] F. Wang, S. Izvekov, and G. A. Voth, J. Am. Chem. Soc. **130**, 3120 (2008).

[24] W. Klopper, J. G. C. M. van Duijneveldt-van de Rijdt, and F. B. van Duijneveldt, Phys. Chem. Chem. Phys. **2**, 2227 (2000).

[25] G. Hura, J. M. Sorenson, R. M. Glaeser, and T. Head-Gordon, J. Chem. Phys. **113**, 9140 (2000).

Chapter 7

Divalent Cations

7.1 Introduction

Traditional (fixed charge) models of zinc are inadequate for studies of zinc partitioning between water and protein binding sites.[1] In fact, zinc will not stay in its binding site at all unless artificial bonds are introduced.[1] For thermodynamic studies, models of bound zinc have been introduced. These models have a reduced zinc charge (i.e. $< +2e$) and are "covalently bound" (via strong harmonic restraints) to the binding site.[2] While these models improve the overall description of the protein, they obviously cannot capture the movement of zinc into and out of the binding site.

The polarization of the binding site by zinc contributes strongly to the energetics.[1] Quantum mechanical (QM) studies show charge transfer (CT) onto zinc in these binding sites as well.[3] We have previously developed a model for ion-water interactions which includes polarizability and CT.[4] This model accurately captures hydration free energies and dynamically adjusts ion and water charges based on the local environment.[4, 5]

A model which incorporates polarizability and CT may provide a more accurate and useful model of zinc for protein-water systems. As a first step towards this type of model, we herein parameterize zinc-water and magnesium-water interactions.

7.2 Methods

When developing molecular mechanics force fields, a variety of parameters need to be set to particular values. While the values of parameters are not necessarily unique, careful choice of parameters will allow for more accurate simulations. Our general approach to parameterization involves

i. quantum chemical calculation of charge transfer amounts,

ii. determination of polarizability (usually available in the literature),

iii. calculation of the ion-water dimer potential energy surface,

iv. simulation of a single ion in bulk water.

The CT and polarizability parameters are set based on the quantum mechanical data. The remaining (five) parameters are adjusted freely to get the best agreement with dimer and aqueous properties known from experiment and high-level quantum calculations. This adjustment can be done manually or using an automated optimization procedure. Finally, the quality of the parameters is confirmed by calculating the single-ion solvation free energy.

7.2.1 Quantum Chemistry Calculations

The geometry of ion-water dimers is optimized using the meta-generalized gradient approximate density functional TPSS [6] in Gaussian 09.[7] The basis set used for magnesium and water is aug-cc-pvTz. For zinc, the effective core potential (ECP) MDF10 is used; the ECP is compared to cc-pvDz for the dimer. The charge distribution is calculated using TPSS, Hartree-Fock (HF), and Moller-Plesset perturbation (MP2) theory. The electron density distribution is analyzed using AIMAll software [8] for quantum theory of atoms in molecules (AIM) charge partitioning. The charges from AIM are compared to the charges

from electrostatic potential (ESP) charges in which the ESP is constrained to reproduce the total system dipole.

In addition to ion-water dimer, clusters of the ions with multiple waters are also studied. Both ions are coordinated by six waters when in bulk liquid; therefore, clusters of six waters were optimized and the charges obtained. Assuming that the presence of a second solvation shell does not alter charge transfer between the first shell waters and the ion, the charge in bulk should be the same as in the clusters with six waters. To confirm that the second solvation shell does not alter CT within the first shell, we also studied 6+4, 6+8, and 6+12 clusters, where the first number is the number of waters in the first shell, and the second number is the number of waters in the second shell.

To simplify the tables, the following letter codes are used to represent the different combinations of basis sets used in the quantum calculations.

Zinc basis set codes:

A Zn cc-pvDz, O aug-cc-pvTz, H cc-pvDz

B Zn aug-cc-pvDz, O aug-cc-pvTz, H cc-pvTz

C Zn MDF10; O aug-cc-pvdz; H cc-pvdz

D Zn MDF10, O 6-31G*, H 6-31G*

Magnesium basis set codes:

J Mg aug-cc-pvTz, O aug-cc-pvTz, H cc-pvTz

K 6-31G*

L Mg cc-pvdz, H cc-pvdz, O aug-cc-pvdz

7.2.2 Molecular Dynamics Simulations

A force field has been developed which incorporates charge transfer (CT) into classical molecular mechanics simulations.[4, 9] In this CT force field, the total charge of the

system is conserved, but the charge of each molecule and ion can change. The amounts of CT between different species are based on quantum mechanical atoms-in-molecules (AIM) calculations. The model calculates charges for each species at each time step, based on the local coordination structure. There is an energy contribution which is a function of the amount of charge transfer, and the Coulombic energy is calculated using the instantaneous charges. The model also includes polarizability with the fluctuating charge (FQ) method in the water model TIP4P-FQ+DCT and Drude polarizability for the monatomic ions. For a more complete description of the model, see References [9] and [4].

The simplex optimization method, described in Section 3.2.1, is used to adjust the Lennard-Jones (ε and σ), CT (χ and J), and damping (a) parameters.

The simulation details are the same as in Section 4.2.

7.3 Results

7.3.1 Properties of Dimers and Clusters

Zinc-water distances in the clusters are slightly shorter than the magnesium-water distances. The water geometry is also more distorted from its isolated form when complexed with zinc. Adding dispersion corrections to the energy increases the optimal zinc-water distance by 0.013 Å. Neither adding diffuse functions nor using an effective core potential (ECP) to the zinc cation alters the CT. MP2 shows CT of $0.21 - 0.23e$ for zinc. The CT to magnesium is about a third of that at $0.0744e$. The difference in amount of CT between Zn^{+2} and Mg^{+2} has been proposed as one source of their different behaviors. As the ion-water distance increases, charge transfer (CT) drops off exponentially, as is seen in previous studies (see Section 2.4).

In clusters with six or more waters, the Zn^{2+}-O_w and Mg^{2+}-O_w distances are nearly the same and slightly greater than their respective ion-water distances in bulk. The amount of CT per water is less when a greater number of waters coordinate the ion, which is consistent with other results (unpublished data). Comparing HF CT from the dimer to

Table 7.1: CT Data for Zinc-Water Dimers from Quantum Calculations.

optimization method	basis sets	r (M–O) A	charge method	basis sets	ESP+d q(M) e	AIM q(M) e	AIM CT e
TPSS	A	1.870	HF	A	1.8798	1.8293	0.1707
			MP2		1.8449	1.7882	0.2118
			TPSS		1.7886	1.7357	0.2643
			HF	B	1.8795	1.8293	0.1707
			MP2		1.8413	1.7852	0.2148
TPSS-GD3BJ	C	1.883	HF	C	1.8587	1.8151	0.1849
			MP2		1.8198	1.7699	0.2301
			TPSS		1.7505	1.7068	0.2932

Table 7.2: CT Data for Magnesium-Water Dimers from Quantum Calculations.

optimization method	basis sets	r (M–O) A	charge method	basis sets	ESP+d q(M) e	AIM q(M) e	AIM CT e
TPSS	J	1.933	HF	J	1.9401	1.9333	0.0667
			MP2		1.9308	1.9256	0.0744
			TPSS		1.9079	1.9079	0.0921

the six water cluster for zinc, 0.1707e is transferred in the dimer, and only 33% of that (0.0576e per water) is transferred in the 6-water cluster. For magnesium, CT per water in the 6-water cluster (0.0280e per water) is 42% of the dimer CT. However, the total amount of CT is still greater for zinc in the cluster than for magnesium in the cluster, i.e. the charge of magnesium is larger when the first solvation shell is present.

Previous studies show that the ions' second solvation shell does not affect CT between the ionand its first solvation shell.[4] To see whether that conclusion holds for divalent ions, waters are added to the second solvation shell of the six-water cluster. Again, little influence of the second solvation shell on the ion charge is seen. Using a large basis set, the charge of the central ion does not change no matter how many waters are in the second solvation shell. The second shell waters are typically accepting two hydrogen and donating none. In this configuration, we expect these waters to have a charge around

Table 7.3: CT in Zinc-Water Clusters

$n_i + n_o$	optimization method	basis sets	r (M–O) Å	charge method	basis sets	AIM $q(M)$ e	$< q(2ss) >$ e
6+0	TPSS	C	2.105	TPSS	C	1.4868	
				HF		1.6546	
	PBE		2.120	HF		1.6586	
6+4	PBEPBE	D		HF	D	1.6087	0.0486
				HF	C	1.6100	0.0409
6+8	PBEPBE	D		HF	D	1.3641	0.0631
				HF	C	1.6047	0.0339
6+12	PBEPBE	D		PBEPBE	D	1.3758	0.0448
				HF		1.6158	0.0270
				HF	C	1.6115	

Table 7.4: CT in Magnesium-Water Clusters.

$n_i + n_o$	optimization method	basis sets	r (M–O) Å	charge method	basis sets	AIM $q(M)$ e	$< q(2ss) >$ e
6+0	PBE	J	2.111	HF	J	1.8374	
	HF		2.098	HF		1.8354	
	TPSS		2.1	TPSS		1.7888	
				HF		1.8321	
6+4	PBEPBE	K		PBEPBE	K	1.7813	0.0798
				HF		1.8365	0.0471
				HF	L	1.8416	0.0393
6+8	PBEPBE	K		PBEPBE	K	1.7746	0.0607
				HF		1.8335	0.0368
				HF	L	1.8383	0.0325
6+12	PBEPBE	K		PBEPBE	K	1.7792	0.0440
				HF		1.8364	0.0265
				HF	L	1.8398	

Table 7.5: Parameters for Divalent Cations. The parameters are the Lennard Jones radius (σ_{LJ}) and well depth (ϵ_{LJ}), the Drude particle charge (q_D), the Thole-type damping parameter (a_{damp}), the maximum amount of charge transfer (Q_{CT}), the cut-off distances for the charge transfer switching function (r_{CT1} and r_{CT1}), the electronegativity (μ_{CT}) and hardness (η_{CT}) for the CT energy.

Ion	σ_{LJ} Å	ϵ_{LJ} kcal/mol	q_D e	a_{damp} Å	Q_{CT} e	r_{CT1} Å	r_{CT1} Å	μ_{CT} kcal/mol/e	η_{CT} kcal/mol/e^2
Mg	1.915	0.0437	-0.475246	0.42	0.050	1.0	3.7	707.3	663.9
Zn	2.26	0.0481	-1.124637	0.35	0.101	1.0	3.9	690.2	663.9

0.040e, which is indeed what we see with the large basis set. This allows us to apply our previous model, which does not have three-body CT, without modifications.

7.3.2 Single-Ion Properties in Bulk Liquid Water

The parameters which best reproduce the target properties are shown in Table 7.5. The parameters were arrived at by a combination of automated and manual optimization. The final weights for the difference function (Eqn. 3.8) are shown in Table 7.7. The table shows all the properties that were originally considered in the difference function. After testing several weighting schemes, it was seen that any weight given to properties in which a range of values are acceptable is too restrictive on the parameter optimization. This restriction is probably due to the functional form of the difference function in which the quadratic is only minimized for a single value. A more complex form of the difference function in which a range of values is allowed may improved the automated optimization.

Table 7.6: Dimer Properties of Divalent Cations. The results of the present MD model are compared with quantum mechanical calculations. Experimental results for E_{min} and r_{min} are given in the second row in the middle columns.

Pair	E_{min} kcal/mol	r_{min} Å	q_{CT} e	
Mg^+ - H_2O	-78.8	1.90		this work
	-78.8[a]	1.942[a]		targets
Zn^+ - H_2O	-98.99	1.86		this work
	-99[b,c]	1.86[b,c]		targets

References for target properties: *a* QCISD/6-311G* [10], *b* CCSD(T)/CBS [11], *c* CCSD(T)/B2 with relativistic corrections [12]

Table 7.7: Weights for the Various Properties in the Merit Function.

	g_{max}	r_{max} Å	g_{min}	r_{min} Å	r_{max2} Å	n_c	E_{min} kcal/mol	d_{min} Å
Weight	0	10	0	0	0	90	20	20

Table 7.8: Properties of Aqueous Divalent Cations. The location of the first maximum (r_{max}) of the radial distribution function, the coordination number (n_c), the average charge ($< q_i >$) and dipole ($< \mu_i >$) of the ion are shown.

Ion	r_{max} Å	n_c	$< q_i >$ e	$< \mu_i >$ D	
Mg	2.1	6.0	+1.81	0.011	this work
Mg	2.044[a]	6.0[a]			targets
Zn	2.2	6.0	+1.61	0.055	this work
Zn	2.078[b]	6.0[c]			targets

References for target properties: *a* XRD [13], *b* EXAFS [14], *c* EXAFS [15, 16]

The dimer properties produced by the parameters in Table 7.5 are shown in Table 7.6. The energies are consistent with the highest level quantum calculations.

The aqueous properties produced by the parameters in Table 7.5 are shown in Table 7.8. The target properties were derived from X-Ray Diffraction (XRD) and Extended X-Ray Absorption Fine Structure (EXAFS) when possible. If these were not available, *ab initio* molecular dynamics (AIMD) was used instead.

7.3.3 Free Energy Calculations

There exists some disagreement on the single ion hydration free energies, ΔG_{hydr}, of multivalent ions. Tissandier et al.'s [17] values are considered the best estimates for monovalent ions. A more recent study from Coe [18] confirms the values from Tissandier et al. Thus, we calculate ΔG_{hydr} of Mg^{2+} and Zn^{2+} from Tissandier et al.'s ΔG_{hydr} of Cl^- and the experimental whole salt ΔG_{hydr} of $MgCl_2$ and $ZnCl_2$. Yu et al. [19] report $\Delta G_{hydr}(MgCl_2)$ = -607.0 kcal/mol and $\Delta G_{hydr}(ZnCl_2)$ = -637.2 kcal/mol. Tissandier et al. calculate $\Delta G_{hydr}(Cl^-)$ = -72.7 ± 2 kcal/mol. Thus we calculate $\Delta G_{hydr}(Mg^{2+})$ = -

461.6 kcal/mol and $\Delta G_{hydr}(Zn^{2+})$ = -491.8 kcal/mol. These values are about 30 kcal/mol more negative than those reported by Marcus [20] or Schmid [21]. This is consistent with Tissandier et al. reporting more negative cation hydration free energies than Marcus or Schmid in general.

For the parameter sets in Table 7.5, the hydration free energies are $\Delta G_{hydr}(Mg^{2+})$ = -460.5 kcal/mol and $\Delta G_{hydr}(Zn^{2+})$ = -490 kcal/mol.

7.4 Discussion

Work is on-going to get better-converged aqueous thermodynamic properties. Also of interest are the kinetic properties. The experimental diffusion constants are $0.71 \times 10^{-5} cm^2/s$ for Mg^{2+} and $0.71 \times 10^{-5} cm^2/s$ for Zn^{2+}.[19] The experimental residence times of waters in the first solvation shell are $2 \times 10^{-6} - 10^{-5}$ for Mg^{2+} from nuclear magnetic resonance (NMR) [22] and $10^{-10} - 5 \times 10^{-9}$ for Zn^{2+} from quasi-elastic neutron scattering (QENS).[23]

Bibliography

[1] J. C. Wu, J.-P. Piquemal, R. Chaudret, P. Reinhardt, and P. Ren, J. Chem. Theor. Comput. **6**, 2059 (2010).

[2] T. Tuccinardi et al., Bioorganic and Medicinal Chem. **14**, 4260 (2006).

[3] D. K. Chakravorty, B. Wang, C. W. Lee, D. P. Giedroc, and K. M. Merz, J. Am. Chem. Soc. **134**, 3367 (2011).

[4] M. Soniat and S. W. Rick, J. Chem. Phys. **137**, 044511 (2012).

[5] M. Soniat and S. W. Rick, J. Chem. Phys. **140**, (2014).

[6] J. Tao, J. P. Perdew, V. N. Staroverov, and G. E. Scuseria, Phys. Rev. Lett. **91**, 146401 (2003).

[7] M. J. Frisch et al., Gaussian 09 Revision A.1, Gaussian Inc. Wallingford CT 2009.

[8] T. G. S. Todd A. Keith, Aimall (version 14.06.21), overland park ks, usa, (aim.tkgristmill.com), 2014.

[9] A. J. Lee and S. W. Rick, J. Chem. Phys. **134**, 184507 (2011).

[10] M. Alcami, A. I. Gonzalez, O. Mo, and M. Yanez, Chem. Phys. Lett. **307**, 244 (1999).

[11] V. M. Rayón, H. Valdés, N. Díaz, and D. Suárez, J. Chem. Theor. Comput. **4**, 243 (2008).

[12] E. A. Amin and D. G. Truhlar, J. Chem. Theor. Comput. **4**, 75 (2007).

[13] R. Caminiti, G. Licheri, G. Piccaluga, and G. Pinna, Chem. Phys. Lett. **47**, 275 (1977).

[14] P. D'Angelo, M. Benfatto, S. Della Longa, and N. V. Pavel, Phys. Rev. B **66**, 064209 (2002).

[15] P. D'Angelo et al., J. Am. Chem. Soc. **124**, 1958 (2002).

[16] A. Kuzmin, S. Obst, and J. Purans, J. Phys.: Condens. Matter **9**, 10065 (1997).

[17] M. D. Tissandier et al., J. Phys. Chem. A **102**, 7787 (1998).

[18] J. V. Coe, Internat. Rev. Phys. Chem. **20**, 33 (2001).

[19] H. Yu et al., J. Chem. Theor. Comput. **6**, 774 (2010).

[20] Y. Marcus, J. Chem. Soc. Faraday Transact. **87**, 2995 (1991).

[21] R. Schmid, A. M. Miah, and V. N. Sapunov, Phys. Chem. Chem. Phys. **2**, 97 (2000).

[22] J. Neely and R. Connick, J. Am. Chem. Soc. **92**, 3476 (1970).

[23] P. S. Salmon, M. C. Bellissent-Funel, and G. J. Herdman, J. Phys.: Condens. Matter **2**, 4297 (1990).

Chapter 8

Damping of Charge Transfer in Ion-Ion Interactions

In attempting to apply the charge transfer (CT) model to concentrated ion solutions, it was found that the large amounts of CT were resulting in ion aggregation rather than dissolved electrolyte. Therefore, further studies of how CT depends on the environment were called for.

8.1 The Dielectric Constant of the Surroundings Alter Charge Transfer.

Table 8.1: NaCl dimer in gas phase and aqueous phase.

Optimization Method		AIM Method		d(Na–Cl) Å	q_{ct} e
HF	gas	HF	gas	2.391	0.079
HF	gas	HF	aq	2.391	0.050
M06-2X	gas	M06-2X	gas	2.359	0.105
M06-2X	aq	M06-2X	aq	2.357	0.102
M06-2X	aq	HF	aq	2.357	0.051

The environment can be included in an average manner in quantum calculations through the use of a polarizable continuum model (PCM). The NaCl dimer is used as a model system. The dimer is optimized either in the gas phase (ε = 1) or aqueous phase (ε = 78). The Slater-type orbital (STO) basis set ATZ2P and built-in atoms-in-molecules (AIM) analysis in the ADF software is used.[1]

As Table 8.1 shows, CT is reduced in an environment with a high dielectric. However, optimization in a high dielectric does not change the geometry.

The amount of CT decreases rapidly as the dielectric constant increases from 1 to 4, as shown in Figure 8.1. For this study, the NaCl dimer is used with the distance fixed at 2.93Å, the as same as in NaCl crystals. The CT amounts are obtained from HF/aug-cc-pvQZ calculations performed in NWChem,[2] varying the dielectric with PCM. The dielectric constant of NaCl is 5.90, [3] indicating that CT in the crystal is about 50% of CT in the gas-phase dimer.

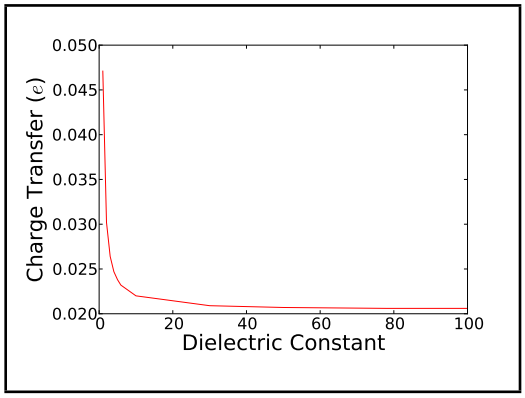

Figure 8.1: The Dielectric Constant of the Surroundings Alters Ion-Ion Charge Transfer.

8.2 The Number of Ligands Alters Charge Transfer.

Figure 8.2 shows the decrease in CT per ligand as the number of ligands increases. The data for cation-water CT are from Ref. [4]. The chloride-water CT data are for optimized clusters from Ref. [5]. The sharp decline in chloride-water CT is partially due to the larger ion-water distances in optimized clusters with a greater number water molecules.

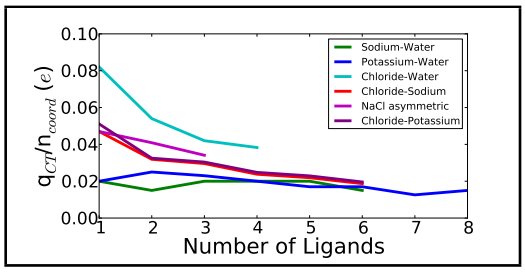

Figure 8.2: Charge Transfer per ligand decreases with the number of ligands. The legend lists the central ion first and the ligands second. NaCl asymmetric refers to a central Cl^- with all Na^+ on one side.

To determine the decrease in CT due only to the increasing number of ligands, ion pairs of Na^+ and K^+ with Cl^- are studied. The ion-ion distance is held at the distance in

salt crystals, listed in Table 8.2. Single-point calculations using HF are carried out in NWChem,[2] using the aug-cc-pvTZ basis for Na and Cl and the 6-311G(2df,2pd) basis for K. This method shows that the decrease in CT per ligand can be due the number of ligands only. In optimized clusters, this decrease in CT is enhanced by the increasing distances between central ion and ligands.

CT decreases less with the addition of ligands if the ligands are all placed to one side of the central ion. This is shown by the "NaCl asymmetric" line in Figure 8.2.

8.3 Charge Transfer in Solids.

Table 8.2: Charge transfer in salt crystals.

Salt	Distance Å	Central Ion	q e	q_{ct}/n_{lig} e
NaCl	2.825	Na	0.909	0.015
		Cl	-0.908	0.015
KCl	3.15	K	0.889	0.018
		Cl	-0.892	0.018
NaI	3.23	Na	0.883	0.019
		I	-0.893	0.018
KI	3.52	K	0.844	0.026
		I	-0.856	0.024

A further study looked at adding ions outside the first solvation shell in order to better mimic the crystalline salt environment. A schematic is shown in Figure 8.3. A central ion is surrounded by six counter-ions; then each face of the crystal is completed by adding more ions and counter-ions. Thus, there are 13 of the central ion type and 14 counter-ions in the system forming a face-centered cubic cell. The ion-ion distance is determined by their lattice constants; the distances are listed in Table 8.2. No periodic boundary conditions (PBC) are applied, and the dielectric is $\varepsilon = 1$. A calculation was attempted with $\varepsilon = 6$, which is more relevant to the solid salt environment but proved to be too computationally demanding. The methods for NaCl and KCl are the same as in Section 8.2, except that the basis sets were reduced to aug-cc-pvDZ and 6-311++G(2d,2p) due to computational expense. For iodide, the effective core potential (ECP) MWB46 is used, and the calculations are done in Gaussian09.[6]

Similarly to the higher dielectric environment above (Fig. 8.1), CT in the "mini-crystal" is reduced to about half of CT seen in the gas-phase dimer. The CT per ligand in NaCl is less than what is seen by Tang, Sanville, and Henkelman.[7] They find $q_{ct}/n_{lig} = 0.0287e$ using the density functional PW91 with PBC. Their larger CT is probably due to the use of density functional theory, which is shown in Chapter 2 to give too much CT.

One way to deal with CT damping is to reduce the Q_{CT} parameter so that the maximum CT is relevant to the aqueous environment, rather than gas phase. This is similar to the way that reduced polarizability in the aqueous environment is handled.[8] Does this create artifacts at that interface? The ion-water CT also becomes damped in the QM calculations. However, due to the smaller amount of CT in ion-water interactions, the ion-water simulations are still reasonable.

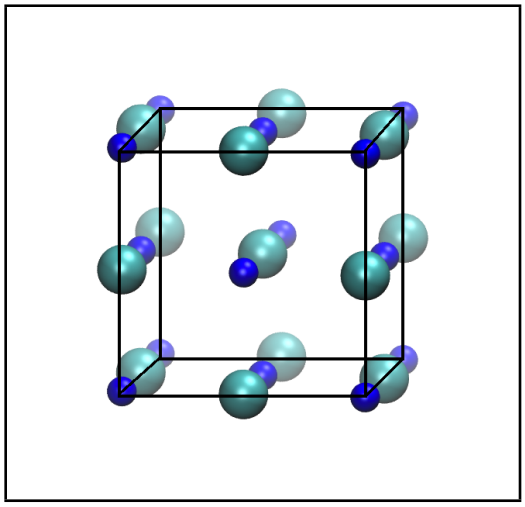

Figure 8.3: NaCl Crystal.

8.4 A Possible Method for Geometry-Dependent Charge Transfer Damping.

In certain situations, e.g. at an interface, it may be important to capture the full CT. Here, a method is proposed for explicit, i.e. geometry-dependent, CT damping. To make the model geometry-dependent, first the coordination number N_i is estimated by

$$N_i = \sum_j S w_{ij}(r_{ij}) \tag{8.1}$$

where $Sw_{ij}(r_{ij})$ is the switching function from Eqn 3.4.

$$Sw_{ij}(r_{ij}) = \begin{cases} 1 & \text{if } r_{ij} < R_1^{CT} \ , \\ \frac{1}{2}[1 + \cos(\pi \frac{r_{ij} - R_1^{CT}}{R_2^{CT} - R_1^{CT}})] & \text{if } R_1^{CT} \le r_{ij} \le R_2^{CT} \ , \\ 0 & \text{if } r_{ij} > R_2^{CT} \ , \end{cases} \tag{8.2}$$

Because the cut-offs R_1^{CT} and R_2^{CT} are designed to allow CT only to the first solvation shell, they exclude molecules outside the first shell. Summing over the neighbors j gives and estimate of N_i. This estimate is made for each molecule first.

Then, the amount of damping d is calculated based on the coordination number of the "central" atom i and the coordination number of each of its neighbors.

$$d(N_i, N_j) = (1 - b \ln N_i)(1 - b \ln N_j) \tag{8.3}$$

where $b = 0.38$ from an empirical fit to amount of damping per ligand. This value of b is fairly consistent for the variety of ligands tested.

Finally, the amount of CT q_{CT} is calculated by multiplying the maximum amount of CT Q_{ij}^{CT} (for the gas-phase dimer) by the damping coefficient d.

$$q_{CT} = Q_{ij}^{CT} d(N_i, N_j) \tag{8.4}$$

This method still conserves charge and will allow for CT to change based on the local environment.

Applying the damping method to the "mini-crystal" described in Section 8.3 improves the CT model's agreement with QM-derived charges. The quantum calculations give $q(\text{Cl}) = -0.91e$. The purely additive model using the dimer amount of CT, described in Chapter 3, predicts $q(\text{Cl}) = -0.46e$. Furthermore, the additive model has a root mean square deviation (rmsd) of 0.29 when the charges of all atoms in the mini-crystal are con-

sidered. In contrast, the damped model predicts q(Cl)= $-0.93e$, and has an rmsd of 0.1 for the total cluster.

Currently, most MD models are appropriate for one phase: gaseous, or liquid/aqueous, or solid. This geometry-dependent method of altering the polarizability and CT could result in a single model that works for all phases of matter.

8.5 Damping in the KcsA Potassium Ion Channel.

The issue of charge transfer (CT) and damping may be important for the KcsA potassium ion channel. CT and polarizability were proposed to play a role in K^+ selectivity over Na^+ in KcsA.[9] However, studies of CT in the selectivity filter (SF) of KcsA suffer from a variety of methodological problems.

Bucher et al.[9] find that carbonyl dipoles are 0.2 D greater than formamide in vacuum when K^+ is present, and 1.2 D greater when Na^+ is present. They conclude that CT does not play a role in K/Na selectivity, even though the CT energy E_{CT} = 17kcal/mol They use QM/MM, which often creates artifacts at the QM-MM boundary. Their boundary cuts through the SF, thus introducing artifacts into the most important region. Has AIM convergence with plane wave basis sets been characterized?

Kraszewski et al. [10] show that more charge is transferred to K^+ than Na^+, though q(K) fluctuates more than q(Na). Also, the sites where q(Na) is at a minimum (in S1 and S3) are the opposite of where q(K) is minimum (in S2 and S4). The minima all occur at the center of the binding sites, and so the differences in CT must be due to some longer-range polarization, i.e. the backbone is the same in all cases, so the side chain must affect CT even though the ions do not directly bind to the side chain. The carbonyl dipoles have the opposite trend, staying at 3.5D with K^+ and fluctuating from 2.9 to 4.1D with Na^+. They perform HF/6-31G(d) calculations on snapshots from an MD trajectory and extract Merz-Kollman-Singh (MKS) charges, a type of electrostatic potential (ESP) charge. These

Table 8.3: CT is Damped in the KcsA Selectivity Filter. The values are charge transferred (q_{ct}) in e.

Number of Carbonyls	NMA	GG		4GG	
	1	2		8	
		expected	actual	expected	actual
K	0.0935	0.1870	0.1058	0.7478	0.0549
Na	0.0089	0.0177	0.0412	0.0709	0.0371

are low levels of theory and have know problems for calculation of CT. They also truncate the SF for the *ab initio* calculations.

Huetz and coworkers [11] [12] find that q(K) varies depending on its position within the SF. The charges reported are Merz-Kollman (MK) ESP charges determined from HF/6-31G(d) calculations. For a discussion of the problems associated with these methods in respect to CT calculations, see Chapter 2.

A molecular dynamics (MD) study which incorporates polarizability and CT would allow for simulations of KcsA at longer timescales, and so better-converged results, than can be achieved with QM or QM/MM methods.

QM studies of Na^+ and K^+ with model compounds help to better understand polarizability and CT within the selectivity filter. The model compounds are N-methylacetamide (NMA) and diglycine (GG). These compounds are often used a mimics of the protein backbone. Four GG (4GG) arranged symmetrically around the central cation give the closest mimic to the S2 site in the SF, shown in Figure 8.4.

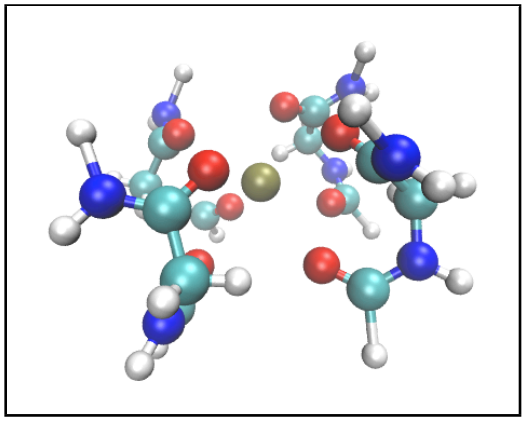

Figure 8.4: S2 site of KcsA SF.

In Table 8.3, the charge transfer amounts are shown for differing number of carbonyl (amide) ligands. The "expected" value is equal to the CT per carbonyl times the number of carbonyl groups. The actual value is from quantum mechanics. Having two carbonyl groups damps the CT to K^+. Oddly, CT to Na^+ increases when coordinated to GG. The reason for this increase in CT is unclear.

In 4GG, we see the importance of including damping of CT in the MD model. The ions are 2.776 Å from each carbonyl group. The CT onto K^+ is expected to be 0.7478 *e* in the additive model, which would results in *q*(K)=0.2522 *e*, a seemingly unreasonable charge. Indeed, the quantum calculations show that only 0.0549 *e* is transferred onto K^+. With only 0.0371 *e* transferred onto Na^+, the charges of the two cations are very similar in the center of the SF. Note that these CT amount are for the ion at the center of 4GG, which corresponds to the minimum energy position for K^+. The minimum energy position for Na+ near the center of one plane of carbonyls. The CT in that position is as yet undetermined.

Bibliography

[1] *ADF2013*, SCM, Theoretical Chemsitry, Vrije Universiteit, Amsterdam, The Netherlands, 2013.

[2] M. Valiev et al., Comput. Phys. Comm. **181**, 1477 (2010).

[3] M. C. Robinson and A. C. H. Hallett, Canadian J. Phys. **44**, 2211 (1966).

[4] S. Varma and S. B. Rempe, Biophys. J. **99**, 3394 (2010).

[5] Z. Zhao, D. M. Rogers, and T. L. Beck, J. Chem. Phys. **132**, 014502 (2010).

[6] M. J. Frisch et al., Gaussian 09 Revision A.1, Gaussian Inc. Wallingford CT 2009.

[7] W. Tang, E. Sanville, and G. Henkelman, J. Phys.: Condensed Matter **21**, 084204 (2009).

[8] H. Yu et al., J. Chem. Theor. Comput. **6**, 774 (2010).

[9] D. Bucher et al., Biophys. Chem. **124**, 292 (2006).

[10] S. Kraszewski, C. Boiteux, C. Ramseyer, and C. Girardet, Phys. Chem. Chem. Phys. **11**, 8606 (2009).

[11] M. Compoint, C. Ramseyer, and P. Huetz, Chem. Phys. Lett. **397**, 510 (2004).

[12] P. Huetz, C. Boiteux, M. Compoint, C. Ramseyer, and C. Girardet, J. Chem. Phys. **124**, 044703 (2006).

Chapter 9

Discussion

From quantum mechanical (QM) calculations, the best method for calculating amount of CT from quantum mechanics was determined to be the MP2/aug-cc-pvDz wavefunction with charges partitioned by AIM. The ion-water CT is affected by the number of waters in the first solvation shell (1ss) but not by the presence of waters in the second solvation shell (2ss). Such damping can lead to a different picture of CT depending on whether dimers or clusters are used.

Our group has developed an efficient charge transfer (CT) method for molecular dynamics (MD) simulations. It avoids non-physical behavior which is a problem in some other CT force fields.[1] I have extended this force field to include ion-water and ion-ion CT.[2] An automated parameter optimization can be useful, especially if some decent starting parameter sets are known; however, the determination of a merit function can be tricky. While debate continues over the need to include CT in models, we are now in a position to determine CT's importance.

So, what have we learned from this CT model? First, though the average charge of a water molecule in bulk is zero, its charge fluctuates based on its local hydrogen bonding (HB) environment.[1] This seems typical of neutral molecules (see Section 1.3.1). At an interface, the HB symmetry is broken, and so waters become charged.[3] Ionic species, on the other hand, have non-integer charges when solvated (see also Section 1.3.1).[2]

Ions have long-ranged effects on the structure of water. In bulk, the some charge from the ion is outside the second solvation shell. This is consistent with the picture of long-ranged perturbation of HB in water due to ions.[4] The excess charge outside the solvation shell alters the diffusivity of that water, leading to better agreement with *ab initio* MD.[5] When an interface is present, the ion can alter the HB of water at the surface even when the ion is not located at the surface.[6]

The charge of the first solvation shell of water is determined by the balance between CT to/from the ion and CT to/from the second solvation shell. For the monatomic, monovalent ions, the 1ss is negative. For the cations, more electron density is gained from the 2ss than is given up to the ion. For the anions, electron density is gained from the ion and less electron density is given to the 2ss. For the divalent cations, the 1ss is positive; more electron density is given to the ion than is gained from the 2ss. For H_3O^+ and OH^-, the charge of the 1ss is of the same sign as the ion. This is because the ion-water CT is greater than the water-water CT. The charge of H_3O^+ and OH^- and their 1ss is also affected by the HB ability of the molecular ions.

In studies of electrolytes which include CT, the anion charge is around -0.8e whereas the cation charge is close to +0.9e.[7] This means that the water has a charge of -0.1e in these systems. It has been shown that this affects the water's diffusivity.[5] What other consequences this charge on water may have are unknown. Such charge imbalance between cation and anion is also seen in KX·6(H_2O) clusters.[8] This charge asymmetry indicates there may be a problem with charge scaling schemes in which the same amount of scaling is used for cations and anions, such as in Ref. [9].

Recently, doubts have been raised about the adequacy of modeling U_{CT} as a second order Taylor expansion in the amount of CT (see Eqn. 3.2). The second order Taylor expansion produces a quadratic function, yet the true energy of an atom as a function of fractional charge should be linear when interpolating between integer charges.[10] The approximation then produces energies that are lower for fractional charges than the true

energy, leading to excess CT. In our model, the linear contribution ($\mu_{CT}q_{CT}$) is typically similar to or less than the quadratic contribution ($\frac{1}{2}J_{CT}q_{CT}^2$). How sensitive the MD model is to this effect is unclear.

As is often the case with research, as many questions are raised as answered. Work in understanding the role of CT molecular interactions would be improved by continuing research in the following areas:

i. parameterization of Zn^{2+} interactions with amino acids for use in studies of zinc metalloproteins

ii. the study of ions in an electric field

iii. testing of the damping method proposed in Section 8.4

iv. comparison of AIM and NBO charge partitioning in Zn^{2+}- and Mg^{2+}-water clusters and comparison of E_{CT} from NBO to our MD U_{CT}

v. calculation of Raman and IR spectra of halide-water clusters in which CT is allowed or prohibited to determine how CT affects these spectra

vi. the study of polarizable (FQ) and FQ+CT KcsA potassium ion channels to determine the importance of these interactions in K^+/Na^+ selectivity

vii. investigation of the effect of negatively charged waters in electrolyte solution

viii. study of the surface charge of metals (electrodes) and their CT to electrolyte solutions

Bibliography

[1] A. J. Lee and S. W. Rick, J. Chem. Phys. **134**, 184507 (2011).

[2] M. Soniat and S. W. Rick, J. Chem. Phys. **137**, 044511 (2012).

[3] C. D. Wick, A. J. Lee, and S. W. Rick, J. Chem. Phys. **137**, 154701 (2012).

[4] S. J. Irudayam and R. H. Henchman, J. Chem. Phys. **137**, 034508 (2012).

[5] Y. Yao, Y. Kanai, and M. L. Berkowitz, J. Phys. Chem. Lett. **5**, 2711 (2014).

[6] M. Soniat and S. W. Rick, J. Chem. Phys. **140**, (2014).

[7] B. Sellner, M. Valiev, and S. M. Kathmann, J. Phys. Chem. B **117**, 10869 (2013).

[8] A. C. Olleta, H. M. Lee, and K. S. Kim, J. Chem. Phys. **126**, 144311 (2007).

[9] I. Leontyev and A. Stuchebrukhov, Phys. Chem. Chem. Phys. **13**, 2613 (2011).

[10] A. J. Cohen, P. Mori-Sanchez, and W. Yang, Science **321**, 792 (2008).

Appendix A

Additional CT Data

See Appendix B for abbreviations of basis sets and methods references.

Table A.1: CT Involving Alkanes.

Electron Donor	Electron Acceptor	Geometry Method	Geometry Basis	Distance Å	AIM Method	AIM Basis	q_{CT} e
CH4	H2O	M06-2X	QZ4P	3.418	same	same	0.006
H2O	CH3CH3	M06-2X	QZ4P		same	same	0.006
Cl-	CH4	HF	ATZP		same	same	0.014
Cl-	CH3CH3	M06-2X	ATZP	3.625	same	same	0.028
CH4	Na+	M06-2X	QZ4P	2.561	HF	ATZP	0.024
CH3CH3	Na+	M06-2X	QZ4P	2.551	HF	QZ4P	0.031
CH4	K+	B3LYP	G-b	3.106	HF	same	0.095
CH4	Ca2+	M06-2X	ATZP	2.509	HF	ATZ2P	0.081
CH4	Zn2+	M06-2X	ATZP	2.016	HF	ATZP	0.296

The optimized geometry and amount of CT involving the alkanes methane and ethane are shown in Table A.1. The distance in Table A.1 refers to the distance from the ion or the water oxygen to the closest carbon. The anion Cl^- binds almost equidistant from both carbons in ethane. CT from alkanes to Na^+ and Ca^{2+} is comparable to that between those ions and water. However, CT from alkanes to K^+ and Zn^{2+} is greatly increased compared to water.

Table A.2: CT Involving Amines.

Electron Donor	Electron Acceptor	Geometry Method	Geometry Basis	Distance Å	AIM Method	AIM Basis	q_{CT} e
NH3	Na+	M06-2X	QZ4P	2.321	same	same	0.052
					HF	ATZP	0.042
NH2CH3	Na+	M06-2X	ATZP		HF	ATZP	0.045
NH3	K+	B3LYP	G-b	2.783	HF	same	0.111
NH3	H2O	M06-2X	QZ4P	2.917	same	same	0.038
					HF	ATZP	0.031
NH2CH3	H2O	M06-2X	TZP	2.874	HF	QZ4P	0.028
Cl-	NH3	M06-2X	TZP		HF	ATZP	0.033
Cl-	NH4+	M06-2X	TZP	2.72	same	same	0.076
NH3	Ca2+	M06-2X	ATZP	2.372	HF	ATZP	0.096
NH3	Zn2+	M06-2X	ATZP	1.955	HF	ATZP	0.336

The optimized geometry and amount of CT involving the amines ammonia, ammonium, and methylamine are shown in Table A.2. The distance is from the ion or the water oxygen to the nitrogen atom. For the cations, CT is greater than from water. The CT between water and ammonia is also greater than water-water CT. CT from Cl^- to NH_3 is reduced compared to water. CT from Cl^- to NH_4^+ is comparable to that from Cl^- to Li^+. The nature of CT in the $Cl^-{\cdot}NH_4^+$ complex is ambiguous from only the AIM analysis. This complex could also be considered as $HCl{\cdot}NH_3$, in which case CT would be from NH_3 to HCl.

Table A.3: CT Involving Alcohols.

Electron Donor	Electron Acceptor	Geometry Method	Geometry Basis	Distance Å	AIM Method	AIM Basis	q_{CT} e
H2O	CH3OH	M06-2X	TZP	2.873	HF	TZP	0.011
CH3OH	H2O	M06-2X	TZP	2.816	HF	QZ4P	0.015

The optimized geometry and amount of CT between water and methanol are shown in Table A.3. The distance is between the water oxygen and methanol oxygen. The CT between methanol and water is less than water-water CT.

The optimized geometry and CT for ions with argon are shown in Table A.4. The distances are large and the CT amounts are small.

Table A.4: CT Involving Alcohols.

Electron	Electron	Geometry		Distance	AIM		q_{CT}
Donor	Acceptor	Method	Basis	Å	Method	Basis	e
Cl-	Ar	M06-2X	ATZP	3.658	HF	same	0.014
Ar	Na+	M06-2X	ATZP	3.847	HF	same	0.002

Table A.5: CT Involving Carbonyls.

Electron	Electron	Geometry		Distance	AIM		q_{CT}
Donor	Acceptor	Method	Basis	Å	Method	Basis	e
H2CO	Na+	B3LYP	acT	2.173	HF	acT	0.0220
(CH3)2CO	Na+	B3LYP	G-b	2.129	HF	G-b	0.0295
					HF	acT	0.0266
H2CO	K+	B3LYP	G-b	2.570	HF	G-b	0.0974
(CH3)2CO	K+	B3LYP	G-b	2.504	HF	G-b	0.1005

The optimized geometry for cations with the carbonyls formaldehyde and acetone are shown in Table A.5. Similarly to the alkanes, CT between the carbonyls and Na^+ is comparable to that between Na^+ and water, yet the CT between carbonyls and K^+ is greater than between K^+ and water.

Appendix B

Methods for CT Data

In the following tables, methods used for geometry optimization of dimers and clusters are shown as well as the methods used to obtain charge transfer (CT) amounts. The references are all placed after the tables. Note that the Amsterdam Density Functional (ADF) software uses Slater-type orbitals (STO's) and has a built-in analysis for atoms in molecules (AIM) charges. With NWChem and Gaussian (G09), the AIM analysis is carried out by another software package. This is either the Henkelman software, which uses Gaussian cube files, or AIMAll, which uses wavefunction files.

To make the tables more legible, the following abbreviations are used for the basis sets:

acX aug-cc-pVXZ

cX cc-pVXZ

G-a 6-311+G*

G-b 6-311++G(2d,2p)

If the atoms are not explicitly listed, then the same basis is used on all atoms.

Table B.1: Methods Corresponding to Tables 2.5 and 2.6.

M	X	geometry optimization		AIM		software
		method	basis	method	basis	
Li	F	M06-2X	QZ4P	HF	same	ADF
	Cl	M06-2X	QZ4P	HF	same	ADF
	Br	M06-2X	QZ4P	HF	same	ADF
	I	M06-2X	QZ4P	HF	same	ADF
	OH2	M06-2X	QZ4P	HF	same	ADF
Na	F	M06-2X	QZ4P	HF	same	ADF
	Cl	MP2	acT	MP2	same	NWChem, Henkelman
	Br	M06-2X	QZ4P	HF	same	ADF
	I	B3LYP	Na acT; I MWB46	HF	same	G09, AIMAll
	OH2	MP2	acT	MP2	same	NWChem, Henkelman
K	F	M06-2X	K G-a; F acT	MP2	same	G09, AIMAll
	Cl	MP2	K G-b; Cl acT	MP2	same	NWChem, Henkelman
	Br	M06-2X	K G-a; Br acT	MP2	same	G09, AIMAll
	I	B3LYP	K G-a; I MWB46	HF	same	G09, AIMAll
	OH2	MP2	K G-b; O, H acT	MP2	same	NWChem, Henkelman
Rb	F	PBE0	Rb MWB28; F acT	PBE0	same	G09, AIMAll
	Cl	PBE0	Rb MWB28; Cl acT	PBE0	same	G09, AIMAll
	Br	PBE0	Rb MWB28; Br acT	PBE0	same	G09, AIMAll
	I	PBEPBE	Rb MWB28; I MWB46	PBEPBE	same	G09, AIMAll
	OH2	PBE0	Rb MWB28; O acT, H cT	HF	same	G09, AIMAll
Cs	F	PBE0	Cs MWB46; F acT	PBE0	same	G09, AIMAll
	Cl	PBE0	Cs MWB46; Cl acT	PBE0	same	G09, AIMAll
	Br	PBE0	Cs MWB46; Br acT	PBE0	same	G09, AIMAll
	I	PBE0	Cs MWB46; I MWB46	PBE0	same	G09, AIMAll
	OH2	M06-2X	QZ4P	HF	same	ADF

Table B.2: Methods Corresponding to Tables 2.7, 2.8, 2.9, and 2.10. The AIMAll program is used for all AIM calculations.

M	X	geometry optimization		aim		software
		method	basis	method	basis	
Be	F	PBEPBE	Be cT; F acT	HF	same	G09
	Cl	PBEPBE	Be cT; Cl acT	HF	same	G09
	Br	PBEPBE	Be cT; Br acT	HF	same	G09
	I	PBEPBE	Be cT; I MWB46	HF	same	G09
	OH2	PBEPBE	Be, H cT; O acT	HF	same	G09
Mg	F	PBEPBE	Mg cT; F acT	HF	same	G09
	Cl	PBEPBE	Mg cT; Cl acT	HF	same	G09
	Br	PBEPBE	Mg cT; Br acT	HF	same	G09
	I	PBEPBE	Mg cT; I MWB46	MP2	same	G09
	OH2	TPSS	Mg, O acT; H cT	MP2	same	G09
Ca	F	PBEPBE	Ca cT; F acT	HF	same	G09
	Cl	PBEPBE	Ca cT; Cl acT	HF	same	G09
	Br	PBEPBE	Ca cT; Br acT	HF	same	G09
	I	PBEPBE	Ca cT; I MWB46	HF	same	G09
	OH2	M06-2X	QZ4P	HF	ATZP	ADF
Sr	F	PBE0	Sr MWB28; F acT	MP2	same	G09
	Cl	PBE0	Sr MWB28; Cl acT	MP2	same	G09
	Br	PBE0	Sr MWB28; Br acT	MP2	same	G09
	I	PBE0	Sr MWB28; I MWB46	MP2	same	G09
	OH2	PBE0	Sr MWB28; O acT; H cT	MP2	same	G09
Ba	F	PBE0	Ba MWB46; F acT	MP2	same	G09
	Cl	PBE0	Ba MWB46; Cl acT	MP2	same	G09
	Br	PBE0	Ba MWB46; Br acT	MP2	same	G09
	I	PBE0	Ba MWB46; I MWB46	MP2	same	G09
	1-4 OH2	MP2	Ba MWB46; O acT; H cT	MP2	same	G09
	5+ OH2	TPSS-GD3BJ	Ba MWB46; O acT; H cT	MP2	same	G09

References:

Software:

ADF [1]

NWChem [2]

Gaussian09 [3]

AIMAll [4]

Henkelman AIM program [5]

Density Functionals:

PBEPBE [6, 7]

PBE0 [8]

M06-2X [9]

TPSS [10]

B3LYP [11, 12, 13, 14]

Post-HF Methods:

MP2 [15]

Basis Sets and Effective Core Potentials (ECP's):

(aug)-cc-pvXz [16]

6-311++G(2d,2p) [17]

MWB (Wood-Boring) ECP [18]

Other:

Grimme's dispersion correction (GD3) [19]

Use of Becke and Johnson's (BJ) damping for GD3 [20]

Bibliography

[1] *ADF2013*, SCM, Theoretical Chemsitry, Vrije Universiteit, Amsterdam, The Netherlands, 2013.

[2] M. Valiev et al., Comput. Phys. Comm. **181**, 1477 (2010).

[3] M. J. Frisch et al., Gaussian 09 Revision A.1, Gaussian Inc. Wallingford CT 2009.

[4] T. G. S. Todd A. Keith, Aimall (version 14.06.21), overland park ks, usa, (aim.tkgristmill.com), 2014.

[5] W. Tang, E. Sanville, and G. Henkelman, J. Phys.: Condensed Matter **21**, 084204 (2009).

[6] J. P. Perdew, K. Burke, and Y. Wang, Phys. Rev. B **54**, 16533 (1996).

[7] J. P. Perdew, K. Burke, and M. Ernzerhof, Phys. Rev. Lett. **78**, 1396 (1997).

[8] C. Adamo and V. Barone, J. Chem. Phys. **110**, 6158 (1999).

[9] Y. Zhao and D. G. Truhlar, Theor. Chem. Acct. **120**, 215 (2008).

[10] J. Tao, J. P. Perdew, V. N. Staroverov, and G. E. Scuseria, Phys. Rev. Lett. **91**, 146401 (2003).

[11] A. D. Becke, J. Chem. Phys. **98**, 5648 (1993).

[12] S. H. Vosko, L. Wilk, and M. Nusair, Canadian J. Phys. **58**, 1200 (1980).

[13] C. Lee, W. Yang, and R. G. Parr, Phys. Rev. B **37**, 785 (1988).

[14] P. J. Stephens, F. J. Devlin, C. F. Chabalowski, and M. J. Frisch, J. Phys. Chem. **98**, 11623 (1994).

[15] C. Möller and M. S. Plesset, Phys. Rev. **46**, 618 (1934).

[16] J. Dunning and H. Thom, J. Chem. Phys. **90**, 1007 (1989).

[17] T. Clark, J. Chandrasekhar, G. W. Spitznagel, and P. V. R. Schleyer, J. Comput. Chem. **4**, 294 (1983).

[18] J. H. Wood and A. M. Boring, Phys. Rev. B **18**, 2701 (1978).

[19] S. Grimme, J. Antony, S. Ehrlich, and H. Krieg, J. Chem. Phys. **132**, 154104 (2010).

[20] S. Grimme, S. Ehrlich, and L. Goerigk, J. Comput. Chem. **32**, 1456 (2011).

Vita

Marielle Soniat was born in New Orleans, LA and raised in Thibodaux, LA. She graduated in 2003 from Louisiana School for Math, Science, and the Arts, a residential high school for academically gifted students in Natchitoches, LA. She attended Mississippi State University, where she was part of the University Honors program and received a variety of awards for academic and extra-curricular activities. Her undergraduate research focused on biomaterials synthesis and characterization. She graduated from MSU in 2007 with a Bachelors of Science in Biological Engineering. From 2007-2009, she worked as a Peace Corps volunteer teaching chemistry and math at Kwabutu Secondary School in Lusanga, Tanga, Tanzania. In 2010, she started the doctoral program in Chemistry at the University of New Orleans. Her research has focused on the development of force fields for molecular dynamics simulations.